University of Alberta

Field Experiment Observations of a Dryline and the Associated Clouds and Precipitation

by

Daniel Martin Brown

A thesis submitted to the Faculty of Graduate Studies and Research
in partial fulfilment of the requirements for the degree of

Master of Science

Department of Earth and Atmospheric Sciences

Edmonton, Alberta
Spring, 2010

Abstract

The *UNderstanding Severe Thunderstorms and Alberta Boundary Layer Experiment* (UNSTABLE) in July 2008 was a field project to investigate the initiation of thunderstorms in southern Alberta. Special field observations included an enhanced surface network augmented with instrumented vehicles. Upper air observations were taken from four sites every two hours.

This thesis focuses on the case study day of 17 July 2008 when a dryline formed parallel to the Rocky Mountains at 1030 MDT and persisted for up to nine hours. The vapour mixing ratio changed from 4.5 to 8.5 g/kg over 5 km. We documented the spatial and temporal distribution of cloud and precipitation relative to the dryline. Initially, extensive cloud formed over the dry air to the west of the dryline, while the capping inversion at 800 mb inhibited cloud formation in the moist air. In the afternoon, convection was triggered along the dryline and severe thunderstorms were observed.

Acknowledgements

i. Data Contributors

This thesis could not have been completed without the raw data provided by certain data contributers. The author would like to thank the following data contributors for supplying and quality controlling the meteorological data used in this thesis.

Neil Taylor (Environment Canada)
- UNSTABLE development and coordination
- ATMOS surface data

Craig Smith (Environment Canada)
- Upper air sounding data
- Upper air sounding data processing and quality control

Dave Sills (Environment Canada)
- ATMOS surface data
- AMMOS mobile transect data

John Hanesiak (University of Manitoba)
- Upper air sounding data

Geoff Strong (University of Alberta)
- Mobile transect data

Alberta Sustainable Resource Development
- Fire tower weather reports
- Automated weather station data

Telvent
- Weather data from Alberta traffic cameras

Environment Canada
- Satellite imagery
- Radar imagery
- Canadian lightning detection network data
- Surface data
- Severe weather reports

ii. Graduate Student Funding

Canadian Foundation for Climate and Atmospheric Sciences
National Science and Engineering Research Council of Canada
Canadian Meteorological and Oceanographic Society
Government of Alberta

iii. Other Contributors

Gerhard Reuter
- For continued support and revisions in the structure and wording of the thesis

Geoff Strong
- For continued support and revisions in the structure and wording of the thesis

Neil Taylor
- For advice on the science and structure of the figures

Paul Myers
- For advice on the science and structure of the figures

Moritz Heimpel
- For advice on the science and structure of the figures

Tom Hutchison
- For extensive proof reading and comments on the structure of the thesis

Other proof readers include: Jan Schmidt, Martin Robillard, Freja Ann Mc Getrick, and Laurie Rac.

Table of Contents

List of Tables

List of Figures

Chapter 1

Introduction

Severe thunderstorms are a common summertime occurrence in Alberta (Etkin and Brun, 2001). Severe thunderstorms can cause significant damage due to hail, flash flooding, powerful winds, and tornadoes (Djurić, 1994). During the summer months, hail falls on over half the days in Southern Alberta (Smith et al., 1997), and an average of 10 tornadoes occur in Alberta every year (Hage, 2003). The 1987 Edmonton tornado (F4 on the Fujita Scale) and the 2000 Pine Lake tornado (F3 on the Fujita Scale) may be the most memorable (Dupilka and Reuter, 2005). Environment Canada must provide watches and warnings in affected areas with lead times to allow those affected to have time to prepare (Environment Canada, 2008). Specifics must be known about when and where thunderstorms will begin in order to accurately forecast the timing and location of severe thunderstorms. The relationship between weather features (e.g. shortwave troughs or fronts) and the organisation of precipitation is important to be able to accurately forecast thunderstorms.

1.1 Severe thunderstorms

When thunderstorm conditions exist, warmer humid air (less dense) is situated below colder air (more dense). Normally, this unstable situation would result in convective overturning of the atmosphere, manifested as thunderstorms. In severe thunderstorm conditions, the warm air and the cold air are separated by a capping inversion (hereafter referred to as the "cap"). The cap is a layer of hot, dry air which prevents the warm, buoyant air at the surface from rising up into the dense cold air in the middle atmosphere. In the lee of the Rocky Mountains, the cap is created when air subsides over the mountain barrier to the west, heats by compression, and is advected eastwards over the plains (Strong, 1986; Smith et al., 1997). A build up of heat and humidity occurs underneath the cap; a result of daytime heating and evapotranspiration. This further increases the instability. In

order to release the instability, the cap must be weakened or removed (Strong, 1986). Once the cap breaks, the warm, humid air rises because it is less dense, and cools as it expands. This causes the water vapour to condense, forming a cumulus cloud. When the water vapour condenses, a tremendous release of latent heat (2500 J g^{-1} for water) warms the rising air, further reducing its density. This release of energy causes additional upward motion and ultimately drives the development of the thunderstorm.

A developing cumulus cloud is characterised by a small plume of rapidly rising air (the updraft). Before precipitation begins, the updraft is compensated by a large area of slowly subsiding air encircling the cloud (Wallace and Hobbs, 1977). As the cloud grows, precipitation (in the form of rain or hail) begins to fall. The precipitation creates a more organised downdraft by dragging air down (precipitation drag), adding extra weight to the air, and by cooling the air as the precipitation evaporates. The thunderstorm now consists of a well defined updraft and downdraft. In non severe thunderstorm conditions, the downdraft suppresses the updraft because it forms in the same spot. These thunderstorms often form and die over the course of about 20 minutes (Wallace and Hobbs, 1977).

Vertical wind shear is the changing of wind direction or velocity with changes in altitude. Wind shear organises the internal storm dynamics by separating the updraft and the downdraft (Djurić, 1994). Separating the updraft and downdraft is necessary to keep them from interfering with each other. The presence of strong wind shear causes thunderstorms to last longer by helping to maintain the storm, although too much wind shear will blow the storm apart (Djurić, 1994). Dupilka and Reuter (2006) found that low level vertical wind shear was a necessary condition for tornadic thunderstorms in Alberta.

Synoptic scale features significantly influence the potential for the development of severe thunderstorms (Strong, 1986). A conceptual model for the synoptic conditions for the development of severe thunderstorms in Alberta has been developed over the past 30 years with data from various field projects.

Strong (1986) developed this model, and Smith and Yau (1993) present a modified version of the model. In this model, an upper level ridge is located over the Alberta/Saskatchewan Border with a corresponding upper level trough located in central British Columbia. This generates a south westerly flow and upper level divergence between the ridge and trough over the Rocky Mountains. Upper level divergence creates surface convergence and can trigger and sustain severe thunderstorms (Beebe and Bates, 1955). As the upper level trough drifts into Alberta, cold air advection occurs in the middle troposphere. This will tend to increase the instability, especially if it is accompanied by warm air advection near the surface. Because of the south west flow over the Rocky Mountains, lee cyclogenesis takes place and a surface low develops. A surface low in southern Alberta and relatively higher pressure in northern Alberta will conspire to produce an easterly component to the surface winds. The easterly flow causes upslope flow and convergence along the foothills, supplementing the already unstable situation (Strong, 1986; and Smith and Yau, 1993). The location of the induced surface low is important for where the strongest easterly component is produced (Strong, 1986).

Smith and Yau (1993) also found that the easterly flow caused by synoptic systems is supplemented by further easterly forcing caused by the mountain-plain circulation. The mountain-plain circulation is caused by differential heating between the east slopes of the Rocky Mountains and the plains to the east. When the sun rises in the east in the morning, the east slopes are facing into the sun. This results in the east slopes receiving more concentrated solar radiation than the plains, which causes them to heat up faster. The warmer air rises, which induces easterly winds on the plains. To create the maximum probability of severe thunderstorms, all of these forcing mechanisms must work together. Ideally the upper level trough discussed in the previous paragraph should arrive between 0800 and 1400 MDT to have the maximum surface convergence coincide with the maximum daytime heating, the maximum moisture content of the air, and the maximum forcing from the mountain plain circulation (Smith and Yau, 1993).

Because the cap initially suppresses convection, a trigger is required to initiate severe thunderstorms. The trigger supplies upward motion to break through the cap and release the buoyant energy. Triggers tend to initiate isolated severe thunderstorms. When the trigger breaks the cap in one spot, the rest of the cap continues to suppress widespread thunderstorm development. If too many thunderstorms are created in the same area, they will interfere and become less severe because they compete with each other for warm moist air (Dupilka and Reuter, 2006). The initiation of severe thunderstorms becomes much more probable when a number of triggers work together. Smith and Yau's (1993) model allows for the prediction of which days will support severe thunderstorms, while Strong's (1986) model allows for an objective prediction of the intensity and a general location of thunderstorms. Neither of these can give specifics about the exact location and timing of the initiation of severe thunderstorms, hence the need for examining other triggers.

1.2 Triggering of severe thunderstorms

A number of different mechanisms can trigger severe storms. Inhomogeneous surface heating can cause the cap to erode preferentially in one place. This can be caused by differences in slope, albedo, vegetation and soil moisture. Upslope flow caused by a topographic barrier can help to punch through the cap. Surface convergence areas caused by upper level disturbances, spatial changes in land cover, lake/sea breezes, storm outflow boundaries, or frontal boundaries can cause upward motion forcing air through the cap (Djurić, 1994). Knowledge about the location, timing, and type of trigger can narrow down the regions where severe storms can be expected, which would improve forecasting of the location and timing of severe thunderstorms.

A front is the boundary between two different air masses. Warm and cold fronts are boundaries between warm and cold air masses. A cold front is advancing cold air while a warm front is retreating cold air (allowing warm air to advance). Fronts cause surface convergence and upward motion, and can be

identified by the different types of clouds they produce. Warm fronts are characterised by large areas of stratiform clouds with light precipitation, while cold fronts are characterised by a line of convective clouds with heavy precipitation. In the summer there is a much smaller difference in the temperatures between different air masses (Djurić, 1994). Strong (1986) claims that most Alberta severe thunderstorms are not caused by warm or cold fronts. Instead, severe thunderstorms in Alberta are post cold frontal, which means that they occur well after a cold front has passed.

1.3 Drylines

Drylines are a different type of surface boundary often found in the summer. Rather than a boundary separating air masses with different temperatures, a dryline is a sharp boundary separating dry air from humid air (Fujita, 1958). A thin line of stronger cumulus convection is often visible along the dryline, with broken to overcast sky conditions on the moist (east) side, and a cloud free sky on the dry (west) side (Fujita, 1970). In North America, a dryline tends to travel eastwards during the morning and afternoon and westwards during the evening and night (Schaefer, 1986). Surface convergence is frequently present along the dryline, leading to interest in the role of drylines in the initiation of severe thunderstorms (Rhea, 1966).

Drylines have not been studied extensively in Alberta (Hill, 2006). It has been found that a dryline was responsible for the initiation of severe storms in Alberta such as the Pine Lake and Holden tornadic storms. A dryline was not detected during the initiation of the 1987 Edmonton tornadic storm (Dupilka and Reuter, 2005). Hill (2006) showed that drylines can occur in Alberta with a narrow boundary between the dry and moist air. The moisture gradients in Alberta were similar to those measured in Texas and Oklahoma (Hill, 2006).

1.4 Detecting drylines

Convergence and divergence are important variables for deriving the vertical motion involved in breaking the cap. Convergence is the shrinking of the horizontal area occupied by a parcel of air, and determines the vertical motion of the air. For example, convergence at the surface will force air to move up, while divergence at the surface will pull air down (Wallace and Hobbs, 1977). Surface convergence is calculated using the wind speed and direction (see Appendix A). Vegetation, topography, and vertical mixing can considerably affect wind direction. Even though the wind speed and direction may be accurately measured, these point wind measurements may not accurately represent the large scale flow, making the accurate computation of large scale surface convergence difficult. In addition, wind measurements are often taken on a sixteen point scale, causing noise due to the lack of resolution (Ogura and Chen, 1977). This is why the dryline is frequently examined in terms of humidity, even though it is the surface convergence caused by the wind which initiates thunderstorms. The humidity of the air serves as a tracer allowing one to identify the moist air (with an easterly component to the flow), and the dry air (with a westerly component to the flow).

1.5 Data requirements

Low level instrumented aircraft transects by Fujita (1958) and McGuire (1962) have established that the dryline boundary between the moist and dry air can be very narrow (sometimes less than 1 km). Surface observations of the dryline by operational weather stations are limited by the spatial resolution of surface weather stations. Surface weather stations often are spaced more than 100 km apart, while the width of the moisture gradient in the dryline can be less than 1 km (Fujita, 1958). A number of different solutions to this problem have been developed. A special dense mesonet of weather stations has provided insight into drylines in Oklahoma (McCarthy and Koch, 1982). Radar and LIDAR observations have remotely sensed the moisture gradient along the dryline (Parsons et al, 1991 and Fujita, 1970). Mobile mesonet vehicles have provided transects across the dryline sampling at very high spatial and temporal resolution

(Pietrycha and Rasmussen, 2003). These measurements are not routinely available, and must be part of a special project.

The same aircraft traverses by Fujita (1958) and McGuire (1962) revealed that large changes in temperature and humidity associated with the dryline occur over small distances throughout the boundary layer. Measurements of the atmosphere above the surface are commonly done using instrumented balloons called radiosondes. Operational radiosonde measurements are performed twice per day with a spacing often greater than 500 km. This is far too few to adequately observe a 1 km wide changing dryline. For example, there is one radiosonde site in Alberta, none in Saskatchewan and one in Manitoba. Soundings are only launched twice per day at these sites. Researchers have used a number of high resolution measurements to fill in these gaps. Bluestein et al. (1988 and 1989) used mobile soundings to obtain upper air data near drylines and thunderstorms. Aircraft measurements have been used extensively by Fujita (1958), McGuire (1962), and others. Parsons et al. (1991) used Doppler LIDAR while Atkins et al. (1998) used airborne Doppler radar. Again, none of these measurements are routinely available, and must be a part of a special project.

Drylines can be identified by remote sensing in a number of different ways. Often, a thin line of cumulus convection visible on satellite imagery indicates a dryline (Fujita, 1970). Drylines can also be identified from satellite imagery as a cloud – no cloud boundary (Parsons et al., 1991). Rhea (1966) identified drylines using radar. Radar echoes, indicating precipitation, persistently developing along a line could indicate a dryline (Rhea, 1966). Understanding the relationship between cloud cover, precipitation, and the location of the dryline helps forecasters determine where the initiation of convection is likely to occur.

The previous discussion shows that in order to further understand the dryline, additional instrumentation is needed to supplement the operational instrumentation. It is necessary to incorporate and assortment of special

instrumentation during a field research experiment to study the finescale structure of the dryline.

1.6 UNSTABLE field project

The purpose of the 2008 UNSTABLE project (UNderstanding Severe Thunderstorms and Alberta Boundary Layer Experiment) was to better understand the boundary layer processes which initiate deep convection in the Alberta foothills. The project consisted of special fixed and mobile measurements, radiosonde launches, and aircraft measurements to help fill in the gaps left by the current observation network (Taylor et al., 2007). An intensive observation period took place in mid-July for about two weeks. Within those two weeks, the full scale deployment of all the instrumentation took place on eight intensive observation days. The author was part of one of the mobile mesonet teams throughout the intensive observation period. This will be discussed further in the experimental setup (Section 3.2). UNSTABLE was a collaboration between scientists from Environment Canada, the University of Alberta, the University of Manitoba, the University of Calgary, York University, and Weather Modification Inc (Taylor et al., 2007).

Sufficient dryline data was collected during the UNSTABLE project on three days. Data was made available to the author for the dryline case of 17 July 2008. The goal of this thesis will be to explore a case study of a dryline event which was suspected to initiate severe convection using the UNSTABLE data measured on the 17 July 2008 in central Alberta.

1.7 Main Scientific Questions

The main scientific questions to be answered in this thesis relate to a case study approach for studying the dryline on the 17 July 2008. The questions are as follows:

1. How are the clouds and precipitation organised relative to the dryline on the 17 July 2008, and how does this evolve with time?

2. How does the structure and evolution of the 17 July 2008 Alberta dryline compare to the classical "textbook" dryline?

A case study approach will be taken to answer these questions. The majority of the UNSTABLE data was obtained from 8 intensive observation days, and numerous researchers are hoping to investigate the UNSTABLE data. This lends itself to a case study approach. A case study allows an extremely detailed analysis of one particular feature using an assortment of different data sources.

1.8 Thesis Outline

The first chapter provided an introduction to the topic of this thesis. Chapter 2 will examine the current knowledge of the dryline. Most of this knowledge consists of work done in Texas and Oklahoma. A discussion on the current state of knowledge about drylines in Canada will also be provided. Chapter 3 is a discussion on the UNSTABLE field project, and the data sources. The UNSTABLE data sources that are used, the known limitations of the data, and the other data sources (not part of UNSTABLE) will be discussed. Chapter 4 is the analysis and results of the case study. The structure and evolution of the dryline will be discussed, along with the associated clouds and precipitation. Chapter 5 is a comparison between the 17 July 2008 dryline and textbook cases and other conceptual models. Chapter 6 is a summary and discussion of the key findings about this case study, with suggestions for further research.

The background on the current knowledge about drylines will be discussed in the next section. Drylines have been extensively studied in Texas and Oklahoma. The conceptual model of dryline structure and motion has been refined over the years by Schaefer (1986), Ziegler and Hane (1993), and others. The limited research on drylines in Alberta (Hill, 2006) will also be discussed.

Chapter 2

Drylines

2.1 Characteristics of drylines

During the spring and early summer, a narrow boundary between relatively moist and dry air sometimes forms parallel to the Rocky Mountains in North America. This boundary separates moist air and dry air flowing in different directions. Often the moist air originates from the Gulf of Mexico, while the dry air flows off the semi-arid high plateau regions of Mexico, or has subsided on the lee side of the Rocky Mountains (Fujita, 1958). In the literature, this narrow zone of moisture gradient has been termed *dewpoint front* (Beebe, 1958), *dry front* (Fujita, 1958) and *dryline* (McGuire, 1962). Beebe (1958), Fujita (1958), and McGuire (1962) all noted that often thunderstorms were triggered near the dryline. Miller (1959) found that most of the severe convection occurred in bands coinciding with the location of a dryline. The dryline affected both the triggering and the intensification of the severe thunderstorms.

Typically the horizontal temperature gradient in the atmosphere is very small in the vicinity of a dryline, which differentiates a dryline from a warm or a cold front. The temperature gradient across a dryline reverses sign diurnally. Usually the dry air is cooler than the moist air at night, while during the day, the dry air is warmer than the moist air (Schaefer, 1986). Fujita (1958) and Beebe (1958) analysed the surface wind field in the vicinity of dry lines. They found that the dryline often moved eastwards. The dry air pushed eastwards while the moist air flowed towards the north, i.e. there was southerly flow on the moist side and westerly flow on the dry side. This change of wind direction across the moving dryline resulted in surface convergence along the moisture transition zone. Fujita (1958) described the dry air as having “Chinook-like characteristics”.

Early research on drylines focused on measuring the sharpness of the moisture gradient across the dryline using research aircraft. Based on low-level

aircraft traverses across a dryline, Beebe (1958) measured a water vapour mixing ratio gradient of about 2 g kg^{-1} km^{-1}. McGuire (1962) reported a moisture gradient across a dryline of 2.5 g kg^{-1} km^{-1}. McGuire (1962) found that the horizontal density gradient at 700 mb was close to zero. His measurements suggest that the slope of the dryline is nearly vertical in the lowest part of the atmosphere, then changing to almost horizontal near the 700 mb level.

In the Great Plains of the United States, drylines occur predominantly in spring and early summer (Schaefer, 1986). Rhea (1966) and Schaefer (1974b) investigated the dryline occurrences and found that drylines are evident on about 40 % of all spring days. Lubbock, Texas has recorded an average of 12 dryline passages over the course of the spring (Peterson, 1983). In Canada, the development of the dryline has only been investigated in the summer months (Hill, 2006). Hill (2006) found that there were 3 or 4 drylines forming over southern Alberta during a summer.

2.2 Locating of drylines

A moisture variable must be chosen for analysing the dryline. Synoptic observations for weather forecasting are recorded and disseminated in dewpoint temperature, which makes this is the most convenient variable in an operational setting. Water vapour mixing ratio and specific humidity are both conserved variables with height, which gives either of them a strong theoretical appeal, especially for studies with variable terrain (Schaefer, 1986). When analysing drylines, there is no convention for whether to place the dryline on the moist or dry side of the front, although Hane et al. (1997) suggested placing the dryline on the moist side of the moisture gradient. Operational surface observations are not spaced closely enough to adequately resolve the dryline, causing the moisture field to appear to exhibit a discontinuity (e.g. a 1 km dryline between two surface stations 20 km apart). This requires that one chooses an arbitrary contour line to define as the location of the dryline within the smoothed moisture gradient.

Remote sensing can help to locate the dryline, with satellite imagery and radar finelines being the most common (Schaefer, 1986).

For analysis of the dryline, Schaefer (1986) recommends the 9 g kg^{-1} isohume (line of constant vapour mixing ratio) for the southern United States. In terms of dewpoint, this corresponds approximately to the 12 °C isodrosotherm (line of constant dewpoint temperature). In cases where high resolution humidity measurements are available, Hane et al. (1997) located the dryline on the moist side of the sharpest moisture gradient.

2.3 Three dimensional structure of drylines

Ziegler and Hane (1993) developed a conceptual model that synthesised many of the findings made by Schaefer (1974a, 1974b, 1986), as well as their own findings. In this model, the dry air (located west of the surface dryline) is well mixed by convective overturning from the surface up to about 500 mb. In contrast, the moist air (located to the east of the dryline) is capped at about 800 mb (Schaefer, 1974a, 1986; and Fujita, 1958, 1970). The properties of the dry air to the west are similar to the properties of the dry air above the moist air to the east. Convective instability often results from this dry adiabatic layer situated above the shallow capped moist layer (Schaefer, 1986). In the Ziegler-Hane (1993) model of a dryline, clouds are often formed in the moist air (east of the dryline), while the dry air to the west tends to be mostly free of clouds (Fujita, 1970; and Bluestein et al., 1988).

The motion of the dryline is driven by the height of the boundary layer. Gently sloping topography towards the east in the lee of the mountains causes the thickness of the moisture layer to increase further east (Schaefer, 1974b). The height of the boundary layer increases during the day due to daytime heating. As this happens, the shallow moist layer is mixed away further and further east, causing the dryline boundary to advance eastwards (Schaefer, 1974b).

Deep vertical mixing in the dry air carries down mid-level momentum with a westerly component (McCarthy and Koch, 1982). Because the moist air to the east has an easterly component, there is a confluence of the wind direction resulting in surface convergence where the dry air and moist air meet to form the dryline (Rhea, 1966). This convergence produces the strong vertical motion required to break through the cap (Wallace and Hobbs, 1977).

In the evening the dynamics of the dryline changes. As the air cools at the surface, a nocturnal inversion begins to form creating an extremely stable stratification. The nocturnal inversion prevents the mixing down of mid-level momentum, causing the surface winds in the dry air to subside due to ground friction (Matteson, 1969; and Schaefer, 1986). The easterly flow in the moist air has not subsided yet, which advects the boundary towards the west (Schaefer, 1986). Furthermore, the depth of the boundary layer has stopped increasing, halting the eastward advance of the dryline (Schaefer, 1974a).

If the dryline succeeds in breaking the cap, severe thunderstorms are often initiated (Rhea, 1966). Not all drylines initiate severe thunderstorms (e.g. Dupilka and Reuter, 2005; and Hill, 2006). Severe thunderstorms tend to form on the moist side of the dryline within about 50 km of the dryline boundary (Rhea, 1966). Some of the most severe tornadic storms have been initiated along a dryline, such as the 2000 Pine Lake tornadic storm in southern Alberta, and the 1993 Holden tornado in central Alberta (Dupilka and Reuter, 2005).

Fujita (1958) found from aircraft transects that the slope of a dryline was 1:30 in the afternoon. McGuire (1962) determined that the slope was essentially vertical in the afternoon at the surface tending towards horizontal as the boundary approaches 700 mb. A modelling study by Miller et al. (2001) showed that the slope could change diurnally from 1:5 in the afternoon to 1:100 in the evening. The much shallower slope in the evening may be the result of the dryline taking on the form of a density current (Schaefer, 1986).

2.4 Dryline motion

Miller et al. (2001) performed numerical simulation of drylines with the focus on investigating the motion of the dryline. The simulated drylines tended to move eastwards during day and westwards during the night. Schaefer's (1974a) observations suggest that vertical mixing was the driving force behind the motion of the dryline during the day. Because the terrain gradually slopes down toward the east, the depth of the moisture underneath the capping inversion is deeper to the east. As daytime heating mixes the lower parts of the atmosphere, the cap is broken. Because of the depth of the mixed layer, this happens earlier in the west, and later in the east causing the dryline to progress eastwards in the morning and early afternoon as a direct result of daytime heating (Schaefer, 1974a). Miller et al. (2001) confirmed that the effect of the changes in static stability were significant in the motion of the dryline. They used a time varying "reduced gravity" (based on the density difference between the dry and moist air) in order to simulate the motion of the dryline, and determined that dryline motions of up to 200 km eastward could result from changes in the stability and density of the dry and moist air. It appears that the reduced gravity effect described by Miller et al. (2001) results from reduced westward density current flow in the morning, and increased westward density current flow in the evening.

Schaefer's (1974a, 1974b, and 1986) observations showed that dryline motion was usually continuous, but could be discrete at times. Discrete propagation occurred if the cap were eroded simultaneously over a large area, which could be caused by uniform surface heating in an area with a uniform capping inversion and uniform elevation. Schaefer (1974b) refers to the dryline "jumping" further east much faster than advection could account for.

The late evening and nocturnal motion of drylines appears to have a different origin from morning and mid-afternoon drylines. There has not been nearly as much research done on nocturnal drylines, but they are known to retrograde westwards after the height of daytime heating, and continue to do so

until late at night (Schaefer, 1986). It was first noted by Matteson (1969) that a possible cause of the westward retreat of the dryline at night was the tendency for the winds in the dry air to become light at night, allowing the moist air to advect the boundary to the west. Schaefer (1974a) suggests that because the dry air cools faster than the moist air, it decouples from the upper level air quicker due to the formation of a nocturnal inversion, and the westerly winds stop due to friction with the surface. This allows the winds with an easterly component in the moist air to advect the dryline in the same way as a density current back to the west. Since the air on the dry side can be as much as 5° warmer than the air on the moist side, faster cooling of the dry air could, in some cases, still result in warmer temperatures to the west, and thus lower density.

2.5 Horizontal density gradient

There has been much debate on whether there is a significant horizontal gradient of air density perpendicular to a dryline, and whether this density gradient contributes significantly to the motion of the dryline. Early studies by McGuire (1962) and Fujita (1958) found no significant horizontal density gradient across the dryline. In contrast, some more recent studies found that there was a horizontal density gradient (e.g. Parsons 1991). Ziegler and Hane (1993) attributed this apparent conflict due to differences in timing of the observations. The diurnal temperature variation in the dry air is much larger than that in the moist air. Parsons et al. (1991) attributes this to cloudiness in the moist air and a cloud free sky in the dry air. Accordingly, the dry air is significantly warmer in the late afternoon and early evening, while it is cooler in the early morning and towards noon (Schaefer, 1986). This supports the idea that the dryline can act as a density current, as the temperature differences between the dry and moist air can be as much as 5 °C, more than offsetting the effect of moisture on the density. The temperature variations lend support to the proposal by Schaefer (1974a, 1974b, and 1986) that the dryline acts as a density current in the evening, but not in the early afternoon and morning.

Most of the research on drylines uses virtual potential temperature as the variable representing density. Virtual potential temperature is essentially the potential temperature corrected for the density differences caused by humidity (See Appendix B). In some cases, there is a notable gradient in virtual potential temperature across the dryline, although this depends on the time of day (Schaefer, 1974a, 1974b, and 1986). Schaefer (1986) postulates that in the evening, the dryline retrogresses westwards as if it were a density current flowing into less dense air. Parsons et al. (1991) and Ziegler et al. (1995) use an equation to calculate the propagation speed of the proposed density current flow of the dryline, and find that it compares well with density current theory. There are a few concerns with the idea of density current flow. In the case of a dryline, the propagation of the density current would be uphill, and be countered by gravity (in this case, a "reduced" gravity). This issue was addressed by Parsons (1991) who found that the uphill flow was not expected to be significant in that particular case. Another issue brought up by Parsons (1991) is the possibility that the variation in potential temperature could be caused by elevation difference.

2.6 Dryline bulges and waves

Synoptic scale dryline bulges form when additional upper level momentum is mixed to the surface (Schaefer, 1986). Schaefer (1986) provides some speculation as to the source of the upper level momentum. He notes that when a synoptic scale dryline bulge is present, an upper level jet is often present and could be the source of the extra momentum. Other proposed sources of momentum are disturbances crossing the dryline providing enhanced convergence or divergence forcing momentum down to the surface, or standing mountain waves (Schaefer, 1986).

Mesoscale dryline bulges are related to mesoscale dryline waves (McCarthy and Koch, 1982), and horizontal convective rolls (Atkins et al., 1998). Schaefer (1986) mentions the possibility of horizontal convective rolls influencing mesoscale dryline bulges. Since the late 1990s, the development of

Doppler radar and LIDAR, the installation of dense mesonets, and the implementation of high resolution modelling studies have furthered the development of these ideas (Ziegler et al., 1997).

Ziegler et al. (1997) found that a 1 km resolution model is barely acceptable to properly simulate horizontal convective rolls. The model that was run managed to partially simulate bands of convergence, which Ziegler et al. (1997) propose are caused by horizontal convective rolls. Atkins et al. (1998) found that there was substantial variability in the horizontal position of the dryline, and that horizontal convective rolls were responsible. Both Bluestein et al. (1988), and Atkins et al. (1998) have observed the formation of cumulus clouds at preferred locations along the dryline, and this is thought to be caused by horizontal convective rolls in the dry air.

2.7 Estimating convergence near drylines

A vertical profile of mesoscale vertical velocity can be obtained by integrating a profile of mesoscale convergence. Different techniques have been developed to estimate mesoscale convergence for different pressure levels based on mesoscale sounding observations. One approach is the kinematic method (Wallace and Hobbs, 1977; Djuric 1994). Ogura and Chen (1977) used the kinematic method to estimated convergence and updraft profiles near a dryline. Parsons et al. (1991) stated that the kinematic computation of convergence and vertical velocity based on sounding data cannot resolve the sharp gradients of kinematic variables in vicinity of drylines. Instead they promoted the use of mobile Doppler radar or LIDAR instead of sounding data. Ziegler and Hane (1993) used aircraft wind measurements to estimate convergence. Strong (1986) discussed the interaction of thunderstorms with the ambient airflow. Typically, the pre-storm environment shows small mesoscale vertical velocity values (< 0.2 m s^{-1}). Once thunderstorms are formed, the mesoscale vertical velocities are often exceeding 0.5 m s^{-1}, consistent with strong low level convergence and upper level divergence.

2.8 Drylines forming over Alberta

Strong (1986) suggested that drylines form in the Alberta foothills region where the subsidence induced capping lid intersects with the ground surface. Knott and Taylor (2000) investigated the meteorological conditions leading to the severe weather outbreak which produced the F3 Holden tornado in central Alberta. Based on the surface analysis of dewpoint, temperature and wind, they identified a long lasting synoptic scale dryline. The severe convection formed close to the dryline. Dupilka and Reuter (2005) compared the initiation of three severe convective storms over central Alberta that spawned intense tornadoes: the 1987 Edmonton tornado, the 1993 Holden tornado, and the 2000 Pine Lake tornado. They found that the Holden tornadic storm and the Pine Lake tornadic storms were triggered along well defined drylines. In contrast, the 1987 Edmonton tornadic storm was not associated with a dryline, as the surface conditions were very humid everywhere. This suggests that some severe convective storms are triggered by drylines, but others are not.

In the studies by Knott and Taylor (2000) and Dupilka and Reuter (2005) the drylines were located based on meteorological data sampled by operational surface weather stations. Hill (2006) was the first to analyse finescale measurements of the Alberta dryline using mobile transects and proximity soundings. In her thesis, Hill described several drylines forming over Alberta. Her observations suggest that the moisture gradient across Alberta drylines was similar to that reported for drylines of the American Great Plains. Alberta drylines are often but not always associated with convection in Alberta (Hill, 2006).

On the Canadian prairies, evapotranspiration over the crops in summer constitutes an important source of humidity. Strong (1986) stressed the large diurnal trend in water mixing ratio. Strong (1997) found that transpiration from crops can add as much as 4 g kg^{-1} of boundary layer moisture from morning to afternoon. An interesting development on the Canadian prairies is the

modification of the pre-storm environment from its natural state by extensive agriculture (Raddatz, 1998). Raddatz (1998) found that the development of agriculture modified the evapotranspiration profile of the prairies causing more moisture to be present in July, while less is present in August. It has been documented that the increase in moisture due to evapotranspiration can double the convective available potential energy (CAPE) resulting in much more severe storms than would be expected without significant evapotranspiration (Raddatz, 2003). Raddatz (2003) suggested that the increase in boundary layer moisture due to evapotranspiration can contribute to the formation of severe convection such as the Winnipeg hailstorm of 1996 and the Pine Lake tornado of 2000. Modelling studies confirmed that the location of drylines is strongly affected by evaporation from soil moisture and transpiration from vegetation (Shaw et al., 1997).

Figure 2.1 and 2.2 illustrate the possible formation of a dryline forming over the Alberta foothill region. A vertical cross section perpendicular to the dryline is shown. Hot dry air develops from the release of moisture and subsequent latent heat from repeated orographic precipitation. The hot dry air is initially sits above the moist air. The surface air to the east gets its moisture by evapotranspiration from crops (Strong, 1997). The easterly component of the flow is driven primarily by the mountain plain circulation (Smith and Yau, 1993). Lee cyclogenesis can also contribute to upslope easterly flow over the foothills (Strong 1986) (Figure 2.1 upper panel). As daytime heating progresses, the dry air to the west is mixed down to the surface, while the moist air (located to the east) continues to be capped at around 800 mb. The dry air can be well mixed as high as 500 mb. The properties of the dry air to the west are similar to the properties of the dry air above the moist air to the east (Schaefer, 1986). Convective instability can result when the dry adiabatic layer rises above the shallow capped moist layer at the surface. Extensive cloud cover is often observed in the moist air, and some researchers have defined the dryline as the cloud – no cloud boundary (Fujita, 1970; and Bluestein et al., 1988). The dry air with a

westerly component interacts with the moist air with an easterly component causing convergence along the boundary (Figure 2.1 bottom panel).

The dry air and moist air mix along the dryline creating plume of intermediately humid air and two sharp moisture gradients separated by about 10 – 20 km. The plume of moisture is forced up by convergence and extends almost as high as the well mixed dry air to the west (Ziegler and Hane, 1993) (Figure 2.2 upper panel). Once the plume of moisture reaches its condensation level, convection is initiated. This convection may intensify into severe thunderstorms (if the instability and wind shear permit) as it drifts into the moist air east of the dryline (Ziegler et al., 1998) (Figure 2.2 bottom panel).

Chapter 3

UNSTABLE 2008 Field Project and Method of Analysis

3.1 Review of Alberta Field Experiments

Most of the convective storms affecting the Canadian Prairie provinces originate from the Alberta foothills region on the lee side of the Rocky Mountains. Once initiated in this region, these convective storms migrate eastwards into central Alberta, Saskatchewan, and Manitoba. Central Alberta is affected by hail on more than half (57 %) of the days during the summer months (Smith et al., 1998) and experiences about 10 to 20 tornadoes annually (Hage, 2003). Alberta farmers suffer about 100 million dollars in crop losses each year (Etkin and Brun, 2001). A particular disastrous event was the Edmonton tornado on 31 July 1987 which left 27 people dead, 300 injured and caused 250 million dollars in property damage. The severe hailstorm which swept over Calgary on 7 September 1991 cost insurance companies more than 400 million dollars (Charlton et al., 1995).

To study the formation and possible modification of hailstorms, field experiments were conducted in central Alberta from 1956 to 1985. Some important findings of these activities involved: formation and growth of hail (English, 1973), hail forecasting (Renick and Maxwell 1977), and water budget of hailstorms (Rogers and Sakellariou, 1986). To investigate the initiation of convection, the LImestone Mountain EXperiment (LIMEX) was conducted in the Alberta foothills in July of 1985 (Strong, 1986). Smith and Yau (1993) used the high resolution surface and sounding data from LIMEX to determine the factors that differentiate severe from non-severe convective outbreaks. They concluded that under generally clear skies, cumulus convection begins over the foothills as strong surface heating removes the capping lid. Convective outbreaks occur when an approaching synoptic scale upper-level trough is in phase with strong surface heating over the Alberta foothills. East and north east surface winds transport

moist air from the plains to the foothills, and the normal mountain-plain circulation is amplified by the deep destabilization which is localized over the foothills (Smith and Yau, 1993). By analysing the LIMEX water vapour mixing ratio fields, Brennand (1992) concluded that low-level moisture convergence tended to precede storm development by two to four hours. Low-level mass convergence remained during the entire period of storm formation.

In 1992, the precipitation research in Alberta summer storms received a major boost with the upgrading of the Carvel radar establishing a digital archive of radar measurements. In addition, the radar upgrade allowed Doppler wind measurements. Carvel radar observations were used to investigate severe storm structure (Holt et al., 1994), organisation of precipitation in flooding storms (Reuter and Nguyen, 1993), the kinematic characteristics of gust fronts and mesocyclones (Larochelle 1994), and convergence lines during the formation of convective storms (Xin and Reuter, 1998).

In the summers of 2003 and 2004, the Foothills Orographic Precipitation Experiment (FOPEX) was conducted to record orographic effects of precipitation and storm initiation. The field observations included a line of automated surface weather stations at different elevations. Hill (2006) used these measurements, supplemented with surface measurements of a mobile weather station, to document the occurrence of drylines in Alberta foothills region.

3.2 UNSTABLE 2008 field project

The UNderstanding Severe Thunderstorms and Alberta Boundary Layer Experiment (UNSTABLE) was a field project, data analysis, and modelling study to investigate the atmospheric boundary layer processes associated with convective initiation and severe thunderstorm development (Taylor et al., 2007). A pilot experiment (UNSTABLE 2008) was conducted during the summer of 2008 to investigate the importance of water vapour stratification and mesoscale convergence boundaries, including drylines. Measurements obtained through a high-resolution network of fixed and mobile surface, upper-air and airborne

instruments were used together with measurements from existing platforms to better understand important mesoscale processes in this thunderstorm genesis zone (Taylor et al., 2007). The following information is summarised from Taylor et al. (2007).

UNSTABLE 2008 was a collaboration between scientists from Environment Canada, the University of Alberta, the University of Calgary, the University of Manitoba, York University, and Weather Modification Inc. The geographical focus of the project was in west central Alberta (Figure 3.1). An intensive observation period took place from 9 to 24 July 2008. The science plan for UNSTABLE outlined several missions which included a mission to study the dryline. Further information on UNSTABLE can be found in the science plan available at the following website: http://www.umanitoba.ca/faculties/environment/envirogeog/weather/unstable/UNSTABLE.html.

UNSTABLE consisted of numerous mobile and fixed observation platforms. There were three mobile mesonet vehicles. The vehicles were equipped with temperature, humidity and pressure sensors, with one vehicle equipped with a wind sensor. These vehicles were responsible for completing mobile transects which differed depending on the selected mission. Balloon soundings were released every two hours from four different locations. A tethersonde was also operational to measure time series of meteorological variables in the atmospheric boundary layer. An instrumented aircraft was used to sample temperature, humidity and wind at mid-levels.

Eight days were selected as Intensive Observation Days (IOD). An IOD would consist of a morning weather briefing to plan where the observing teams would go to sample the pre-storm environment. Once storms developed, teams would conduct storm observations. Most of the data have been processed and quality controlled, but there are still some data that have not been made available and are not used in this thesis.

My participation in UNSTABLE 2008 consisted mainly of helping operate one of the three vehicles to sample surface measurements at critical locations. My partner was Dr Geoff Strong throughout the three weeks of field work. I also participating in weather briefings, and recorded observations of severe thunderstorms.

3.3 UNSTABLE instrumentation networks

a) Surface weather station network

Figure 3.2 depicts the location of surface weather stations. The operational surface network consisted of data acquired from Environment Canada, Alberta Sustainable Resource Development (ASRD), and Telvent. Environment Canada operates 39 weather stations located within the UNSTABLE study area. Most of the Environment Canada weather stations are located in the agricultural land in the east part of the study area and report hourly. ASRD operates 11 weather stations with hourly measurements and 15 stations with measurements twice daily within the UNSTABLE study area. Most of the ASRD weather stations are located in the forested foothills of Alberta. Telvent operates a network of road cameras and weather stations for Alberta Transportation and the Alberta Motor Association. Telvent provided data from 14 weather stations which report every 20 minutes. The weather stations operated by Telvent are located along major highways.

The operational weather stations mentioned above record temperature, humidity and rainfall amounts. About two thirds of the operational weather stations also sampled wind speed and wind direction. Surface pressure measurements were taken only at Environment Canada surface weather stations, and even there not all EC stations recorded pressure.

A major component of the UNSTABLE project included a number of additional surface weather stations at special locations to complement the existing operational network. The ATMOS (Automated Transportable Meteorological

Measurement System) weather stations were specifically installed for UNSTABLE. The ATMOS weather stations measured wind speed and direction, air temperature, relative humidity, surface pressure, solar radiation, precipitation, and dewpoint at one minute intervals. Five ATMOS weather stations were installed for the UNSTABLE project. These stations were strategically placed in two lines perpendicular to what is thought to be the climatological location of the dryline. They are labelled P1, P2, P3, P4, and P5 (Figure 3.2).

Some of the surface weather stations set up for the FOPEX project were still operational and used for UNSTABLE. The FOPEX stations recorded surface pressure, temperature, relative humidity, precipitation, and wind speed and direction at one minute intervals. The FOPEX weather stations are labelled AB1, AB3, and AB4 (Figure 3.2). Each of the four upper air sites also reported surface weather conditions. All of them recorded temperature, humidity and pressure, while some of them recorded wind speed and direction. The temporal resolution of the upper air surface weather stations ranged from one to fifteen minutes.

The University of Calgary operates a dense mesonet of weather stations in the south half of the study area. The spacing between the weather stations for the most part varies between 5 and 15 km. These stations record temperature and humidity every hour, while precipitation is monitored continuously. These data have not been quality controlled and is currently not available for analysis.

The average distance between the available surface weather stations is approximately 35 km. The spacing of the weather stations is reasonably uniform. There is one significant hole in the data south of Calgary, where the spacing is closer to 80 km. Research has shown that the width of the dryline in Alberta can be on the order of 1 km (Hill, 2006), which prevents the surface weather stations from adequately resolving the dryline. With a spacing of 35 km, it is only possible to get an approximate location of the dryline, hence the need for the mobile mesonet vehicles.

b) Mobile Mesonet Vehicles

There were three mobile mesonet vehicles which participated in the UNSTABLE project. The mobile mesonets consisted of a weather station mounted on a car. One of the mobile vehicles had a full weather station including temperature, humidity, pressure, wind speed and direction, and lightning detection. The other two vehicles just took temperature, humidity, and pressure measurements. The meteorological data were sampled and recorded every 15 s or better. All three vehicles were equipped with a GPS receiver to provide precise (within 10 m) information on the location of each vehicle at all times. The GPS locations were monitored in real time from mission control. At the time of this study, data from only one of the mobile mesonet vehicles have been quality controlled and are available for analysis.

Hill (2006) discussed the accuracy of mobile measurement systems. She found that measurements were accurate provided there was adequate ventilation. When the mobile mesonet system was stopped, there often were ventilation problems. Without proper ventilation, the temperature would read anomalously high due to heat radiating from the roof of the vehicle. As long as the vehicle was moving, the wind would provide adequate ventilation for the system. One of the mobile systems had a fan which provided continuous airflow when the vehicle was stopped. For more information on errors with mobile mesonet systems, see Hill (2006). Data preparation and quality control for one of the mobile mesonet systems was performed at the University of Alberta.

At the beginning of the UNSTABLE project, two of the mobile mesonet vehicles and one of the mobile sounding units completed an intercomparison of measurements. The intercomparison between vehicles indicated that temperature and pressure measurements differed by less than 0.5 °C and 0.5 mb. Relative humidities agreed within 1 % of each other. Absolute humidity measurements agreed within about 0.2 g kg^{-1} in water vapour mixing ratio.

c) Soundings

Upper air soundings consist of instrumentation attached to a helium filled balloon. Soundings measure the temperature, humidity, pressure, and winds as they ascend through the atmosphere. The only operational sounding that is close to the UNSTABLE project area is located in Stony Plain (53° 31.8'N, 114° 06.0'W). This is the only operational upper air station located in Alberta. The Stony Plain sounding is released twice per day at 0000 UTC and 1200 UTC.

Due to the lack of operational soundings, four additional upper air stations were included in the UNSTABLE instrumentation. These soundings were scheduled to be launched every 2 hours. Two of the upper air sites were at fixed locations. One was located at the Olds – Didsbury Airport (51° 42.0'N, 114° 06.0'W) while the other was located at the fire hall in the town of Water Valley (51° 30.0'N, 114° 36.5'W). The other two upper air sites were mobile and had different locations on different days. The locations of the mobile sounding units were decided on during the morning briefing and were fixed throughout the rest of the day.

Quality control of the sounding data was performed by Craig Smith of Environment Canada. When examining sounding data it is important to note that soundings are normally launched fifteen minutes before the hour of the sounding. The sounding balloons typically take about 45 minutes from the launch time until the reception is lost. For example, the 2000 UTC sounding would be launched at 1945 UTC and contact with the transmitter usually would occur until 2030 UTC. During this time, the balloon will drift with the prevailing winds by as much as 50 km from the launch location. Sounding teams launched more than 200 balloons during the UNSTABLE intensive observation period.

Dupilka (2006, p. 32-36) describes the accuracies of balloon soundings measurements. Temperature measurements are accurate to within 0.5 °C. Relative

humidity measurements are accurate to within 5 %. Wind speeds are accurate to within 3 knots, while wind directions are accurate to within 5 degrees. Pressure measurements are accurate to within about 1 %.

The temporal resolution of balloon soundings is limited by both the cost of the expendable materials and the amount of time required for taking measurements. This usually limits the frequency of sounding launches to every 2 hours. In order to alleviate this issue, measurements were performed by a tethersonde during the UNSTABLE project. The tethersonde consisted of a balloon tethered to the ground with six sondes (measuring equipment) placed at approximately equal intervals along the rope. Measurements at each location include temperature, humidity, pressure, and wind speed and direction at ten second intervals. The tethersonde had the ability to be extended 3 km, but NAV Canada restricted the maximum altitude of the balloon to 200 m above the ground to prevent conflict with low flying aircraft.

d) Remote Sensing

Weather radars provide measurements of the spatial and temporal distribution of the precipitation. Weather radars send pulses of microwave radiation focused into a narrow beam. When the radar beam encounters precipitation, the beam is scattered, and echoes are returned to the radar station. The radar beam is rotated through 360 degrees horizontally and as much as possible vertically. Radar stations allow maps of precipitation location and intensity to be constructed (Rogers and Yau, 1989).

All radar images were provided by Environment Canada. There were two Environment Canada radar stations which provided data in the UNSTABLE study area. The Carvel Radar (53° 33.6'N 114° 08.7'W) is located west of Edmonton, while the Strathmore Radar (51° 12.4'N 113° 24.0'W) is located east of Calgary. Environment Canada provides a detailed discussion on how to interpret radar images along with common misinterpretations on the following website: http://www.msc-smc.ec.gc.ca/cd/factsheets/weather_radar/index_e.cfm

The spatial and temporal distribution of clouds were sampled remotely from the GOES (Geostationary Operational Environmental Satellite) West satellite. Satellite images in the visible light wavelength band have spatial resolution of about 2 km at 55 °N latitude. Infrared satellite images over Alberta have a spatial resolution of about 4 km. Water vapour satellite images record a different wavelength of infrared radiation. Water vapour images show the amount of water vapour in the middle levels of the atmosphere. Water vapour images over Alberta have a spatial resolution of 8 km. All the satellite images previously discussed have a temporal resolution of 15 minutes.

Satellite images from the GOES west satellite suffer from a phenomenon known as parallax. This error is particularly noticeable for images of high latitudes taken from geosynchronous satellites. The viewing angle of the satellite causes the location of objects above the surface of the Earth to be positioned in the wrong spot. Objects at greater altitudes are subject to greater parallax errors. Within the UNSTABLE study area, objects with a height of 2 km (low level cumulus clouds) will be displaced 3.5 km NNE, while objects with a height of 10 km (thunderstorm tops) will be displaced closer to 20 km NNE. The 3.5 km error in the low level clouds is not significant. It is much less than other errors in the dryline location, and it is almost parallel with the dryline.

The University of Calgary and the University of Manitoba took measurements of the boundary layer using radiometers and Doppler Sodar. Many of these measurements were taken at the same location as the radiosonde balloon launches in order to make comparisons between the two. The data from this instrumentation are not yet available for analysis.

e) Aircraft

Weather Modification Incorporated (WMI) provided an aircraft for taking airborne measurements. The aircraft (a Piper Cheyenne II) had equipment which took measurements of temperature, humidity, and winds. The aircraft

accumulated just under 28 hours of flight time during the 8 intensive observation days of the UNSTABLE project. The aircraft data have not been quality controlled yet and are not available for analysis.

3.4 Observational Data used for 17 July 2008 Case Study

a) Surface Weather Station Network

All surface data that could be acquired were used for our surface analysis. There were some errors and inconsistencies which required certain data from the operational surface network to be excluded from the analysis. The problems were a combination of elevation and instrument inconsistencies. The reasons for the exclusion of any operational weather station are discussed in Appendix D. In the UNSTABLE instrumentation network, the sites P3 and AB3 (shown in Figure 3.2) were not used because these sites were not operational due to technical difficulties.

b) Mobile Mesonet Vehicles

Data for only one of the three mobile mesonet vehicles have been prepared and quality controlled. The data from the other two mobile mesonet platforms are not available for analysis. The vehicle which provided the data used in this thesis travelled along a transect on Highway 54 on the 17 July 2008. This transect was completed between the tethersonde site (52° 12.6'N 114° 50.1'W), and Corkscrew Mountain (52° 00.4'N 115° 22.7'W). The vehicle tracks as recorded by GPS are displayed in Figure 3.3. The system was operated from 1430 UTC 17 July until 0130 UTC 18 July.

c) Soundings

On the 17 July 2008, all four upper air sites were operational, and scheduled to launch sounding every two hours. A few problems occurred, some of which resulted in lost data. Soundings were launched at Water Valley every 2 hours from 1200 UTC until 0000 UTC with no problems. The sounding at 1400 UTC at Water Valley was dubious in that all the data had a warm bias. We did not

use this particular sounding for our analysis. Soundings were launched from the Olds – Didsbury airport from 1200 UTC until 0000 UTC, but there was a problem with the 2000 UTC sounding. Contact was lost with the receiver and none of the data were recorded. However, hand written data of pressure, temperature, and humidity are available every 50 mb between 700 mb and 250 mb. The hand written data were used in the sounding analysis.

The two mobile sounding teams were located in the foothills on the 17 July 2008. The sounding teams were coded MB1 (51° 39.0'N 115° 15.0'W) and MB2 (51° 57.6'N 115° 16.8'W). An early sounding was launched at MB1 at 1630 UTC. After that, soundings were launched at MB1 at 1800 UTC, 2000 UTC, 2200 UTC, and 0000 UTC. The sounding launched at 2200 UTC was lost at 615 mb, but otherwise there were no problems with the soundings. Soundings were launched from MB2 at 1800 UTC, 2000 UTC, 2200 UTC, and 0000 UTC without any problems.

d) Remote Sensing

Since the Strathmore radar is closer to the study area than the Carvel Radar, we used the Strathmore radar data. Specifically, we examined the 1.5 km CAPPI (Constant Altitude Planned Position Indicator) images, Doppler wind velocity images, and echo top images. The Strathmore radar is prone to ground clutter caused by the radar beam reflecting off the Rocky Mountains. For the radar images shown in this thesis, all ground clutter caused by the Rocky Mountains has been removed.

Visible satellite images are the only satellite images used in our analysis. Due to the long daylight hours in Alberta during the summer, the period of analysis for this case study is entirely during daylight hours. This allows visible satellite images to be used at any time throughout the analysis. Visible satellite imagery provides much higher resolution images than either infrared or water vapour imagery. Because the dryline is so narrow, it is important to have the highest resolution images possible. Parallax error corrections were not performed

because Ziegler and Rasmussen (1998) suggest that parallax errors are not significant. Although parallax errors in Alberta are greater than they would be in Texas, they still are not any more significant than other errors.

The data from the radiometers and SODAR are not currently available for analysis. These data are not fully necessary because much of it was collected at the same sites as the sounding launch sites and provides the same data as the upper air soundings.

e) Aircraft

The UNSTABLE team decided at the morning briefing that the aircraft would not fly on the 17 July 2008. Thus there are no aircraft data used in this case study.

3.5 Method of Analysis

a) Surface Maps

Surface maps were created using data from all of the available surface weather stations. Data were interpolated to a regular 1 km by 1 km grid using the kriging method of interpolation. Contour maps of mixing ratio, temperature, and derived variables such as virtual potential temperature were created, while vector wind maps were overlaid on the contour maps.

The interpolation and creation of contour and vector maps were done using the Surfer 8 surface mapping software. We also hand drew contour maps for comparison with the computer generated maps. This form of quality control was to ensure that the computer generated maps were consistent with the hand drawn maps. Because of the fairly regular spacing of the surface measurements, the software performed an adequate analysis of the data.

b) Single Sounding Analysis

The analysis of a single sounding was done using the RAOB sounding analysis software using the tephigram. Severe storm indices (CAPE, LI, CIN, etc.) were calculated by uniformly mixing the lowest 50 mb of the atmosphere, and all were calculated using virtual temperature, which takes into account the effect of humidity on air density. Since the severe storm indices are based on density, virtual temperature provides more realistic values of instability than temperature alone (Doswell and Rasmussen, 1994).

c) Vertical Cross Sections

In order to investigate the two dimensional boundary layer and upper air features of the dryline, we constructed height – distance cross sections with contour plots of different meteorological quantities. The vertical cross section was oriented perpendicular to the direction of the quasistationary dryline. The four vertical soundings were projected onto the cross section (see Figure 3.3). The cross section is about 80 km long and ranges in height from the surface to 500 mb. In addition to the soundings, transects from the mobile mesonet were also projected onto the cross section when they were available. Contour maps of humidity, virtual potential temperature, and equivalent potential temperature were constructed every two hours coinciding with the sounding observations.
These variables were contoured by hand onto the cross section and the subsequent contour lines were digitised. We tried to use the Surfer 8 mapping software to objectively analyse the data but the measurements were too sparse. Each of the four soundings and the mobile mesonet transect provided lines of extremely high resolution data separated by large areas without measurements. The software struggled to suitably interpret the empty space between the each of the soundings and the transect while preserving the small scale features present in the data.

d) Area Averaged Profiles of Kinematic Variables

Divergence and vorticity can be evaluated kinematically using a triangulation of wind velocities from three soundings. See Appendix A for a detailed discussion of the equations and mathematics behind the evaluation. Triangulation requires that three soundings be chosen. In order to be consistent, the same three soundings must be compared at all times. This requirement causes some problems when soundings are missing. For this case study, EA3, WVX, and MB2 (see Figure 3.3) were chosen for the triangulation analysis. These sites were chosen because they had a more complete dataset, they were positioned more uniformly, and their positions focused on one of the locations for the initiation of a severe thunderstorm.

Determining convergence and vorticity through triangulation is sensitive to small changes in the u and v components of the wind velocities. The accuracy of wind velocity is at best 3 knots, and the accuracy of the wind direction is at best 5 degrees (see section 3.3 c). The end result was a very noisy profile of the variables. Considerable smoothing was performed to filter out the noise. Vertical smoothing was executed via a 21 point moving average.

The kinematic vertical velocity can be evaluated using the convergence. The equations for the vertical velocity calculations are also discussed in Appendix A. The vertical velocity calculation requires one boundary condition. There are two ways of satisfying this boundary condition. One can either set the vertical velocity to be zero at the surface or at the tropopause. Setting the vertical velocity to be zero at the surface can be problematic because the vertical velocity can change substantially very close to the surface. For this reason, the vertical velocity was chosen to be zero at the tropopause. Most often, the soundings were cut off at 250 mb, while the tropopause was at 230 mb. In the cases where all three soundings did not reach the tropopause, the vertical velocity was set to zero at the highest altitude possible.

e) Locating the Dryline on Surface Maps

Ideas differ on the methods used for locating the dryline on a surface map (see section 2.2). The use of differing methods arises from the lack of enough surface stations to fully resolve the dryline. It seems that the method chosen for the location of the dryline is dependent on each particular case. For this case study, the lack of resolution of the surface observations does not allow positioning the dryline on the sharpest gradient (like Atkins et al., 1998), and there is a lack of sufficient moisture to use Schaefer's (1986) suggestion of the 9 g kg^{-1} isohume (12 °C isodrosotherm). In this case, moisture varies from 4.5 – 5.5 g kg^{-1} on the dry side to 8.5 – 9.5 g kg^{-1} on the moist side. Using a value half way between the dry and moist air seems to provide the best estimate for the dryline location, therefore the dryline will be positioned on the 7 g kg^{-1} isohume for this case study. If another isohume had been chosen (such as 6 g kg^{-1} or 8 g kg^{-1}), the location of the dryline would not have changed more than about 20 km, and these changes would not significantly affect the results.

Chapter 4

17 July 2008 Dryline and Convective Storms

In this chapter, we will analyse the meteorological data observed in Alberta for the UNSTABLE case study event of 17 July 2008. The main objective of our analysis is to address the question: how are the clouds and precipitation organised relative to the dryline? Our approach will be to first describe the synoptic scale airflow. Thereafter we will focus on the evolution of the mesoscale weather, and finally we will deal with the convective scale phenomena. The chapter ends with a discussion synthesising the findings into a coherent picture.

4.1 Synoptic airflow

Figures 4.1 through 4.3 depict synoptic weather maps over western Canada. The maps show height contours of constant pressure levels (500 mb, 700 mb, and 850 mb). We have also added isotherms (contoured every 0.5 °C). Times are given in UTC time, which is 6 hours ahead of Mountain Daylight Time (MDT).

The upper level flow was characterised by a closed low (Figure 4.1) with an associated trough extending from it over British Columbia. The trough was evident at 500 mb (Figure 4.1), 700 mb (Figure 4.2), and 850 mb (Figure 4.3). The trough was coupled with a weak ridge in central Alberta at 1200 UTC. By 0600 UTC, the axis of this ridge moved over the Alberta – Saskatchewan border. A thermal ridge accompanied the pressure ridge at the 500 and 700 mb levels. Cold air advection was occurring at 500 mb and 700 mb over the study area by 0000 UTC as the thermal ridge drifted into Saskatchewan along with the pressure ridge. At the 850 mb level, the thermal ridge remained close to the foothills as a pressure trough developed along the foothills, consistent with a lee trough developing.

The 700 mb flow (Figure 4.4) was almost perpendicular to the Rocky Mountain Barrier at 5 m s^{-1} to 7 m s^{-1} with the strongest wind speed occurring over Rocky Mountain House. This supported the development of a weak lee trough or low pressure centre. As the day progressed, cold air advection into the upper levels in western Alberta helped to increase the convective instability and supported the development of deep convection.

A surface analysis of the sea level pressure (contoured every 1 mb) is shown in Figure 4.5. At 1500 UTC, higher pressure dominated southern Alberta, with relatively lower pressure in the north. The pressure gradient was weak. There was only a 4 mb pressure difference along the entire province (greater than 1000 km). As the day progressed, the pressure fell in southern Alberta. The high pressure centre drifted in to Saskatchewan, while low pressure pushed in from British Columbia with the pressure gradient supporting a south easterly flow by the mid afternoon. The pressure gradient strengthened throughout the day. By 2100 UTC, there was 7 mb difference across southern Alberta (about 500 km). This surface pattern is significantly different from the Strong (1986), and the Smith and Yau (1993) models, but it accomplished the same thing. An easterly component of the surface wind was present creating upslope flow and surface convergence along the foothills.

4.2 Timeline of Events for 17 July 2008

In this section, we will discuss the major events of the day in chronological order. This will include the formation of the dryline, the structure and evolution of the dryline, the organisation of clouds and precipitation relative to the dryline, and the dissipation of the dryline. We refer to numerous figures compiled using special observations from the UNSTABLE project. Again, all times are given in UTC time, which is six hours ahead of local time (MDT).

a) Dryline development (late morning)

Figures 4.6, 4.7, 4.8, and 4.9 are surface analyses of water vapour mixing ratio (contoured every 0.5 g kg^{-1}) and wind velocity within the study area. Each figure shows data at different times. At 1200 UTC, a weak moisture gradient was present, with drier air in the foothills and more humid air over the plains (Figure 4.6, left). Between 1200 UTC and 1400 UTC, the surface humidity increased throughout the study area, but the weak moisture gradient remained (Figure 4.6, right).

A height – distance cross section of water vapour mixing ratio was created using soundings and mobile transects. This can be seen in Figure 4.10 at 1600 UTC, 1800 UTC, 2000 UTC, and 2200 UTC. At 1600 UTC, significant vertical mixing was not occurring near the surface. Vertical mixing forms areas of uniform mixing ratio, or slightly decreasing mixing ratio between the surface and the top of the mixed layer. At 1600 UTC, there was still strong moisture stratification and intense vertical moisture gradients throughout the boundary layer in the cross section. Satellite images (Figure 4.11, upper left) indicate that the sky was clear over the UNSTABLE study area at 1400 UTC.

Between 1600 UTC and 1630 UTC a sharp horizontal gradient in water vapour mixing ratio formed near the surface. This sharp moisture gradient will hereafter be referred to as the dryline. Figure 4.7 is a surface map showing the mixing ratio and winds in the study area at 1600 UTC and 1630 UTC. Between 1600 UTC and 1630 UTC, high resolution surface measurements depict the rapid drying that occurred in the northern half of the region on the dry side of the dryline. The moisture gradient intensified at approximately the same time everywhere within a time span of about 30 minutes. The moisture gradient between the dry and the moist air was about 4 g kg^{-1} over a horizontal distance of about 50 km throughout the UNSTABLE domains. The dryline was oriented roughly parallel to the Rocky Mountain continental divide.

We note that the sharp moisture gradient developed very rapidly, suggesting that it formed as the capping inversion was eroded through vertical mixing in the western half of the study area. This process of rapid dryline genesis is discussed by Schaefer (1974b) for the classical dryline formation over Texas. The similarities in the development and motion of this dryline with the results of Schaefer (1974b) are not unexpected. The motion of the dryline analysed by Schaefer (1974b) is driven by the gently eastward sloping topography. Figure 4.12 shows that this topographical feature is also evident in Alberta.

Each panel in Figure 4.13 is a comparison between the best "textbook" sounding in the dry air and the best "textbook" sounding in the moist air (the red lines are the temperature and dewpoint in the moist air while the blue lines are the temperature and dewpoint in the dry air). At 1800 UTC, the air on the dry side was predominantly well mixed in both temperature and humidity, while air on the moist side was capped at about 800 mb (see Figures 4.10 and 4.13 at 1800 UTC). Below the cap, the air was moist, while above the cap, the air had properties similar to the air on the dry side of the dryline. The cap prevented the moist air from mixing with the dry air above it, which allowed the moisture to build underneath the cap.

b) Maximum Dryline Structure (Noon)

A line of convective clouds began to form at 1630 UTC. At 1700 UTC the line of clouds was well-developed. The location of this line of convection coincided with the location of the surface dryline based on the surface analysis (Figure 4.14). Fair weather cumulus convection developed west of the dryline. At this time the moist air on the east side of the dryline remained cloud free as the capping lid suppressed ascending motion (Figure 4.11, upper right, and Figure 4.15). While the convective clouds developed in the dry air, there was still an enhanced area of convergence which formed an enhanced line of clouds along the cloud – no cloud boundary (Figure 4.11 – upper right).

At 1700 UTC the vehicle with meteorological sensors sampled the dryline. As the vehicle proceeded from the moist air (east) into the dry air (west), the instrumentation recorded the mixing ratio dropping from 8.2 g kg^{-1} to 5.5 g kg^{-1} over about 5 km (Figure 4.16). The high resolution measurements recorded by the mobile mesonet help to establish the width of the dryline.

An analysis of the convective instability parameters is shown in Figures 4.17 and 4.18. The source data for these analyses are a combination of the surface observations, vehicle measurements and the soundings. Figure 4.17 is a distance cross section showing the convective available potential energy (CAPE), and the convective inhibition (CIN). The CAPE built up on the moist side of the dryline to greater than 1000 J kg^{-1} throughout the day, indicating support for relatively strong thunderstorms. The measurements at 1800 UTC read anomalously high CAPE and anomalously low convective inhibition (CIN) in the moist air due to sparse data from the EA3 sounding. The most insightful image is at 2000 UTC, because it is later in the day and has a complete set of soundings. The dryline is characterised by very little CAPE and CIN on the dry side, moderate CAPE (300 J kg^{-1}) and significant CIN (25 J kg^{-1}) around the dryline, and high CAPE and low but non-zero CIN on the moist side (12 J kg^{-1}). This can be seen on the map in Figure 4.18 as well. Figure 4.18 shows no CAPE and varying CIN (due to the calculation method) on the dry side and a quick transition (50 km) to high CAPE (over 1000 J kg^{-1}) and low CIN (around 10 J kg^{-1}) on the moist side. There appears to be an axis of the highest CAPE another 50 km east of the dryline, caused by the axis of moisture visible on the surface maps in Figure 4.8. The axis of moisture can likely be attributed to moisture convergence along the dryline.

The surface analysis at 1800 UTC (Figure 4.8, left) produced the highest resolution image of the dryline because it includes special ASRD measurements at fire towers. ASRD fire tower measurements are taken at 1200 UTC and 1800 UTC daily. The surface position of the dryline appeared better defined at this time due to these measurements. It is likely that the dryline was as well defined during the other times of the day when the fire tower measurements were not

available. The confluence of the surface winds in the moist and dry air was also best defined at 1800 UTC (Figure 4.8, left) due to these extra measurements. The south easterly winds in the moist air and the south westerly winds in the dry air converged along the dryline. Wind speeds in the moist air averaged around 20 km h^{-1} while winds in the dry air were closer to 10 km h^{-1}. It is also apparent from Figure 4.8 that there was a horizontal mesoscale structure to the dryline with specific undulations noticeable at North Ghost, Elbow, and Willow Creek. These horizontal bulges or waves are similar to observations by McCarthy and Koch (1982), and Atkins et al. (1998).

Figure 4.19 shows four selected analysed dryline locations on a single map. Aside from some small mesoscale perturbations, the dryline was quasistationary on a synoptic scale throughout the day. The 700 mb winds (Figure 4.4) did not show a jet. If there was a jet of enhanced winds at the 700 mb level, subsidence and mixing could bring this extra momentum down to the surface causing the dryline to bulge eastwards throughout the day (Schaefer, 1986). Surface winds remained relatively light in the dry air (about half the speed of the surface winds in the moist air). Although the dryline was quasistationary on a synoptic scale, there were several smaller scale movements that occur along the dryline. The surface weather station network had sufficient resolution to detect hints of some of these movements, yet the observational network was not fine enough to fully resolve the mesoscale bulges and movements. The first of these happened between 1800 UTC and 1900 UTC when the dryline retrograded westward through North Ghost (B6). Between these times, the mixing ratio rose from 5 g kg^{-1} to 8 g kg^{-1} at North Ghost (Figure 4.8). There were no reliable wind measurements at North Ghost. The first radar echoes appeared at 1900 UTC (Figure 4.20), and were mostly weak echoes of the fair weather cumulus variety. The radar echoes appeared earlier, and were more dense and widespread in the north half of the study area.

At 1915 UTC, the vehicle crossed the dryline a second time. It appears from the second crossing (Figure 4.16) that two distinct steps developed in the

moisture gradient: the first from 4.7 g kg^{-1} to 7.4 g kg^{-1}, and the second from 7.4 g kg^{-1} to 8.3 g kg^{-1}. These two steps were separated by an intermediate mixing zone (mixture of the dry and moist air) about 15 km wide. It is interesting to note that Ziegler and Hane (1993) also reported a characteristic two steps variation in moisture in their dryline observations separated by a mixing zone.

The sounding cross section at 2000 UTC (Figure 4.10, lower left) revealed that the sounding at WVX was within the mixing zone. The depth of the mixed layer increased substantially with the formation of the mixing zone as seen in Figure 4.10 at 2000 UTC. A large plume of moisture was visible extending as high as 700 mb. Significant drying at the surface also occurred over WVX. The coarse temporal resolution of the sounding data of 2 hours do not allow to ascertain the exact time that the mixing zone developed. However, some insight was obtained using the time series of meteorological data sampled with the tethersonde. The tethersonde was positioned within the mixing zone for part of the day. The development of the mixing zone was evident (Figure 4.21) when the air became distinctly drier around 1830 UTC. The first evaluations of convergence and vertical motion were completed for data at 2000 UTC. Suitable soundings were not available earlier in order to compute these parameters earlier in the day. Convergence and vertical motion were evaluated based on the triangulation of three soundings (Appendix A). Overall divergence was visible, but the magnitude of the divergence and convergence was much lower at 2000 UTC than at the later times. Some subsidence was occurring between the surface and 500 mb with a maximum rate of 0.06 m s^{-1}.

c) Convective Initiation and Dryline Dissipation (Early Afternoon)

The behaviour of the dryline became more unusual at 2000 UTC in the northern part of the study area. Between 1900 UTC and 2000 UTC, the moisture gradient weakened and retrograded westwards in the northern part of the region. The reasons for this are not apparent. The moisture gradient weakened to the point that this cannot be called a dryline in the northern half of the region at 2000

UTC. Deep convection began to be seen on visible satellite imagery (Figure 4.11) at 2015 UTC. This convection developed on the moist side of where the dryline used to be half an hour earlier. Strong radar echoes of 40 dBZ appeared (Figure 4.20) at around 2040 UTC. Thunderstorms developed at different preferred locations along the dryline at approximately the same time (within an hour of each other), with the strongest radar echoes reaching up to 60 dBZ.

UNSTABLE participants (including the author) measured a maximum hail diameter of 21 mm from one of these storms (Figure 4.22). The hail was variable in size and was opaque. Figure 4.23 shows a map of all severe weather events reported to the Environment Canada storm line. Strong cyclonic rotation was observed in another thunderstorm later in the day. A rotation period of about 10 minutes was determined through time lapse photography. The source of this cyclonic rotation may have been the low level vorticity which built up later in the day (Figure 4.24). Based on radar images (Figure 4.20), the convection in the north seemed to be more severe and longer lasting than the convection in the south at this time. It is also apparent from Figure 4.25 that the initiation of all of the strong convection occurred within about 20 km from the dryline. It also occurred mostly on the moist side of the dryline. Some of the convection formed on what used to be the dry side of the dryline, but this convection appears to have been forced by the already existing convection to the north.

While the dryline dissipated with the initiation of convection in the north, the dryline persisted in the south half of the study area. There were no special UNSTABLE measurements in the southern half of the domain which detected the dryline, so the surface analyses consisted of operational datasets from Environment Canada, ASRD, and Telvent. These analyses are shown in Figure 4.9. Throughout most of the day, the dryline in the south half of the domain stayed quasistationary within the resolution of the surface measurements. There were no mobile mesonet vehicles that took measurements in the area. Convection in the area remained limited to small pulsing short lived thunderstorms which did not leave the vicinity of the dryline. At 2300 UTC, the dryline retrograded

westwards through Bow Valley. The mixing ratio in Bow Valley rose from 3.7 g kg^{-1} to 7.3 g kg^{-1} while the wind shifted from 270° to 130°. Throughout the day a stronger easterly component of the wind was present in the moist air near Bow Valley. We think that the stronger easterly component near Bow Valley was due to the channelling effect of the Bow River Valley. This pushed the dryline back towards the west.

The most interesting event in the southern part of the study area occurred at 0000 UTC where a mesoscale bulge formed in the dryline near Willow Creek. Before this bulge formed, the dryline was positioned between Highwood and Willow Creek (Figure 4.9). This was the case throughout the day. At 0000 UTC, the dryline advanced eastwards through Willow Creek. The mixing ratio at Willow Creek dropped from 8.7 g kg^{-1} to 5.4 g kg^{-1} between 2300 UTC and 0000 UTC while the wind direction varied between 270° to 180°. It is apparent that the dryline proceeded eastwards, but it is not known how far due to the lack of available observational data. The strongest storm of the day was initiated along the north west boundary of the mesoscale bulge at 0030Z. This storm produced 2 cm diameter hail and radar echoes in excess of 60 dBZ. After this time the dryline boundary becomes more diffuse and dissipates.

4.3 Dryline Criteria

In this section, we will determine whether the dryline observed on 17 July 2008 meets the "textbook" dryline criteria. The dryline on 17 July 2008 had a maximum moisture gradient of about 1 g kg^{-1} km^{-1}, as measured by mobile transects (Figure 4.16). This is similar to most moisture gradients measured in "textbook" cases in Texas and Oklahoma (e.g. Fujita, 1958, McGuire, 1962).

Schaefer (1974b) suggests that the narrow moisture boundary must last for 6 consecutive hours in order to qualify as a dryline. On 17 July 2008, the narrow moisture boundary lasted for different lengths of time in different parts of the domain. The narrow moisture gradient was present for as much as 9 consecutive hours. Because it lasted longer than the required amount of time, it is reasonable

to identify this as a dryline. It is unlikely that this dryline could be mistaken for the rear flank downdraft of a supercell thunderstorm as cautioned by Schaefer (1986). Surface analysis shows that the dryline was synoptic in scale, and was present long before and after convection was initiated (Figures 4.7 and 4.8).

Throughout the study area, stations in the dry air had south westerly winds, while stations in the moist air had south easterly winds. There were two times throughout the day where the dryline crossed a weather station with wind measurements. In one case, the dryline crossed the Bow Valley weather station. The mixing ratio in Bow Valley rose from 3.7 g kg^{-1} to 7.3 g kg^{-1} while the wind backed from 270° to 130°. According to Schaefer (1986), backing winds are associated with a retrograding dryline (a dryline moving from the east toward the west), while veering winds are associated with an advancing dryline (moving from west to east).

Another dryline crossing occurred at the Willow Creek weather station between 2300 UTC and 0000 UTC, and again between 0000 UTC, and 0100 UTC. The mixing ratio dropped from 8.7 g kg^{-1} to 5.4 g kg^{-1} at 0000 UTC and then rose back up to 7.8 g kg^{-1} at 0100 UTC. The winds were erratic near the time that this happened, shifting from a south easterly component to a westerly component and back. The wind directions did not correlate well with the dryline. It appears that the dryline boundary must have been very close to Willow Creek, and that the convergence line was not precisely correlated with the dryline boundary. In fact the convergence line appeared to be located just to the east of the boundary. Matteson (1969) found that the line of convergence indeed does not always coincide with the moisture gradient.

All of the evidence presented indicates that the moisture boundary observed on 17 July 2008 should be classified as a dryline. It lasted the required amount of time, the moisture gradients were sufficiently large, and the wind directions and convergence are in agreement with the “textbook” cases.

4.4 Mesoscale structure, motion, and topographic influences

McCarthy and Koch (1982) attribute some of the mesoscale variability of the dryline to the presence of mesoscale dryline waves. Mesoscale dryline waves ripple along the dryline and appear to be a factor in the motion of the dryline. McCarthy and Koch (1982) do not speculate about the origin of the waves, they focus more on discussing the characteristics of the waves. In more recent years the focus on the mesoscale variability of the dryline has been on the effect of horizontal convective rolls. Atkins et al. (1998) suggest that horizontal convective rolls may have an effect on the mesoscale structure of the dryline. Atkins et al. (1998) also found that horizontal convective rolls may cause convergence causing the dryline to initiate deep convection.

The 2008 UNSTABLE field project did not include sufficient data to analyse these factors. Atkins et al. (1998) used airborne Doppler radar and other aircraft measurements to investigate the effects of horizontal convective rolls. McCarthy and Koch (1982) completed surface analysis using a high spatial and temporal resolution mesonet of surface weather stations in Oklahoma. The analysis for this case study does not include Doppler radar at all, and does not include aircraft measurements. The surface analysis also is not sufficient to adequately analyse mesoscale dryline waves. There are hints of waves in the location of the dryline on surface maps, but there is not enough temporal or spatial resolution to further analyse these features. One difficulty in using surface analyses during the UNSTABLE project was the proximity of the dryline to the Rocky Mountains. This limited the number of measurements in the dry air.

Small mesoscale variations in the location and motion of the dryline may also be caused by variations in local topography. There is considerable variability in the local topography in the foothills of Alberta. Numerous rivers carve valleys through the mountains and foothills, while there is considerable variation in the structure of the foothills themselves. The effect of local topography on the location of the dryline has been presented as a side note by a number of

researchers (e.g. Atkins et al. (1998) and Parsons et al. (1991)). Hill (2006), and Strong (1986) note that the dryline (or the structure of the capping inversion) in Alberta is susceptible to certain topographical restraints, and the location and evolution of the dryline can be influenced significantly by topographical features. The terrain and indications of where the topography could allow air movement within the UNSTABLE study area are shown in Figure 4.26.

Topography seems to be important for the 17 July 2008 case. The mesoscale bulges seem to be associated with breaks between the foothill peaks and with river valleys. In Alberta, the dry air often pushes further east south of Red Deer, and through the Calgary area (Hill, 2006). This did not happen on 17 July 2008. Instead, the moist air seemed to be advected further into the valley by the enhanced winds in the moist air, creating a moisture bulge to the west. The channelling of the winds in the Bow River valley could be the cause of these enhanced winds, similar to observations by Atkins et al. (1998). Another bulge that appears to have been affected by local topography was the eastward bulge in the dryline that occurred in the vicinity of the Willow Creek weather station. It is possible that the Highwood River Valley funnelled the dry air enhancing the winds and allowing the dry air to push into the moist air causing the bulge.

It is not known why the dry air bulged in this case and the moist air bulged in the previous case. The wind field was generally uniform in both the dry and moist air. The effect of local topography will require further study.

4.5 Discussion

The synoptic scale airflow supported a convective outbreak. In general the results were consistent with the conceptual model of severe thunderstorm initiation suggested by Strong (1986) and Smith and Yau (1993). One important difference between the 17 July storm and the conceptual model was the location of the surface pressure lows.

The dryline developed late in the morning, and was quasistationary throughout the day. This is supported by the lack of strong 700 mb winds. There is no extra momentum forcing the dryline to bulge. Surface analyses indicate that small mesoscale fluctuations in the location of the dryline occurred throughout the day. They appear to be associated with local topography. In particular, it seems that the oscillations across the Bow Valley weather stations are a result of wind channelling in the Bow River Valley. It also appears that the Highwood River Valley allowed the dry air to push out of the river valley creating a dry bulge that formed through the Willow Creek weather station.

On 17 July 2008, the cloud features and the initiation of severe thunderstorms were intimately connected to the location and evolution of the dryline. The first convective clouds to develop were a line of cumulus clouds located above the surface dryline. The convection was sustained by the convergence of surface wind along the dryline. Shortly afterwards, cumulus clouds developed on the western (dry) side of the boundary, while the sky remained cloud free on the eastern (moist) side of the dryline. The cloud – no cloud boundary (evident on the visible satellite imagery) remains within less than 20 km of the surface dryline.

The development of deep convection began to be visible on satellite imagery at 2015 UTC, while strong radar echoes were recorded at 2040 UTC. Hail was observed at 2110 UTC by UNSTABLE participants. The deep convection visible on satellite and radar developed along the dryline boundary (within about 20 km). Radar indicates that most of the severe convection developed on the moist side of the boundary.

Chapter 5

Comparison with the Textbook Dryline

In this chapter, we will compare the dryline and severe thunderstorm outbreak that occurred on the 17 July 2008 with the "textbook" dryline developed from research in Texas and Oklahoma, and with some of the severe thunderstorm research carried out in Alberta and Saskatchewan. The dryline has been studied extensively in Texas and Oklahoma and a conceptual model of the dryline was developed by Ziegler and Hane (1993). Dryline research in Alberta and Saskatchewan has been limited to a few case studies.

5.1 A comparison with the Ziegler-Hane conceptual model

The dryline is generally considered the boundary between moist air and dry air (Schaefer, 1986). The interactions between the moist and dry air cause the initiation of convection (Rhea, 1966). Research by Ziegler and Hane (1993) and Hane et al. (1993) has revealed some of the dynamics which may be involved in the process. Ziegler and Hane (1993) developed a conceptual model of the dryline development from their results (see section 2.3). This conceptual model will be discussed in this section along with a comparison with the results obtained on the 17 July 2008. The main addition to the model by Ziegler and Hane (1993) is the mixing zone. The mixing zone is an intermediate mixture of dry and moist air along the dryline (Ziegler and Hane, 1993).

It appears that the dryline event on the 17 July 2008 started out at 1630 UTC as a single dryline (Figure 4.16, toward the left) with a relatively narrow 5 km wide mixing zone. Later in the day, a uniformly moist mixing zone about 15 km wide was observed producing two separate narrow moisture gradients on either side (Figure 4.16, toward the right). The air in the mixing zone appeared to be intermediate between the moist and dry air. This is similar to measurements performed by a mobile mesonet vehicle by Ziegler and Hane (1993). They found that there were two intense moisture gradients separated by a mixing zone about

15 km wide which consisted of air that was intermediate between the dry air and the moist air. Hane et al. (1993) also detected a mixing zone in a different dryline case. In their case, the "double dryline" was observed by both mobile transects and as two radar finelines, lending further credibility to the phenomenon. The discontinuous dryline motion noted by Hane et al. (1993) could be the cause of such a mixing area, and may arise from the vertical mixing model proposed by Schaefer (1974b). A schematic of the double dryline observed on the 17 July 2008 is shown in Figure 5.1.

Various studies of the dryline utilising aircraft traverses (Fujita, 1958; McGuire, 1962; Parsons et al., 1991) have shown that there is a plume of moisture above the dryline. Hane et al. (1993), and Ziegler and Hane (1993) propose that vertical motion caused by convergence along the dryline transports moisture up into a vertical bulge above the dryline. On the 17 July 2008, the WVX sounding at 2000 UTC shows a plume of moisture extending up to 700 mb (Figure 4.10, lower left). This plume of moisture was not evident in the earlier soundings. The plume of moisture may have resulted from the convergence as it built up later in the afternoon along the dryline. The presence of the plume of moisture is similar to the model proposed by Ziegler and Hane (1993).

An interesting phenomenon noted by Hane et al. (1993), and by Ziegler and Hane (1993) is that the vertical plume of moisture advects eastward above the cap and the moist air. Ordinarily, soundings in the moist air will have an abrupt decrease in moisture above the capping inversion (Schaefer, 1986). The eastward advection of the moisture causes a small increase in moisture just above the cap in the dry air (Ziegler and Hane, 1993). A plume of moisture is evident on the sounding cross section (Figure 4.10, lower right) constructed for 2200 UTC on the 17 July 2008. The vertical moisture plume formed at 2000 UTC above the WVX sounding site, while the horizontally advected moisture plume occurred at 2200 UTC above the EA3 sounding site. The distance between the two soundings was about 40 km, and the 700 mb winds were about 20 km h^{-1} directed from WVX to

EA3, This suggests that the moisture plume was advected eastwards similar to the conceptual model proposed by Ziegler and Hane (1993).

The location and movement of moisture on the 17 July 2008 agree well with the conceptual model proposed by Ziegler and Hane (1993). The mixing zone, vertical moisture plume, and horizontal moisture plume described in the Ziegler and Hane (1993) model are all discernable on the 17 July 2008.

5.2 Convergence and vertical velocity

The convergence, vorticity, and vertical velocity were evaluated based on a triangulation of three soundings. The methods for doing this are given in Chapter 3 of this thesis, and the equations used in the evaluation of these parameters are given in Appendix A. One must remember that evaluating these parameters using triangulation calculates the area-averaged convergence, vorticity, and vertical velocity for the entire triangle.

The divergence, vorticity and vertical velocity are calculated in this case for three soundings at 2000 UTC, 2200 UTC, and 0000 UTC (Figure 4.24). There were soundings taken earlier, but some soundings were lost and to maintain consistency it is necessary to limit the calculation of the fields to these times. Convergence values (negative divergence) range from (-20 m s^{-1}) / (100 km) to (15 m s^{-1}) / (100 km) (Figure 4.24). This is comparable to previous studies by Ogura and Chen (1977), McGuire (1962), and Strong (1986).

Vertical velocity can be calculated from the convergence values. Ogura and Chen (1977) computed relatively low upward vertical velocity values prior to convective initiation (15 cm s^{-1}), while much larger upward values after convective initiation in the afternoon (more than 60 cm s^{-1}). The values calculated on the 17 July 2008 were mostly similar to values discussed in Ogura and Chen (1977). Vertical velocity values earlier in the day were negative, indicating subsidence was present. A maximum downward vertical velocity of 6 cm s^{-1} was

evaluated at 2000 UTC. Immediately after the initiation of convection, vertical velocity values were positive and reached as high as 50 cm s^{-1}.

Strong (1986) presented an ambiguity in the calculation of vertical velocity using the sounding triangulation method. Strong (1986) determined that although the sounding triangulation correctly analyses the average vertical velocity, strong thunderstorms in the vicinity of the soundings can greatly modify the convergence and vertical velocity profile. Rather than sampling the large scale pre-storm vertical velocity to determine the initiation of convection, the triangulation includes the vertical motion of the thunderstorm itself. In order to illustrate how this problem occurred on the 17 July 2008, the tracks of the soundings for 2200 UTC are overlaid on the CAPPI radar map in Figure 5.2. The tracks of the soundings diverge significantly aloft. The cause of this divergence is most likely the strong thunderstorm located near the MB2 sounding. The results of the divergence calculations are therefore subject to the restrictions imposed in the discussion in Strong (1986): the influence of convective storms must be taken into account when analysing vertical velocities.

A discrepancy in the magnitude of the vertical velocity arises when comparing the vertical velocities computed with soundings (both on the 17 July 2008 and values derived from other research) with higher resolution measurements by Doppler LIDAR and aircraft. While pre storm vertical velocities evaluated from soundings are often around 0.1 m s^{-1} directed upward (Ogura and Chen, 1977), Doppler LIDAR and aircraft traverses show that vertical velocities within the dryline can range from 1 m s^{-1} to 5 m s^{-1} (Parsons et al., 1991, Atkins et al., 1998). It is likely that the cause of this is due to the inability to resolve sharp gradients, as discussed by Parsons et al. (1991).

5.3 Convective initiation

All of the initial convection on the 17 July 2008 occurred on the moist side of the dryline within 20 km of the boundary, as seen in Figure 4.25. Some of the later convection did not coincide with the dryline, but it can be traced to the

effects of the initial convection (such as outflow boundaries). Radar echoes as strong as 60 dBZ were observed from the severe thunderstorms. UNSTABLE participants measured hail with a 21 mm diameter and observed cyclonic rotation in the clouds. Callers to the Environment Canada storm line provided several reports of hail with a diameter greater than 20 mm, and one report of a weak tornado. Many of the severe weather events occurred well after the dryline had dissipated, but the storms which generated the events were either initiated along the dryline or related to a storm that was initiated along the dryline.

The analysis of the relation of the initiation of convection to the location of the dryline on the 17 July 2008 is in agreement with the textbook dryline. Rhea (1966) found through the analysis of many cases that the dryline most often initiated convection within 50 km of the dryline on the moist side. Many severe thunderstorms tend to be associated with dryline events, and a large proportion of destructive tornadic thunderstorms are initiated along a well defined dryline (Fawbush et al., 1951; Rhea, 1966; Bluestein and Parker, 1993; etc.). Dupilka and Reuter (2005), Hill (2006) and Knott and Taylor (2000) have associated drylines with tornadic thunderstorms in Alberta.

More recent studies suggest that the mesoscale variability of the dryline may be associated with the location of the initiation of convection. Severe thunderstorms tend to be initiated in preferred locations and these locations seem to be related to the mesoscale variability of the dryline (Atkins et al, 1998). The structure of the radar echoes and the pattern of the development of severe storms on the 17 July 2008 are similar. Severe storms seemed to develop in preferred locations and the preferred locations seemed to be associated with mesoscale bulges in the dryline. The possible causes of these bulges are discussed in section 5.2. Adequate data are not available to allow us to confirm that this is the case.

5.4 Which drylines initiate convection?

The problem of whether a specific dryline will initiate convection or not has been an ongoing issue that has yet to be fully resolved (Ziegler and Hane,

1993). Based on our findings, we propose the following mechanism for the initiation of convection. Since the strongest convergence, and subsequently the strongest updrafts are often (but not always – see Matteson (1969)) coincident with the strongest moisture gradient (e.g. Ziegler and Hane, 1993), convection would be expected to be initiated along the moisture boundary. Because convection should be initiated along the moisture boundary, it occurs within the mixing zone proposed by Ziegler and Hane (1993). The stability of the air in the mixing zone should then be the important factor in determining whether convection will occur, although the strong vertical motions measured within the mixing zone (e.g. Parsons et al., 1991; and Ziegler and Hane, 1993) will help convection start with less instability. If the air in the mixing zone (a first guess could be a 50-50 mixture of the dry and moist air if measurements are not available) is close to convectively unstable (i.e. there is positive CAPE), then convection would be expected to start at the mixing zone. Ziegler et al. (1998) states that in order for deep convection to form, the air within the dryline mixing zone must reach its condensation level and the level of free convection (where it is virtually warmer than the surrounding air), before leaving the dryline induced updraft.

Once sustainable convection is initiated within the mixing zone, the prevailing south westerly winds in the upper atmosphere often associated with the dryline will advect it eastward into the moist air, which provides much more convective instability. It is here that the convection develops into severe storms visible on radar. This could be the cause of the observations of convection developing to the east of the dryline (Rhea, 1966), since convection supporting precipitation may not develop until it is into the more unstable airmass. The cloud dynamics and convective activity should be in place before the storm is visible on radar, since radar measures precipitation, not the development of the cloud. Comparisons of satellite and radar imagery for the 17 July 2008 indicate a 30 minute delay between the development of the cloud, and the development of strong radar echoes.

On the 17 July 2008, the sounding at WVX was within the mixing zone for part of the day, and although the CAPE was much lower (Figure 4.17), and the predicted cloud tops from the soundings were much lower, thunderstorms would still be expected from the instability on the sounding. There was more convective inhibition, but we suspect that it would be easily overcome by the convergence and upward motion along the dryline. Thus it appears that the thunderstorms developed and strengthened as they advected eastwards into the moister air, which has much greater instability (Figure 4.17 and Figure 4.18). The location of the initiation of deep convection can be seen in Figure 4.25. Figure 4.25 plots initiation of convection relative to the location of the dryline. The initiation of deep convection was defined as when the radar echoes surpassed 45 dBZ. Note that often the radar echoes were visible before they intensified in the moist air, and often began right on the dryline. Some even were visible in the dry air before they entered the dryline.

This mechanism for the initiation and development of severe thunderstorms on the 17 July 2008 does not cover all the effects on convection. Ziegler et al. (1998) found that the effect of strong wind shear, the width of the dryline, and the effects of the mesoscale updraft also are important in determining whether a dryline will initiate convection.

5.5 Clouds, differential heating, and density gradients

For this case study, satellite imagery provides important information about the location of the dryline. The location and growth of clouds is intimately connected to the location of the dryline. The most unusual aspect from this case study is the presence of clouds in the dry air (relatively low absolute humidity) and a cloud free sky in the moist air (relatively high absolute humidity). This is not normally observed. Textbook cases of the dryline almost always refer to the presence of clouds in the moist air and a cloud free sky in the dry air (Schaefer, 1986). Some cases have referred to cumulus clouds in the dry air (Hane et al.,

1997), but there is no case known to the author that demonstrates the presence of extensive cloudiness in the dry air and an extensive cloud free sky in the moist air.

Satellite imagery for the southern part of Alberta shows a distinct cloud – no cloud boundary developing approximately parallel to the Rocky Mountains. This boundary is present from west central Alberta as far south as Montana (Figure 4.11, upper right). Fair weather cumulus clouds formed on the west (deep, dry, well mixed air) side of the boundary, while the sky remained cloud free to the east (shallow, moist, capped air). As the clouds developed, an enhanced line of cumulus convection is observed along the boundary. The cloud – no cloud boundary (and the line of enhanced cumulus convection) coincides with the dryline (as analysed from surface analysis) within less than the resolution of surface measurements (Figure 4.14). This is well within other errors, and shows that the dryline was the most likely cause of the clouds.

If the cloud – no cloud boundary is caused by and coincides with the dryline, then clouds are present on the dry side of the dryline, while the sky is cloud free on the moist side. This situation is extremely unusual, and it has not been documented before to the knowledge of the author. The following mechanism for the formation of clouds associated with the 17 July 2008 dryline is illustrated in Figure 5.3. To understand the process that could cause clouds in the dry air and a cloud free sky in the moist air, it is insightful to look at soundings (Figure 5.4). On the 17 July 2008, there were soundings placed on both sides of the dryline. The moist sounding (Figure 5.4, right side) is capped close to 800 mb, which is below the condensation level for convective clouds. Essentially, the cap is preventing clouds from forming due to thermal convection. The dry air is not capped in the lower levels which allows the dry air (Figure 5.4, left side) to be well mixed from the surface as high as 650 mb (later in the day it mixes as high as 500 mb (Figure 4.13, lower left)). In fact, one of the soundings in the dry air (Figure 4.13, lower left) exhibits a change from a well mixed dry adiabatic layer to a well mixed moist adiabatic layer. The presence of a large area of well mixed dry adiabatic layer, and a thin moist adiabatic layer just above it supports the

presence of cumulus convection. Field observations also support these observations, as seen in Figure 4.15.

There is often a gradient in density (θ_v) in addition to the gradient in moisture (see section 2.5). Parsons et al. (1991) attributed the θ_v gradient to differential heating caused by cloudiness in the moist air. This cannot be the case on 17 July 2008, because although there is a θ_v gradient, the differential heating is opposite. In this case, the θ_v gradient must be caused by a something else. Ziegler and Hane (1993) also attribute the θ_v gradient to differential heating, but without giving a reason for the differential heating. It is possible that the differential heating across the dryline may be caused by differing evapotranspiration due to changes in land use (Ziegler et al., 1995). Because the moist air is capped, the moisture (and the subsequent cooler air due to the evapotranspiration) tends to build under the cap. Any moisture (and subsequent cooler air) added to the dry air is mixed away. A factor in the availability of moisture is the change in land use from west to east. In Alberta, there is more cropped land to the east, and more forest and pasture to the west. This would result in greater evapotranspiration to the east (Raddatz, 1998). Research by Strong (1997) and Raddatz (1998) show that evapotranspiration by plants can contribute as much as 4 g kg^{-1} of moisture to the atmosphere over the course of a day. An example of a thermal gradient that could be caused by evapotranspiration is shown in the lower panel of Figure 5.5. Three different land covers have three different evapotranspiration rates. This causes the air to cool more in areas of high evapotranspiration creating the thermal gradient.

If the air on both sides of the dryline were from the same airmass, and evapotranspiration were the sole contributor to the moisture in the moist air, then θ_e should be mostly constant on the surface map. For this case study, an axis of higher θ_e is present on the plains immediately adjacent to the foothills (Figure 5.6). On either side of this axis, θ_e is very similar – it is about one degree cooler on the dry side. This implies that moisture convergence is taking place along the foothills. Similar θ_e values on both the dry and moist side of the dryline outside

of the axis of higher θ_e support the idea that the some of the thermal gradients could be caused by cooling due to evapotranspiration.

5.6 The dryline as a density current

More recent high resolution studies of drylines indicate that there is often (but not always) a density gradient across the dryline (Schaefer, 1986, Parsons et al., 1991, Ziegler et al., 1995). In order to determine whether a density gradient exists across the dryline, it is necessary to use a variable with a one-to-one monotonic relationship with density. The most commonly used variable in the literature is the virtual potential temperature (θ_v). This is the temperature corrected for altitude and humidity (See Appendix B). For this case study, the virtual potential temperature will be analysed in three separate ways: surface maps (Figure 5.7, left side), sounding cross sections (Figure 5.7, right side), and mobile transects (Figure 4.16).

Analysing the θ_v derived from the MM2 mobile transect reveals some interesting yet inconclusive results. The first dryline crossing was at 1700 UTC. The θ_v rose from an average of 300.7 K to 304.8 K steadily over about 50 km, while the mixing ratio dropped from 8.9 g kg^{-1} to 4.7 g kg^{-1} sharply over about 3 km. It is unlikely that all the change in θ_v can be attributed to changes across the dryline. The magnitude of the gradient in θ_v does not seem to coincide with the magnitude of the gradient in the mixing ratio, and since the transect took place over about an hour, it is necessary to filter out how much of the change is due to daytime heating (which is close to a maximum during this time), or due to elevation changes (as described previously). In fact, during the time that θ_v rose 4 °C, the temperature at nearby stationary stations (P1 and P2) rose an average of 1.5 °C due to daytime heating. The transect performed at 1900 UTC provides more insight. As we drove the vehicle from the dry air into the moist air, the θ_v dropped from 306.6 K to 305.8 K over 50 km, while the moisture rose from 4.7 g kg^{-1} to 8.3 g kg^{-1} over 25 km (in 2 discrete steps). In this case daytime heating would have acted against the observed gradient. The effect of elevation change

could have enhanced this gradient. The problem of the effect of daytime heating on θ_v while performing a mobile transect has been mentioned by Crawford and Bluestein (1997).

Analysing surface maps of virtual potential temperature provide a time independent analysis, but do not include the finescale measurements of the mobile transect. The analysis for the 17 July 2008 gives a definite density gradient (about 5 K per 100 km) with warmer temperatures (lower density) in the west and cooler temperatures (higher density) in the east. This is similar to some of the gradients observed in the United States (Ziegler and Hane, 1993 and Parsons et al., 1991). The θ_v gradient is much more diffuse than the moisture gradient across the dryline visible on the surface maps in Figure 4.8. Some previous research reports a sharp θ_v gradient along the dryline (e.g. Ziegler et al., 1995 and Parsons et al., 1991), while others report both diffuse and sharp θ_v gradients superimposed on one another (Atkins et al, 1998 and Ziegler and Hane, 1993).

Given the difficulty in assessing the density gradient from the mobile mesonet transects and the poor resolution from surface analyses, it is also possible to assess the density gradient from soundings. Because the dry air above the capping inversion supposedly has the same source as the dry air at the surface (Schaefer, 1974b), there should exist a θ_v gradient from below the inversion to above the inversion (θ_v being conserved with altitude). From the EA3 2000 UTC sounding, the θ_v rises from 303.0 K in the dry air to 305.4 K in the moist air giving a 2.5 K difference. This method also may not be the most accurate. Since the dryline advances by mixing away moisture from the surface (Schaefer, 1974b) the dry air should be somewhat moister than the air above the capping inversion. This is indeed the case. The average mixing ratio of the dry air is 4.7 g kg^{-1} while the mixing ratio of the dry air above the cap varies between 2 and 3 g kg^{-1}. This problem in assessing the density difference from soundings is also stated by Atkins et al. (1998). Using soundings to analyse the density gradient is most accurate (but not fully accurate) because it does not suffer from the effects of poor spatial and temporal resolution. Daytime heating and the smoothing of the

gradient are essentially eliminated. The downfall is the differences in moisture (and thus potential temperature) between the dry air at the surface and the dry air aloft.

It is possible that the observed density gradient is not a result of the dryline or synoptic setup at all. Under synoptically quiescent conditions without any gradients in moisture, gradient of θ_v can set up over sloping terrain (Figure 5.5). This θ_v gradient is due to the effect of the slope of the terrain alone. Daytime heating from equal solar radiation will warm areas relatively equally, but because of the slope, the θ_v values will be quite different. A 500 m difference could automatically produce a 5 degree change in θ_v. It appears that this phenomenon could be a significant factor in the observed density (θ_v) gradients for 17 July 2008.

An examination of equations for the propagation speed of a density current has been applied to the dryline in a number of different cases. The equation used is as follows:

$$c = \sqrt{gh\frac{\Delta\theta_v}{\theta_v}} \qquad (1)$$

c is the speed of the density current relative to the mean flow, g is gravity, h is the height of the denser fluid, and $\Delta\theta_v / \theta_v$ is the virtual potential temperature buoyancy (Parsons et al., 1991; and Ziegler et al., 1995). Derivations of different variations of this equation and general theories on the movement of fronts are shown in the appendices in Djurić (1994). The movement of the boundary is caused by the weight of the denser air, which in most dryline cases is the moist air (Djurić, 1994).

Applying equation (1) to the 17 July 2008 gives a propagation speed of 10 m s^{-1}. This calculation uses the virtual temperature gradient measured by the soundings. The calculated speed is considerable, but may not be accurate as the moisture content of the dry air on the west side of the dryline is higher than the

moisture content of the dry air above the moist air. Higher moisture content implies more evapotranspiration, more cooling (Figure 5.5), and a slower propagation speed (Equation 1). Another consideration from both Parsons et al. (1991) and Miller et al. (2001) is that the flow of the density current is opposite the gradient of the terrain (i.e. the boundary moves uphill). Parsons et al. (1991) has determined that the slope is insignificant in Texas, but it is insightful to examine it for Alberta. Since gravity will resist the density current flowing uphill, the acceleration due to gravity can be calculated using the slope (in the general vicinity of the dryline) and a reduced gravity (from Miller et al., 2001). This acceleration will result in the density current losing its speed in approximately 5 hours, which is certainly enough to noticeably retard the flow. It appears that the slopes where the 17 July 2008 dryline occurred are steeper than the cases analysed in Texas and Oklahoma.

It is possible that due to the timing of the mobile transect measurements on 17 July 2008, the correct conditions for the formation of the density current were not observed. As the dryline measurements were taken around noon, and drylines typically acquire a density gradient later in the afternoon and early evening (Schaefer, 1986), the density gradients may have been missed. Another problem with analysing the density gradient is whether the density measured at the surface is consistent throughout the boundary layer. Mobile surface transect and aircraft analysis by Ziegler and Rasmussen (1998) indicate that gradients of moisture and density can be almost double the surface value as little as 150 metres above the ground. This seems to be the case with the data from the 17 July 2008, with much stronger density and moisture gradients visible on the soundings than at the surface. There were no aircraft measurements to supplement this.

5.7 Discussion

In many ways the dryline on the 17 July 2008 resembles "textbook" drylines. The strength of the moisture gradient and the duration of the dryline were similar to other studies. The confluence of the south west winds in the dry air and the south east winds in the moist air agrees with the textbook case. There is some disagreement with the location of the confluence line and the location of the dryline, but this amounts to less than 10 km.

The mesoscale structure and motion of the dryline appears to agree with some of the literature. Many recent studies of the dryline with high resolution instrumentation detect a mesoscale variation in the location and motion of the dryline. This was observed on the 17 July 2008, and appears to be significant in the development of severe thunderstorms. It appeared that the cause of the mesoscale variability could be variations in local topography. There is little research on this and it needs to be investigated further.

The conceptual model provided by Ziegler and Hane (1993) discusses several features that are present in this case study also. The dryline on the 17 July 2008 consisted of 2 moisture gradients separated by a 15 km wide mixing zone. There was a plume of moisture above the mixing zone which advected downwind (eastwards) of the dryline. It is likely that the plume of moisture was caused by convergence along the dryline. The features resolved in the dryline on the 17 July 2008 compare remarkably well with the conceptual model proposed by Ziegler and Hane (1993).

Convection on the 17 July 2008 occurred mostly within 20 km of the dryline location, on the moist (east) side of the dryline. This is in agreement with textbook cases. The convection developed in isolated preferred locations and appeared to be associated with the mesoscale variability in the dryline. This has also been noted in other research with finescale measurements. The measurements taken during UNSTABLE were not sufficient to analyse this further.

The dryline on the 17 July 2008 is vastly different from the "textbook" dryline in one way. The textbook dryline has clouds in the moist air and a cloud free sky in the dry air. On the 17 July 2008, there was extensive fair weather cumulus cloud cover in the dry air, while the moist air remained essentially cloud free. This situation has not been documented before to the knowledge of the author. Section 5.7 provides an explanation as to why this occurred.

More recent research into the dryline often finds that there is a density gradient associated with the dryline, and this density gradient drives the motion of the dryline in accordance with the theory of density currents. For the 17 July 2008, a gradual density gradient was observed, but the source of this density gradient did not appear to be the dryline. It appeared that there was no density gradient directly associated with the dryline, and that the motion of the dryline was influenced by other factors much more than differences in density.

Chapter 6

Conclusions

This thesis documents the case study of the dryline forming on 17 July 2007 over Alberta. The focus is on the evolution of the dryline and the associated clouds and precipitation. The major observational data came from the operational network of surface weather stations, Alberta Sustainable Resource Development (ASRD) weather stations, satellite images, weather radar, and UNSTABLE special instrumentation. UNSTABLE special instrumentation included mobile transects, 2 hourly soundings from 4 sites, boundary layer observations, and eight supplemental weather stations. Another important component of the UNSTABLE dataset included manual observations and extensive cloud photographs by UNSTABLE participants.

6.1 Dryline structure, clouds, and precipitation

This section deals with our science question #1: How are the cloud and precipitation organized relative to the dryline?

a) Dryline characteristics

A sharp water vapour mixing ratio boundary formed parallel to the Rocky Mountains around 1030 MDT. The boundary was located in the western part of the UNSTABLE study area and lasted a maximum of 9 hours. This boundary was synoptic in scale. Based on satellite imagery, the moisture boundary was suspected to have been more than 1000 km long, stretching from central Alberta south to Wyoming. The width was estimated by mobile weather stations to be approximately 5 km with a water vapour mixing ratio change from 4.5 to 8.5 g kg^{-1} giving a moisture gradient of about 1 g kg^{-1} km^{-1}.

The properties of the moisture boundary were indicative of a dryline. A narrow transition zone between the dry and moist air was observed, and convergence was found in the vicinity of the boundary. Mass convergence

appeared to occur on both sides of the boundary, although the scale of analysis made it difficult to say this for certain. The boundary remained quasistationary throughout its existence. The dry (west) side of the boundary was well mixed from the surface up to as high as 500 mb (about 4 km AGL). The moist (east) side consisted of a shallow moist layer at the surface capped at around 800 mb (about 1 km above the ground). The length of the boundary suggests a synoptic scale boundary. The weak temperature gradient (about 2°C per 100 km) precludes a baroclinic front. The dryline was evident on satellite imagery as a stationary line of convective clouds along a cloud – no cloud boundary.

b) Horizontal structure and motion of the dryline

On a synoptic scale the dryline was quasistationary. It persisted along approximately the same line for as much as nine hours depending on the location. The weak 700 mb flow and the approximately equal easterly component at the surface support this conclusion.

Although the location of the dryline was quasistationary on a synoptic scale, there was a distinct mesoscale variation in the location of the dryline. The undulations visible in the dryline appear to resemble the mesoscale dryline waves. There were small bulges both into the moist and dry air, and these bulges changed over the course of the day.

The mesoscale bulges in the dryline were affected by the local topography. In the one case the moist air bulged westwards into the dry air through Bow Valley, with the stronger winds in the moist air advecting the dryline westwards. It is possible that the winds were stronger due to the channelling of winds into the Bow River valley, as suggested by Atkins et al. (1998). In another case, the dry air bulged eastwards through the Highwood River valley.

c) Organisation of clouds

The sky remained cloud free over the entire UNSTABLE domains from daybreak until 1100 MDT. At 1100 MDT, the dryline was visible on satellite imagery as a line of convection along the cloud – no cloud boundary. The cloud – no cloud boundary coincided with the dryline within 20 km. The mesoscale movements of the dryline were not noticeable in the satellite imagery of the line of convection.

Within 30 minutes of development of the line of convection, fair weather cumulus clouds formed in the dry air to the west of the dryline. In contrast, the moist air to the east of the dryline remained cloud free. Cumulus clouds developed on the dry (west) side of the dryline because there was no low level capping inversion on the west side, and the air was relatively well mixed from the surface as high as 500 mb. The temperature and humidity on the dry side allowed for the boundary layer air to reach the condensation level forming clouds. The sky remained cloud free on the moist side of the dryline until about 1500 MDT. The height of the capping inversion (about 800 mb) in the moist air prevented deep vertical mixing which did not allow the air to reach its condensation level, preventing the formation of clouds.

After 1500 MDT cumulus convection continued on the dry side of the dryline as the boundary layer deepened, while cumulonimbus clouds associated with deep convection occurred just to the east of the dryline. The cirrus anvils associated with these clouds drifted eastwards over the moist air, although there were still no convective clouds that formed well within the moist air.

e) Organisation of precipitation

Strong radar echoes (exceeding 50 dBZ) developed within 20 km of the dryline on the moist side. The storms remained stationary when they were most

intense. Hail accumulated 10 cm deep on the ground. UNSTABLE participants measured maximum hail size with diameter 2 cm. The storms that developed were multicellular storms which formed along the dryline. The radar data showed three-dimensional characteristics of the precipitation associated with the dryline.

The location of the dryline bulges sometimes coincided with the location of the first strong radar echo formation. The initiation of strong convection appeared to be more prevalent where the dry air advanced eastwards, particularly near the bulge that formed over the Highwood River Valley. As this bulge formed, a radar echo exceeding 55 dBZ formed to the north east of the bulge and drifted eastwards. Large hail fell from this storm.

2 cm diameter hail, and one weak tornado were reported to the Environment Canada storm line. UNSTABLE participants observed cyclonic rotation in the cloud base in one of the intense thunderstorms. A rotating wall cloud was seen that lowered the cloud base. It is likely that the intense small scale vorticity observed in the thunderstorm was spawned from the mesoscale vorticity found at low levels by sounding triangulation. No tornados or funnel clouds were reported for this rotating thunderstorm.

The convergence associated with the dryline was evident on surface wind maps, calculated using sounding triangulation, and implied by convection seen on satellite imagery. The convergence combined with the proximity of the dryline to the initiation of severe storms shows that the dryline was instrumental in initiating the convection.

6.2 Comparison with textbook cases

This section deals with our science question #2: How does this dryline compare to the textbook drylines?

a) Comparison with conceptual models

The dryline on the 17 July 2008 is similar to conceptual model of a dryline developed by Ziegler and Hane (1993). The textbook dryline tends to have two bands of strong moisture gradients which are separated by a mixing zone about 10 to 20 km wide. Within the mixing zone, a plume of moisture extends well above the altitude of the cap and is advected eastwards above the moist air. The mixing zone consists of a mixture of the moist and dry air (Ziegler and Hane, 1993). In the 17 July dryline, the same structure was found after 1300 MDT. Two moisture gradients were associated with the dryline separated by a mixing zone. A sounding was located within the mixing zone and recorded a deep moisture plume above the dryline. Two hours later, remnants of the same moisture plume had moved about 50 km eastwards above the capping inversion (at about 700 mb).

A major difference between the 17 July dryline and the textbook dryline was the spatial distribution of the clouds relative to the dryline. In the textbook dryline, clouds are present on the moist (east) side of the dryline. These clouds are usually stratocumulus or altocumulus in nature and quite often are broken to overcast. A cloud free sky prevails on the dry (west) side of the dryline, although there are occasional reports of high based cumulus clouds (e.g. Ziegler et al., 1998). On the 17 July 2008, extensive fair weather cumulus clouds were present on the dry (west) side of the dryline while the sky was cloud free on the moist (east) side of the dryline until the initiation of severe thunderstorms. This is in complete contrast to the textbook case.

b) Convective initiation

For the textbook dryline, thunderstorms tend to be initiated near the dryline on the moist side (Rhea, 1966). In many cases this convection develops into severe thunderstorms. On the 17 July 2008, the initiation of convection occurred within 20 km of the dryline also on the moist side. It also occurred just after the moisture plume was observed on the WVX sounding, indicating that the convergence associated with the dryline most likely triggered the convection.

c) Density current flow

There is ongoing debate over whether drylines act as density currents (Hill, 2006). Some drylines have strong density gradients resulting in density currents (Parsons, 1991), while other drylines lack density variations (McGuire, 1962). With the limited data available for the 17 July 2008 dryline an attempt was made to determine whether there was a density current, and if so, whether the density current controlled the movement of the dry line. A weak density gradient was detected, but the location of this density gradient did not always coincide with the location of the moisture gradient. It is possible that in this case, the density gradient was not associated with the dryline, but was rather formed by differential heating due to evapotranspiration. Alternatively, changes in elevation could have generated a density gradient. We conclude that the motion of the dryline on the 17 July 2008 was not significantly driven by density differences.

d) Synoptic and mesoscale motion

The textbook dryline moves eastwards during the day, and moves westwards during the night (Schaefer 1986). However, there are many deviations from this diurnal pattern. For example, there have been cases of stationary drylines. On a synoptic scale, the motion of the dryline of 17 July was quasistationary. On the mesoscale, however, the location and movement of the 17 July dryline had significant variations. Also, the mesoscale horizontal structure varied. Mesoscale dryline waves (McCarthy and Koch, 1982), horizontal

convective rolls (Atkins et al., 1998), and variations in local topography (Atkins et al., 1998) have been postulated as different causes of such variations.

e) Summary

Table 1 compares some characteristics of the Alberta dryline of 17 July 2008 to the classical textbook dryline (for southern United States).

	Textbook Dryline	**17 July 2008 Dryline**
Length of Dryline	~ 1000 km	~ 1000 km
Width of Dryline	0.1 – 10 km	3 km
Duration of Dryline	4 – 48 hours	4 – 12 hours
Moist Air (east of dryline)		
Sky Conditions	BKN - OVC SC/AC	CLR
Wind Direction	South to Southeast	Southeast
Humidity	12 -20 g kg^{-1}	9 – 11 g kg^{-1}
Height of Cap	800 mb	800 mb
Depth of Moist Air	~ 1 km	~ 1 km
Dry Air (west of dryline)		
Sky Conditions	CLR - FEW CU	SCT CU
Wind Direction	Southwest	Southwest
Humidity	2 – 5 g kg^{-1}	5 g kg^{-1}
Mixing Height	~ 500 mb	~ 500 mb
Multiple Moisture Gradient	Sometimes present	Present by 1300 MDT
Mixing Zone Width	10 - 20 km	15 km
Moisture Plume Present	Yes	Yes
Convective Initiation	Sometimes	Severe thunderstorms
Initiation Location	Near dryline on moist side	Near dryline on moist side
Motion		
Early Afternoon	Eastward	Quasistationary
Evening	Westward	Quasistationary
Mesoscale variation	Yes	Most of the time

Table 1: This table is a comparison between the dryline on 17 July 2008 with textbook cases.

6.3 Recommendations for Further Research

Our recommendations for future research are mostly focused on analysing data with an enhanced data network for a possible future field experiment.

A major limitation of this study in terms of analysing kinematic variables for the initiation of convection was the shortage of upper air measurements. Using the four soundings in this study, it was barely possible to estimate the mesoscale convergence and thus vertical velocity. Because some soundings were not available at all locations all the time, a complete set of observations was not available for the calculations. Using additional soundings will allow for the computation of divergence, vorticity, and vertical velocity at every level in enough different areas to produce the three dimensional structure in the same way as has been analysed by Ogura and Chen (1977). They found that the kinematic variables were extremely variable over small spatial scales around the dryline. This would be done in the same way as described in Appendix A, and could be done in a limited way with the addition of as little as two or three additional sounding sites, as shown in Figure 6.1. It is also necessary to launch soundings earlier in the morning to evaluate the pre storm environment, and to ensure that the soundings included measurements at least as high as the tropopause.

All field projects suffer from a shortage of high resolution data due to costs of collecting the data. A numerical model can help to alleviate this problem. Models allow researchers to investigate features which may not be observed at high enough resolution in a field experiment. For example, the field experiment could not properly resolve the dryline at all times, where a high resolution model may be able to. Other researchers involved in the UNSTABLE project are analyzing numerical simulations of UNSTABLE for selected case study events.

Another future study could look at the data provided by the Foothills Climate Array mesonet operated by the University of Calgary when these data become available. This could provide insight into a number of topics discussed in the literature such as mesoscale dryline circulations (McCarthy and Koch, 1982),

and horizontal convective rolls (Atkins et al., 1998). The resolution of the mesonet is similar in resolution to some of the mesonets used in Oklahoma, but it only provides temperature and humidity data. The lack of pressure and wind data will make it more difficult but it will still be possible to get some insight into the variability of the position and motion of the dryline in Alberta.

Aside from a brief mention of agriculture by Schaefer (1986), and a short section by Carlson and Burgan (2003) on fire meteorology, there have been very little detailed studies on the effect of drylines on both agriculture and forest fire meteorology. A further study into either of these two subtopics could provide more insight into the importance of understanding the dryline in both Canada and throughout the world.

Figures

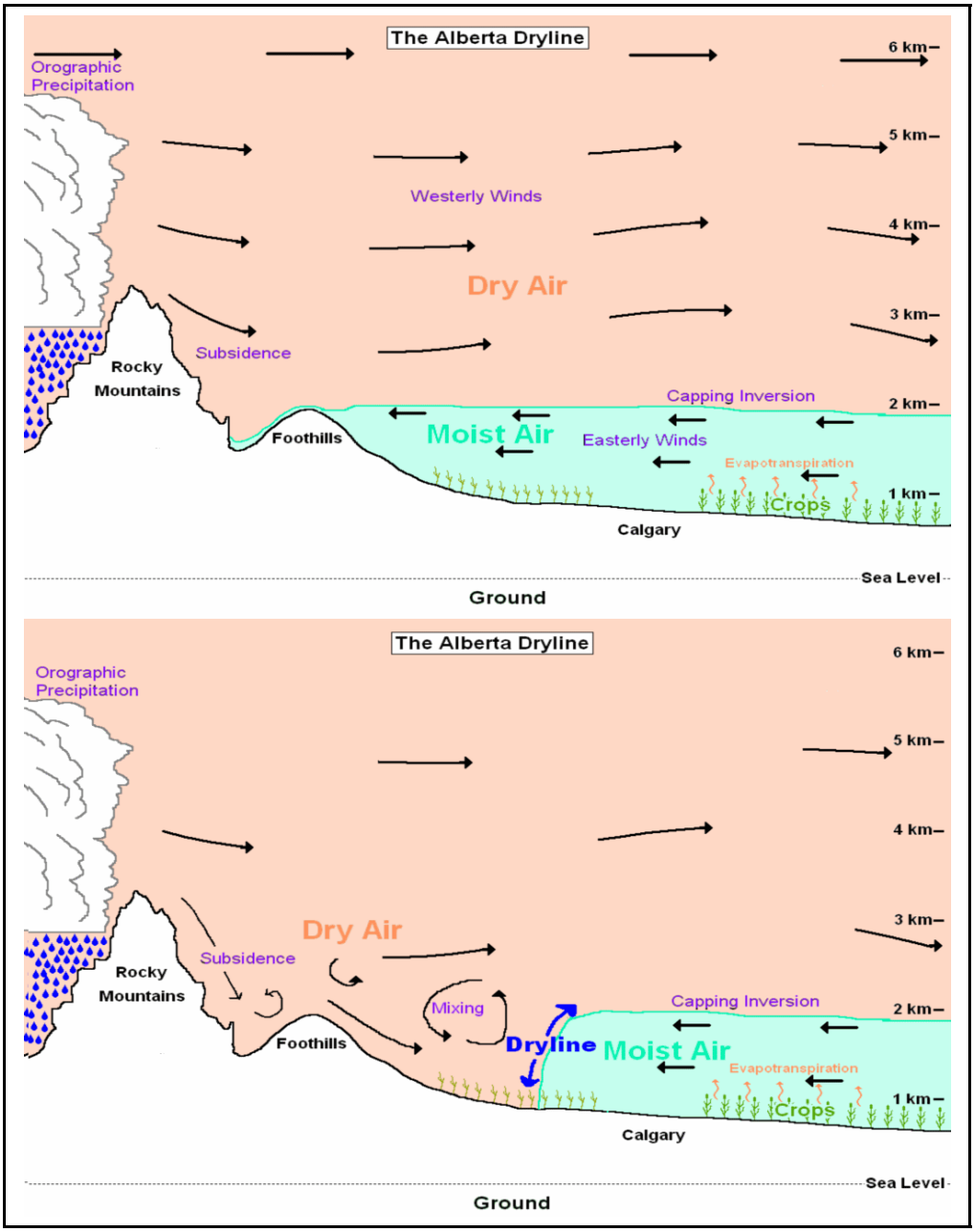

Figure 2.1: A schematic diagram showing the formation and motion of the Alberta dryline. The top panel shows the morning, where the dryline has not formed yet. The moist air is present up to about the same level everywhere, and thus gets deeper further east as the topography drops off. In the lower panel, daytime heating mixes away the cap to the west and the dry air (and westerly winds) come to the surface. The moist air does not because the cap has not been mixed away yet. The boundary between these is the dryline.

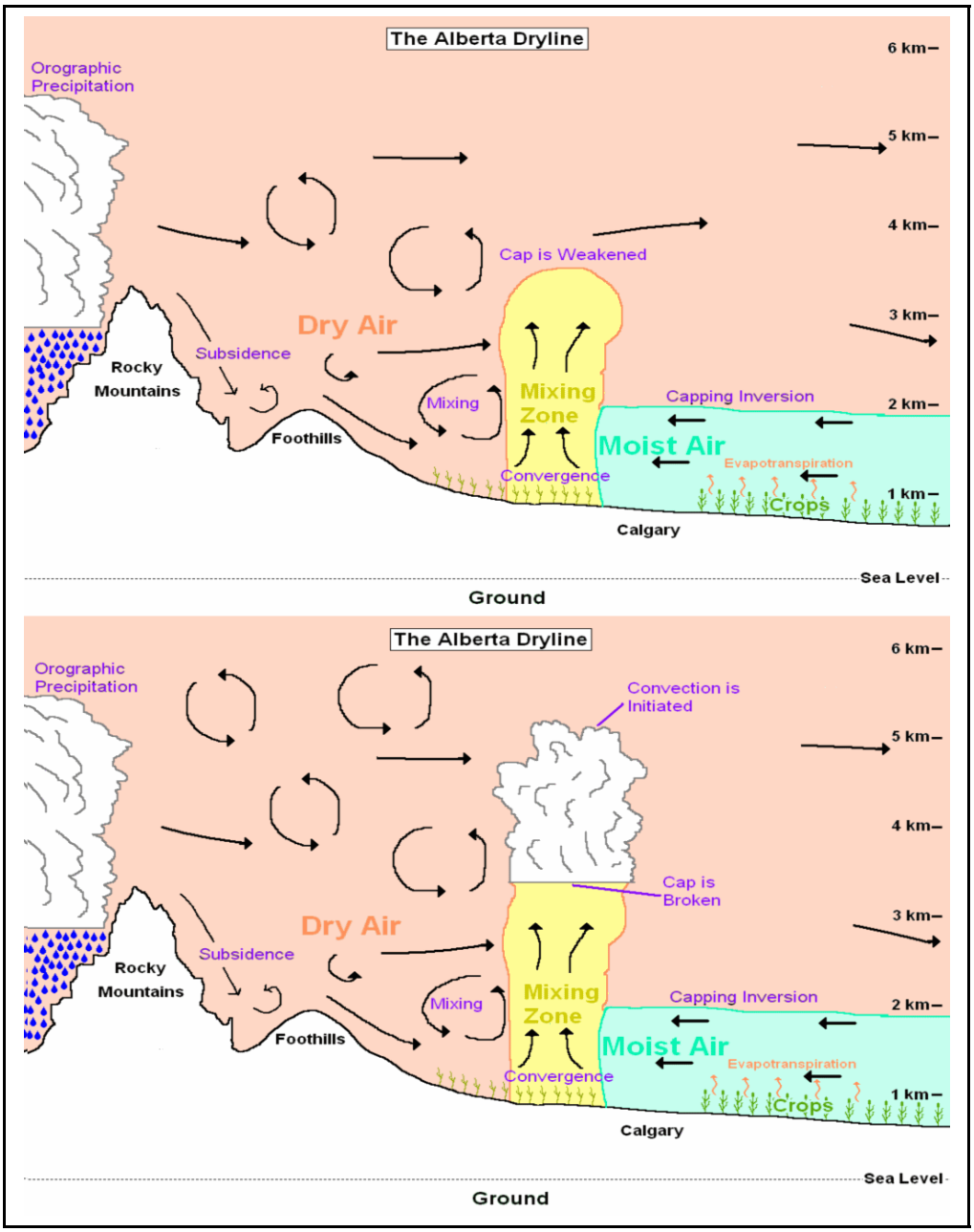

Figure 2.2: A schematic diagram showing the formation and motion of the Alberta dryline. The top panel shows the boundary layer deepening in the dry air. Mixing along the dryline creates a mixing zone. The mixing zone contains a mixture of dry and moist air. In the bottom panel, convergence along the dryline eventually raises the air past its condensation level, and convection is initiated. The convection then will drift into the moist air and intensify.

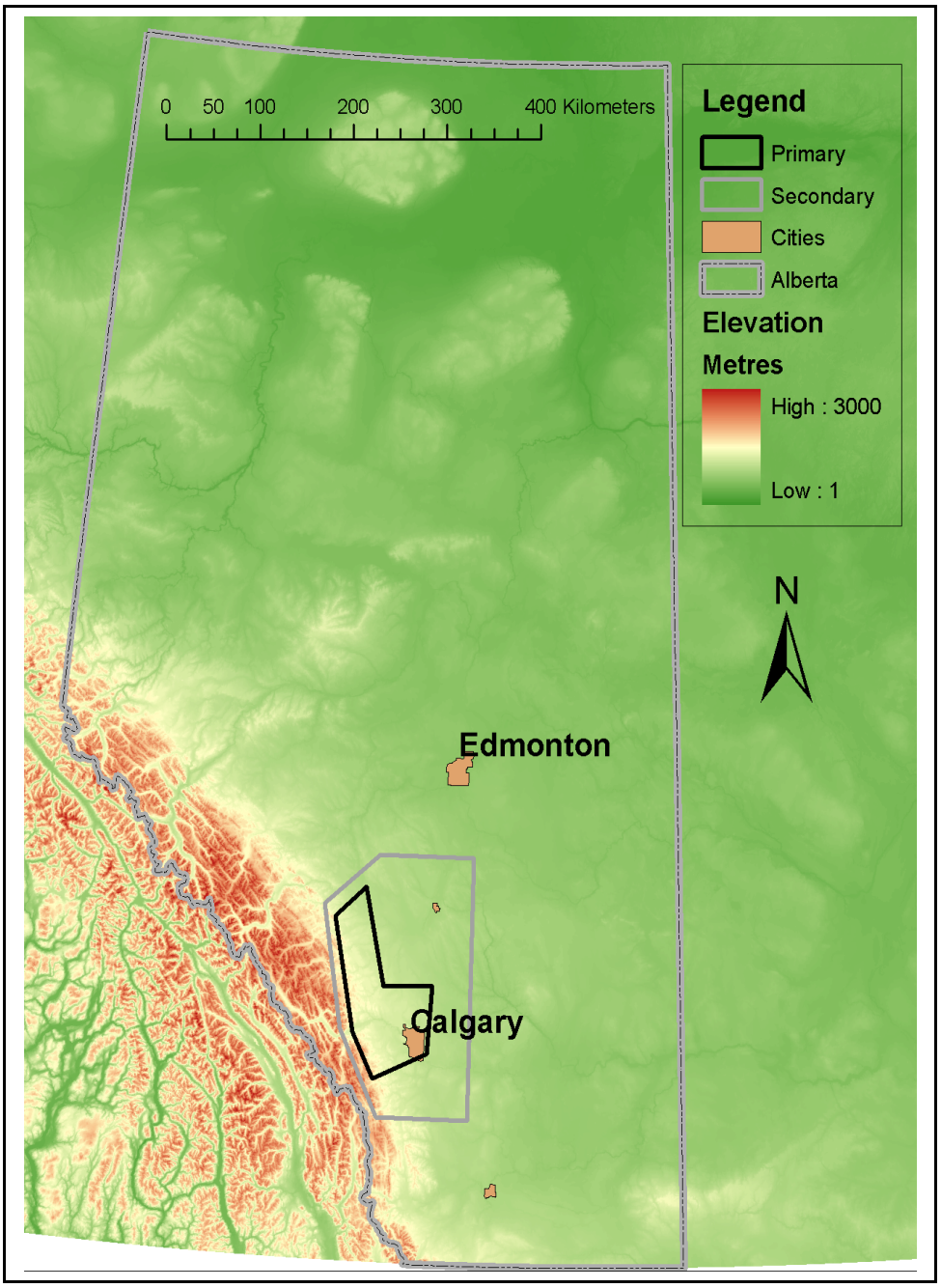

Figure 3.1: An overview map of the location of the UNSTABLE Study area within the province of Alberta, Canada. Edmonton and Calgary are shown, as well as the boundaries of Alberta and the UNSTABLE Primary and Secondary Domains. The colours represent a digital elevation model with greens being the lowest elevations and reds being the highest.

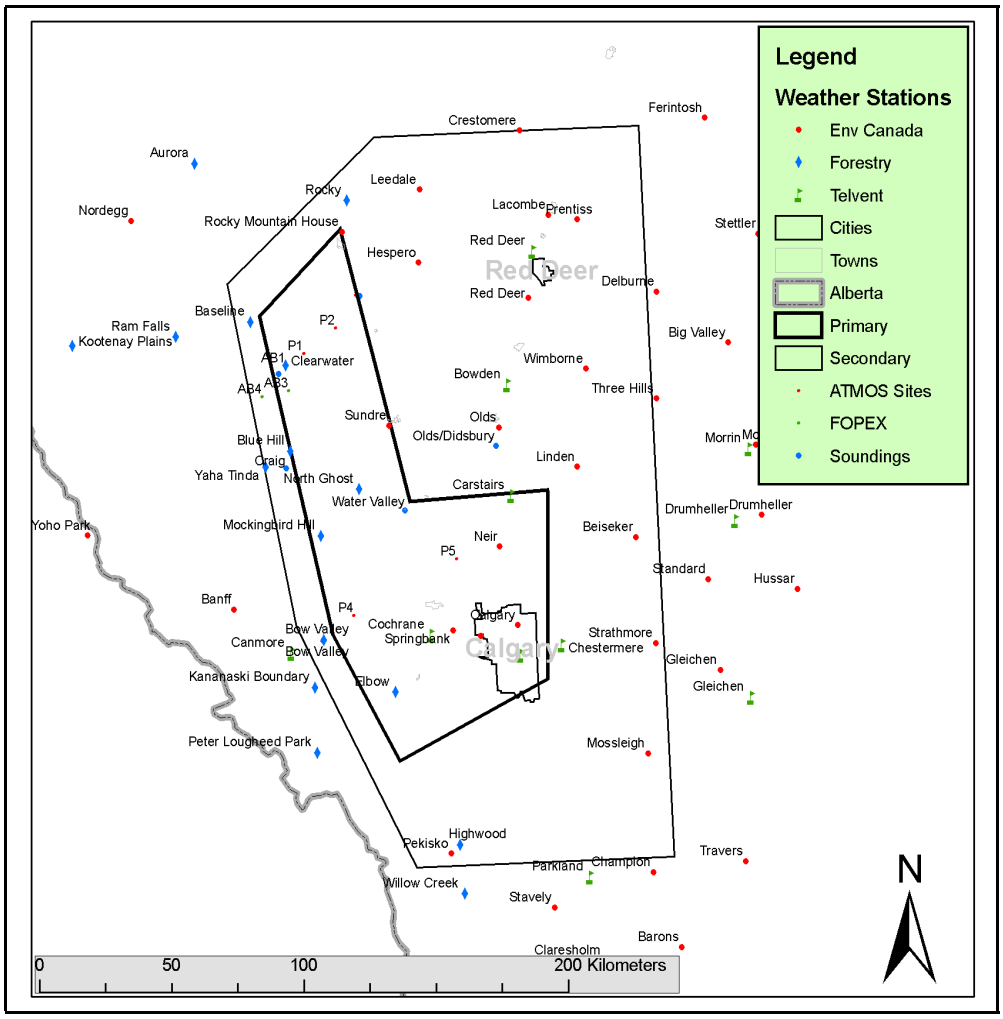

Figure 3.2: The surface weather stations used in the surface analysis are shown here in the context of the UNSTABLE area. The red ones are Environment Canada stations, the blue ones are provided by Alberta Sustainable Resource Development (Forestry), and the green ones are provided by Telvent, and are used for road reports for Alberta Transportation. Also located on the map are the soundings (each sounding site had a surface station) and the special UNSTABLE surface stations.

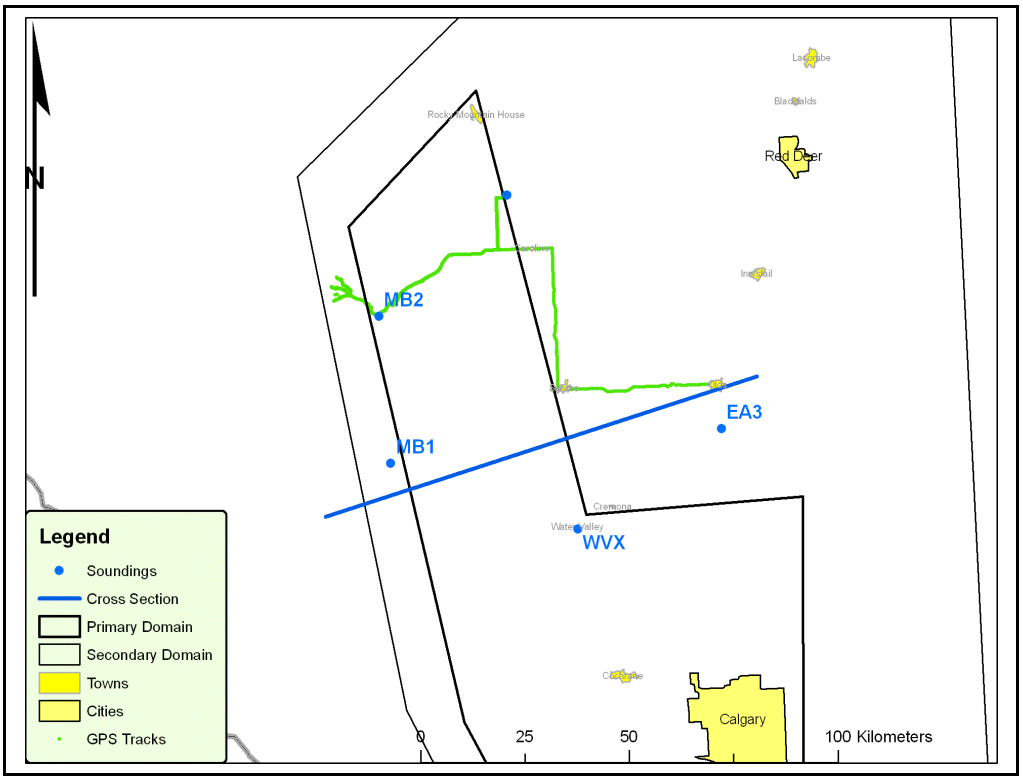

Figure 3.3: The locations of the upper air sounding sites on 17 July 2008 and the tethersonde. MB1 and MB2 were the mobile soundings while WVX is located in the town of Water Valley and EA3 is located at the Olds – Didsbury Airport. The thick blue line represents the line for which the cross section in Figure 4.10 lies on. This line was oriented perpendicular to the dryline and as close to all four soundings as possible. The tracks of one of the mobile mesonet vehicles are shown in green.

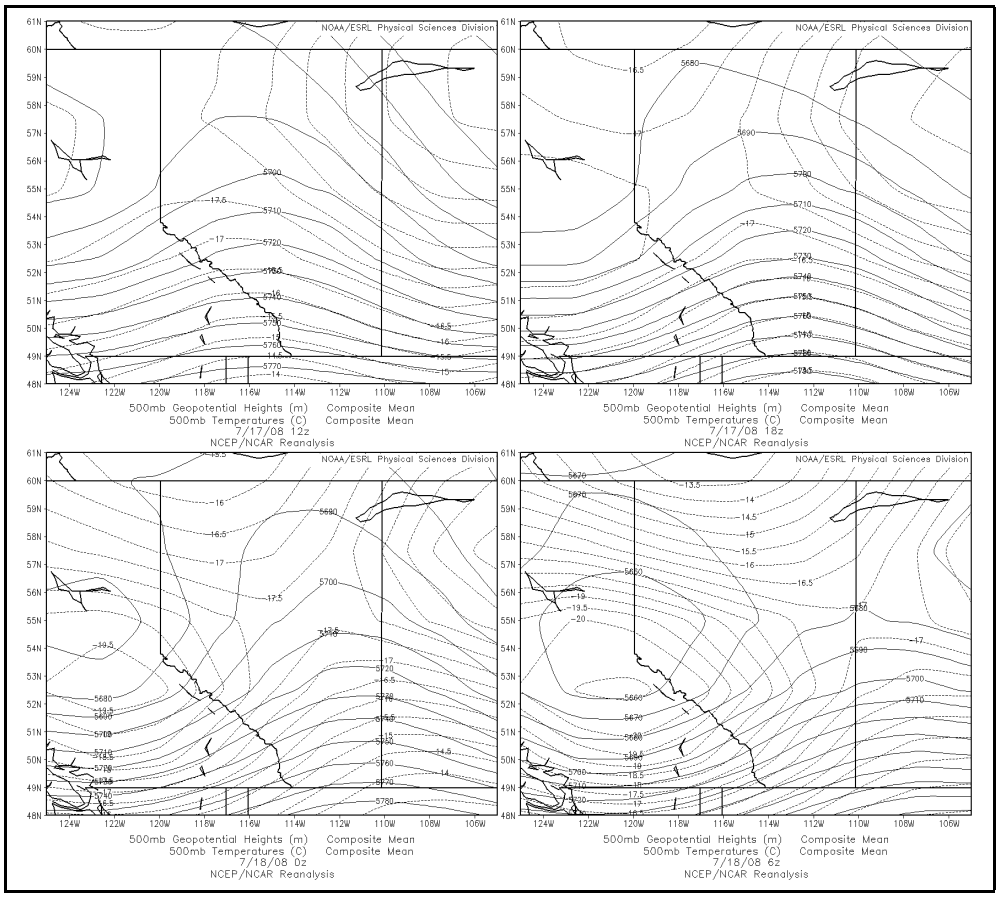

Figure 4.1: 500 mb heights and 500 mb temperatures from 1200Z 17 July 2008, 1800Z 17 July 2008, 0000Z 18 July 2008, and 0600Z 18 July 2008. Solid lines are geopotential heights in metres, and dashed lines are temperatures in degrees Celsius. Image provided by the NOAA/ESRL Physical Sciences Division, Boulder Colorado from their Web site at http://www.esrl.noaa.gov/psd/.

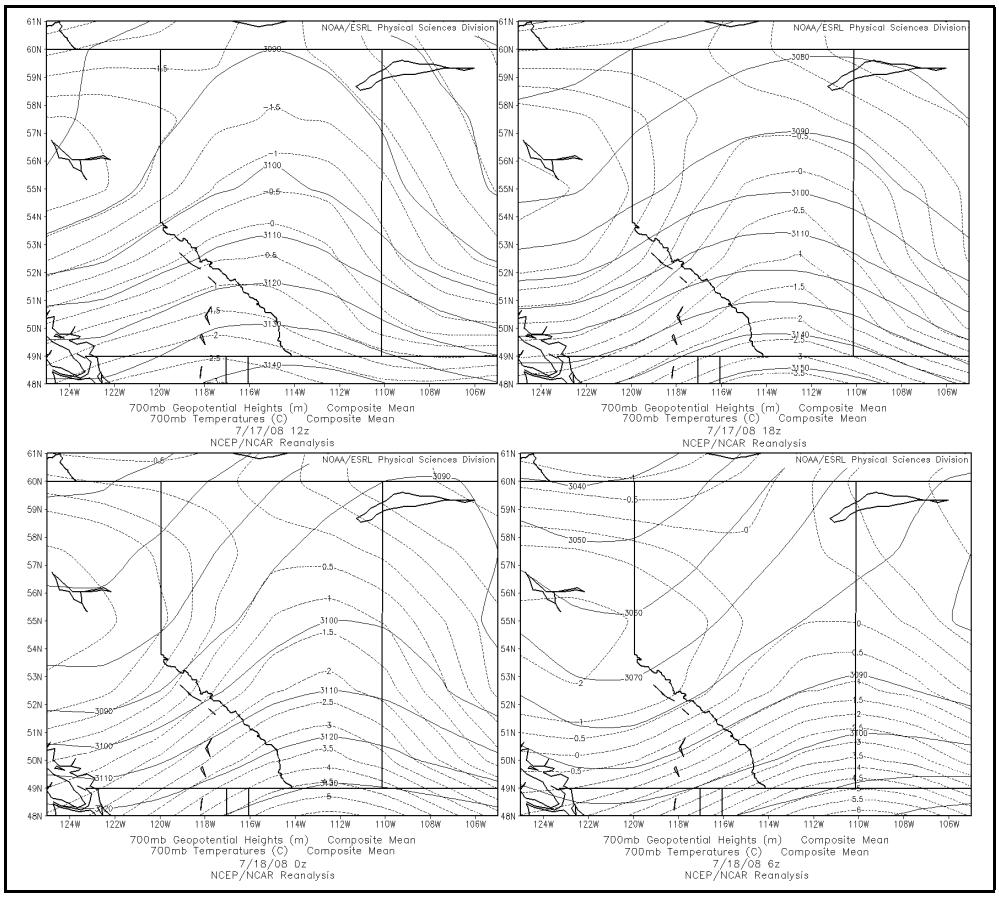

Figure 4.2: 700 mb heights and 700 mb temperatures from 1200Z 17 July 2008, 1800Z 17 July 2008, 0000Z 18 July 2008, and 0600Z 18 July 2008. Solid lines are geopotential heights in metres, and dashed lines are temperatures in degrees Celsius. Image provided by the NOAA/ESRL Physical Sciences Division, Boulder Colorado from their Web site at http://www.esrl.noaa.gov/psd/.

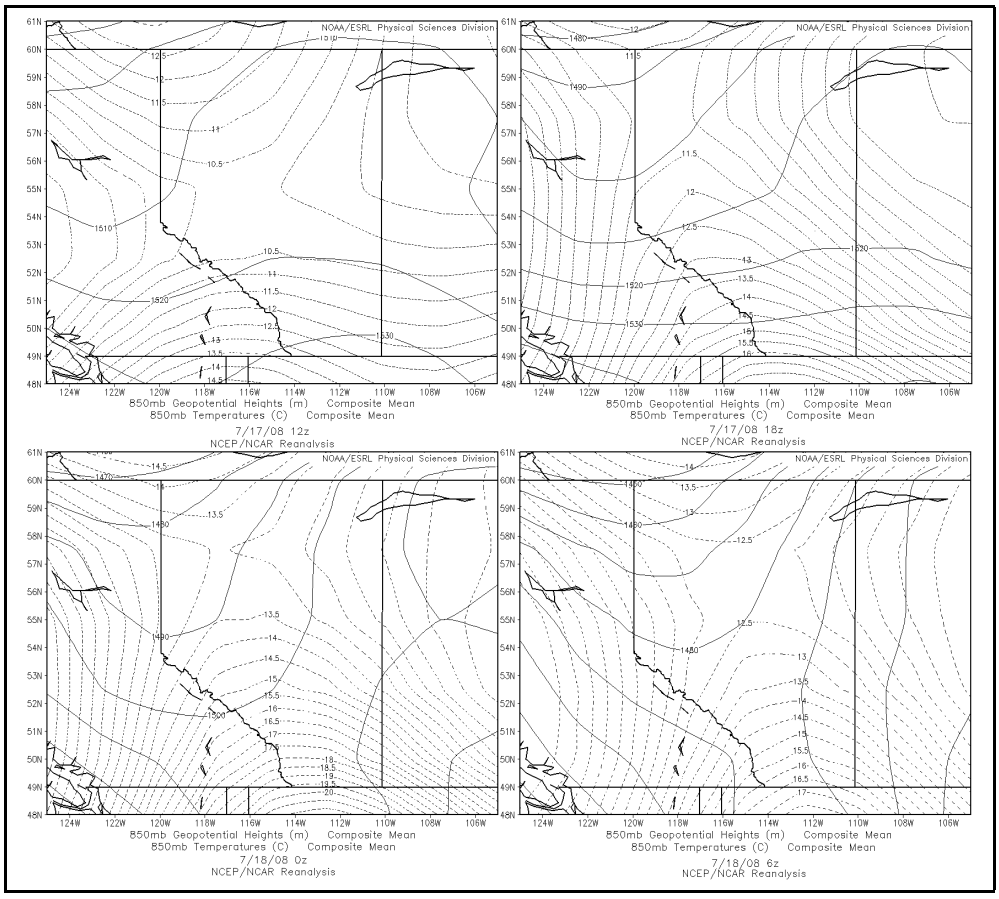

Figure 4.3: 850 mb heights and 850 mb temperatures from 1200Z 17 July 2008, 1800Z 17 July 2008, 0000Z 18 July 2008, and 0600Z 18 July 2008. Solid lines are geopotential heights in metres, and dashed lines are temperatures in degrees Celsius. Image provided by the NOAA/ESRL Physical Sciences Division, Boulder Colorado from their Web site at http://www.esrl.noaa.gov/psd/.

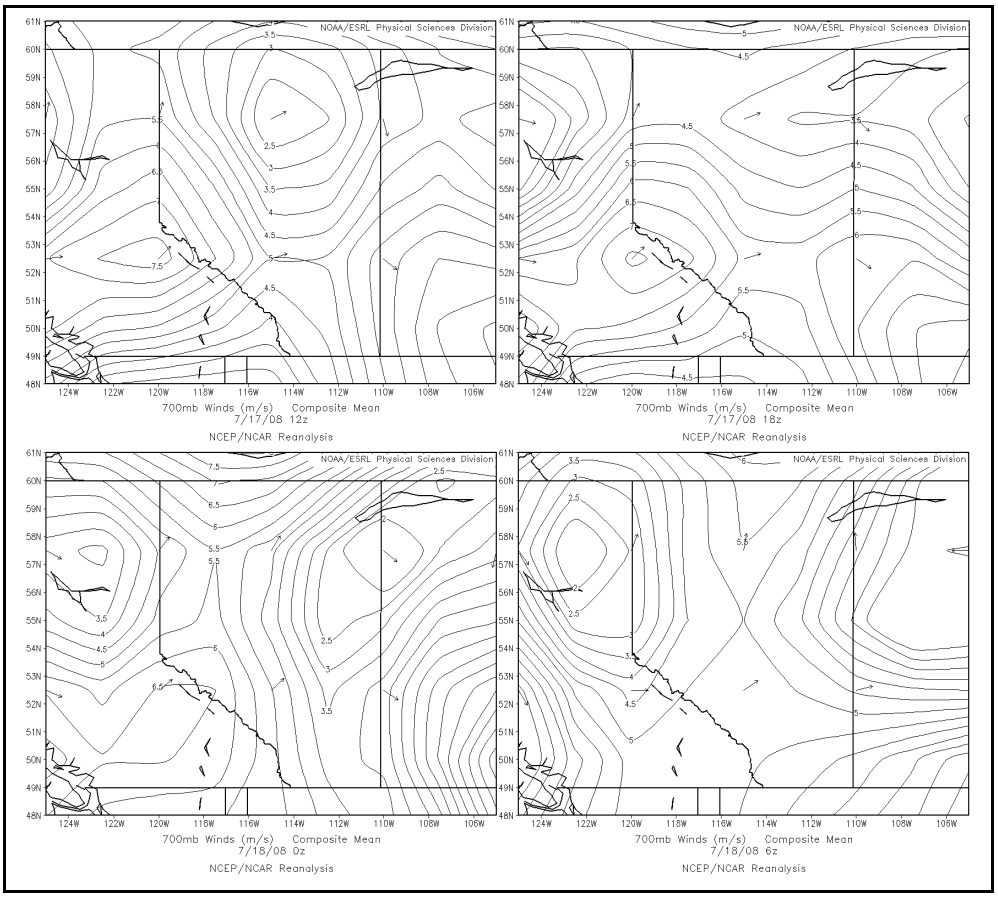

Figure 4.4: 700 mb winds over Alberta for 1200Z 17 July 2008, 1800Z 17 July 2008, 0000Z 18 July 2008, and 0600Z 18 July 2008. Winds are contoured in 0.5 m s^{-1} intervals with arrows indicating the wind direction. Image provided by the NOAA/ESRL Physical Sciences Division, Boulder Colorado from their Web site at http://www.esrl.noaa.gov/psd/.

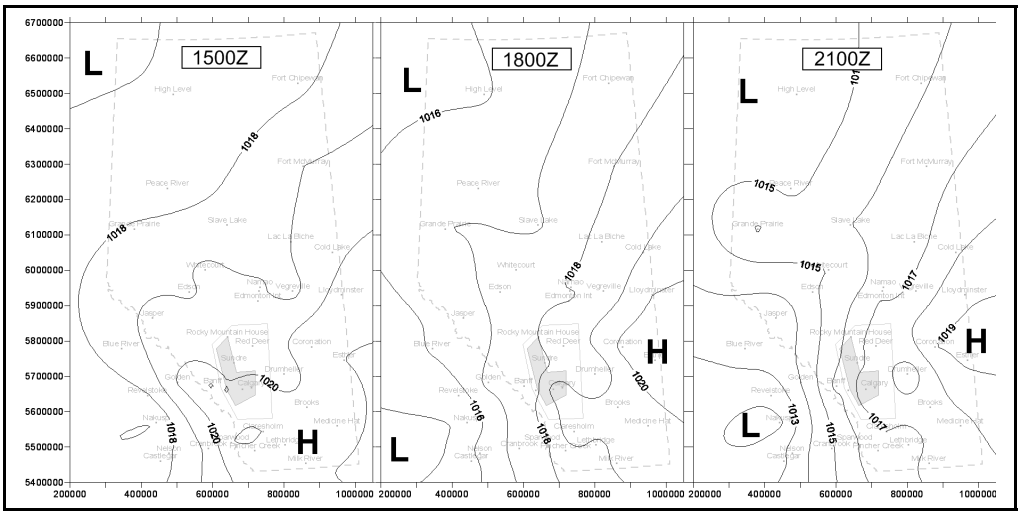

Figure 4.5: Sea level pressure analysis over Alberta for 1500 UTC, 1800 UTC, and 2100 UTC. The sea level pressure is contoured at 1 mb intervals with relative high and low pressure centres labelled. The boundaries of Alberta, the UNSTABLE domains, and the appropriate geography are also shown.

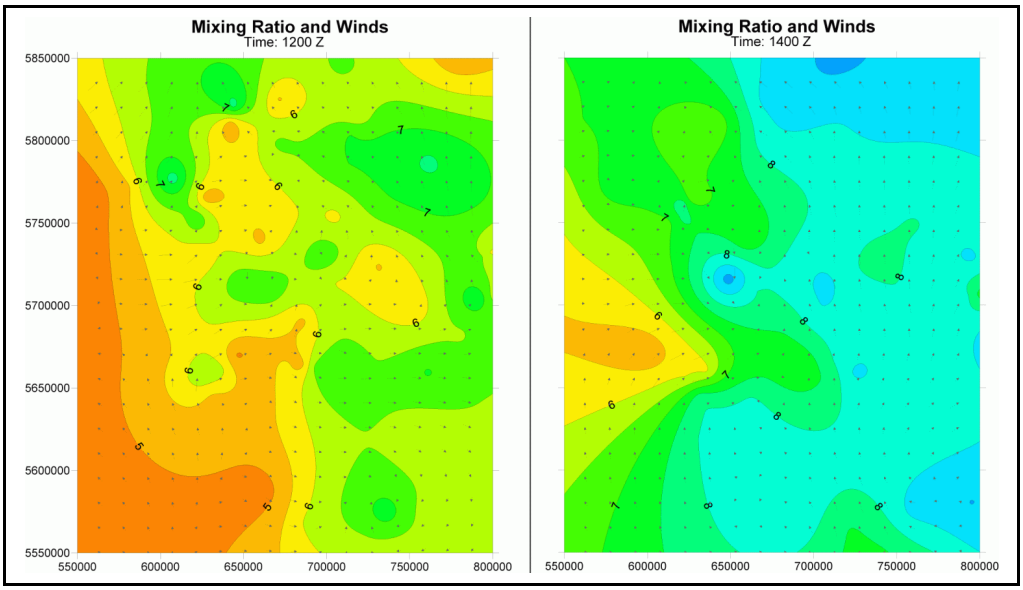

Figure 4.6: Mixing ratio values and the wind vectors for the UNSTABLE domains at 1200 UTC, and 1400 UTC. The mixing ratio is graduated in 0.5 g kg^{-1} intervals with the labels on the image. The arrows represent the wind vectors and point in the direction of the wind flow with longer arrows indicating stronger winds. Dry air is indicated by orange and yellow colouring, while moist air is indicated by shades of blue.

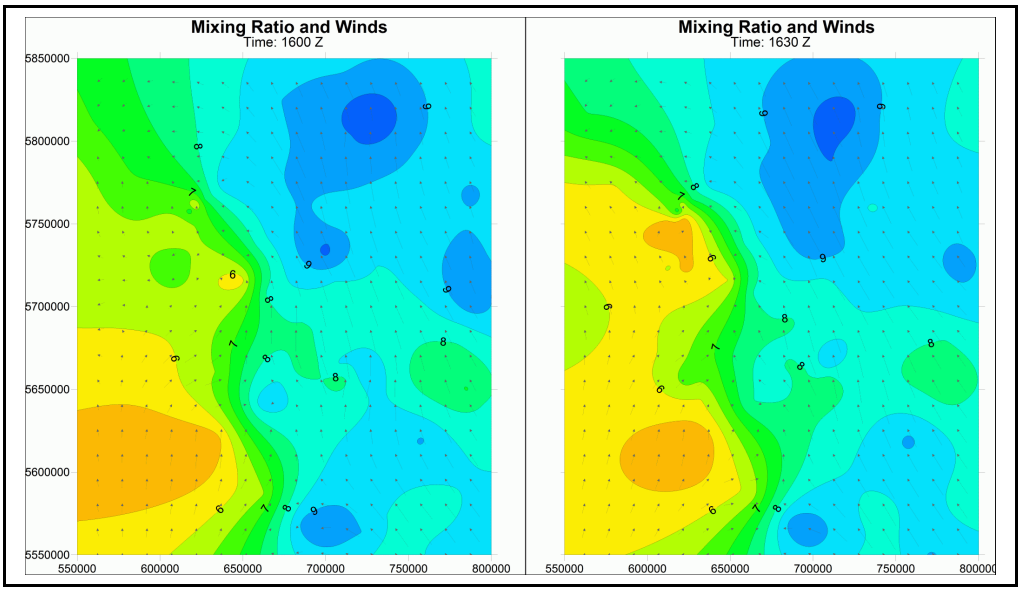

Figure 4.7: Mixing ratio values and the wind vectors for the UNSTABLE domains at 1600 UTC, and 1630 UTC. The mixing ratio is graduated in 0.5 g kg^{-1} with the labels on the image. The arrows represent the wind vectors and point in the direction of the wind flow with longer arrows indicating stronger winds. Dry air is indicated by orange and yellow colouring, while moist air is indicated by shades of blue.

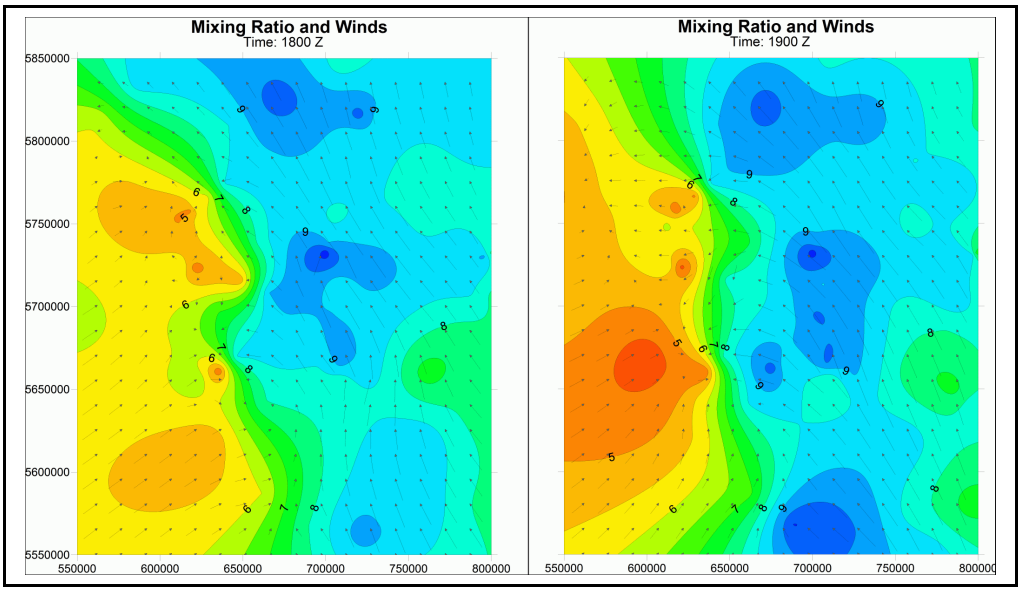

Figure 4.8: Mixing ratio values and the wind vectors for the UNSTABLE domains at 1800 UTC, and 1900 UTC. The mixing ratio is graduated in 0.5 g kg^{-1} with the labels on the image. The arrows represent the wind vectors and point in the direction of the wind flow with longer arrows indicating stronger winds. Dry air is indicated by orange and yellow colouring, while moist air is indicated by shades of blue.

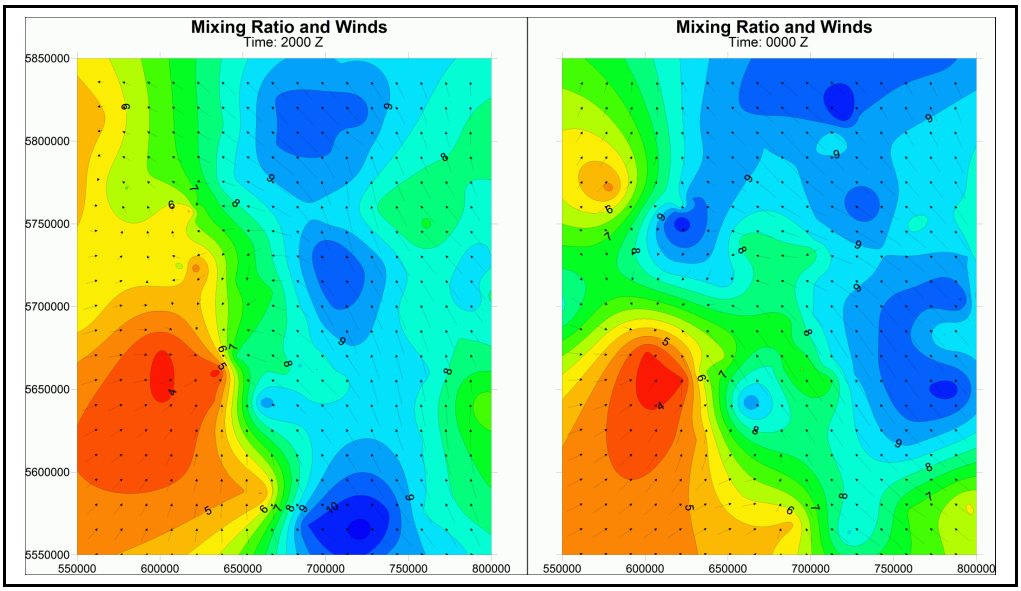

Figure 4.9: Mixing ratio values and the wind vectors for the UNSTABLE domains at 2000 UTC, and 0000 UTC. The mixing ratio is graduated in 0.5 g kg^{-1} with the labels on the image. The arrows represent the wind vectors and point in the direction of the wind flow with longer arrows indicating stronger winds. Dry air is indicated by orange and yellow colouring, while moist air is indicated by shades of blue.

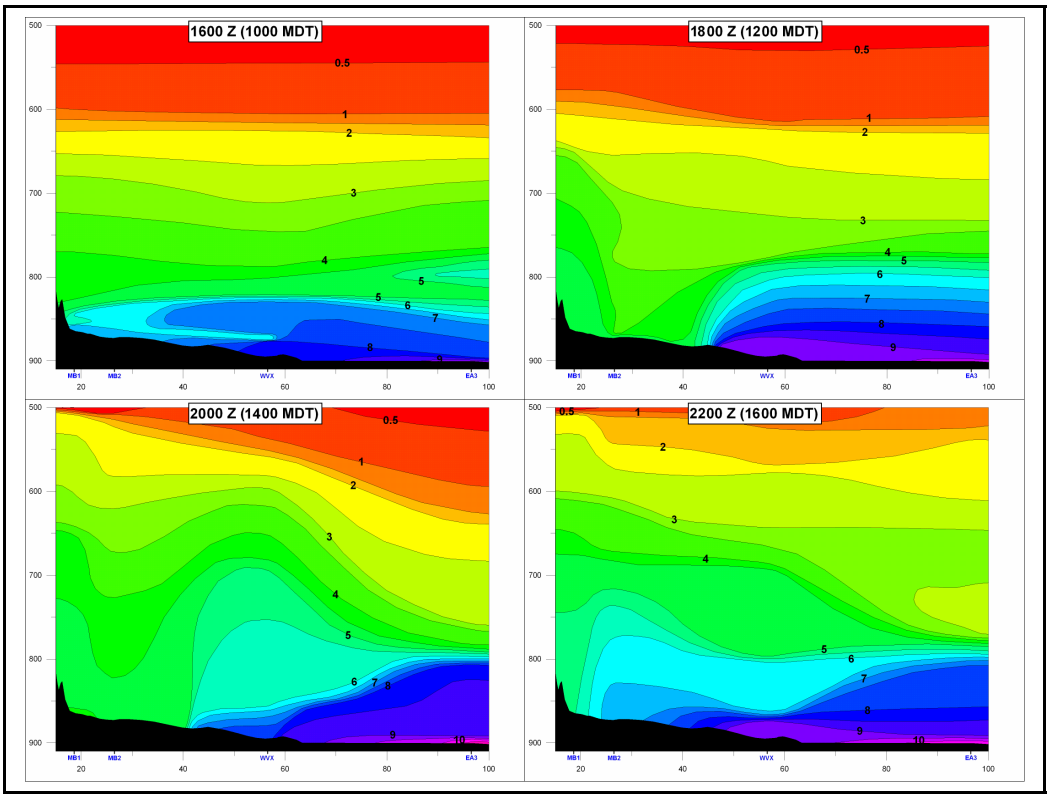

Figure 4.10: Vertical cross section depicting contours of water vapour mixing ratio (g kg^{-1}) across the dryline for 1600 UTC, 1800 UTC, 2000 UTC, and 2200 UTC. The vertical axis is the pressure in mb, while the horizontal axis is the distance along the cross section (shown in Figure 3.3) in km. The black area at the bottom represents the topography. The figure was constructed using soundings and mobile transects. The location of the sounding sites (MB1, MB2, WVX, and EA3) along the transect are shown on the horizontal axis. The moist air is indicated by the blue and purple colours, while the dry air is indicated by the green colours. The red colours at the top are extremely dry air in the upper atmosphere.

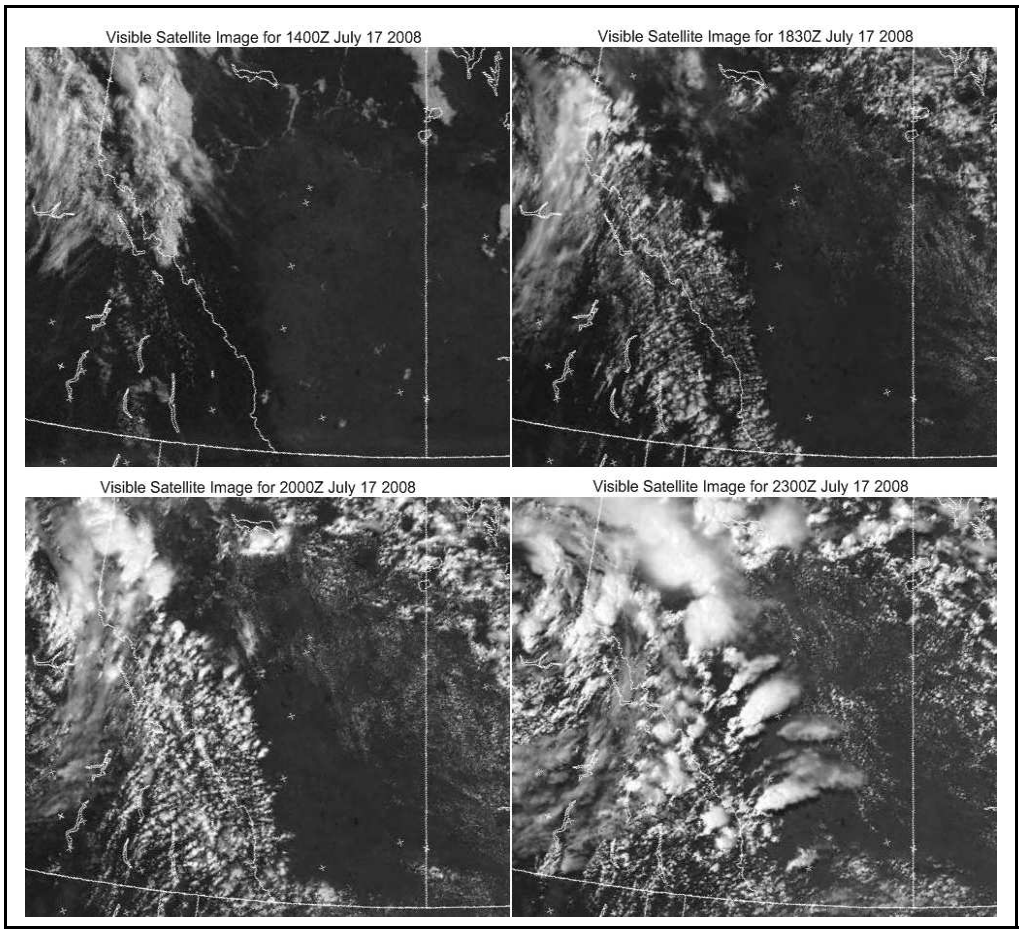

Figure 4.11: GOES West visible satellite images of southern Alberta on 17 July 2008 for 1400 UTC, 1830 UTC, 2000 UTC, and 2300 UTC. White areas indicate clouds, while dark areas indicate clear skies. The boundaries of Alberta are shown. The line of convection along the cloud – no cloud boundary is visible, as are the storms which developed later.

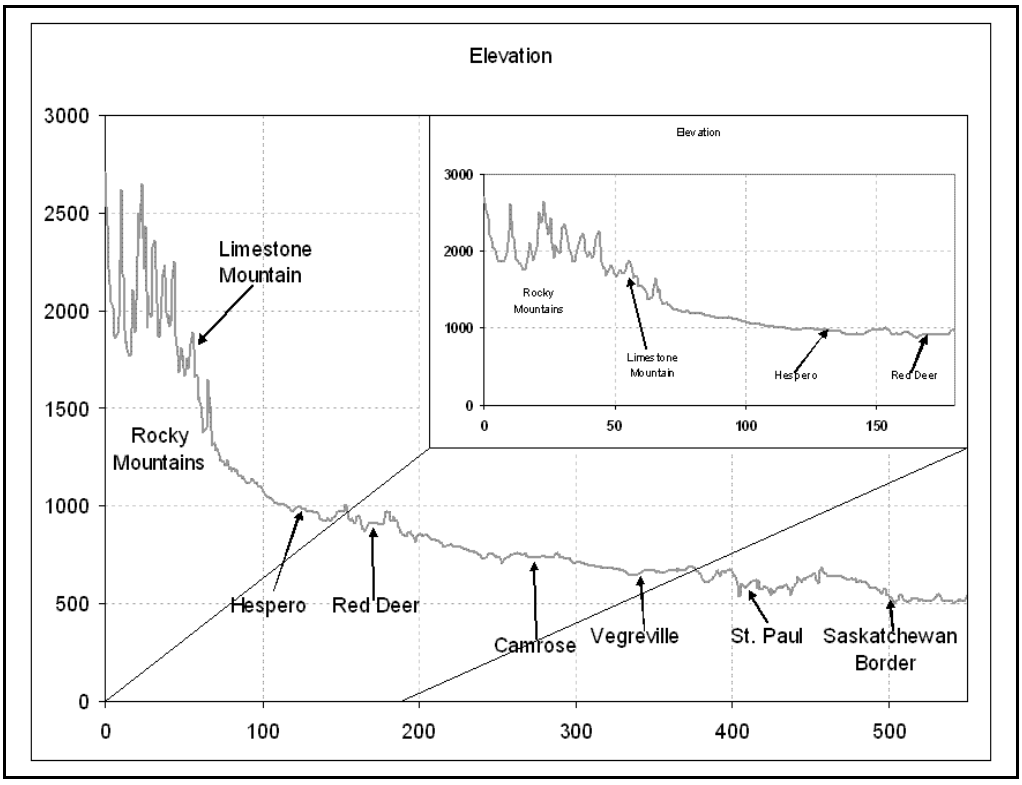

Figure 4.12: A cross section of the elevation profile in Alberta near the UNSTABLE domains. The elevation is in m, while the distance along the cross section is in km. Notable geographical features are displayed for reference. The inset is a close up look at the Rocky Mountains and the foothills.

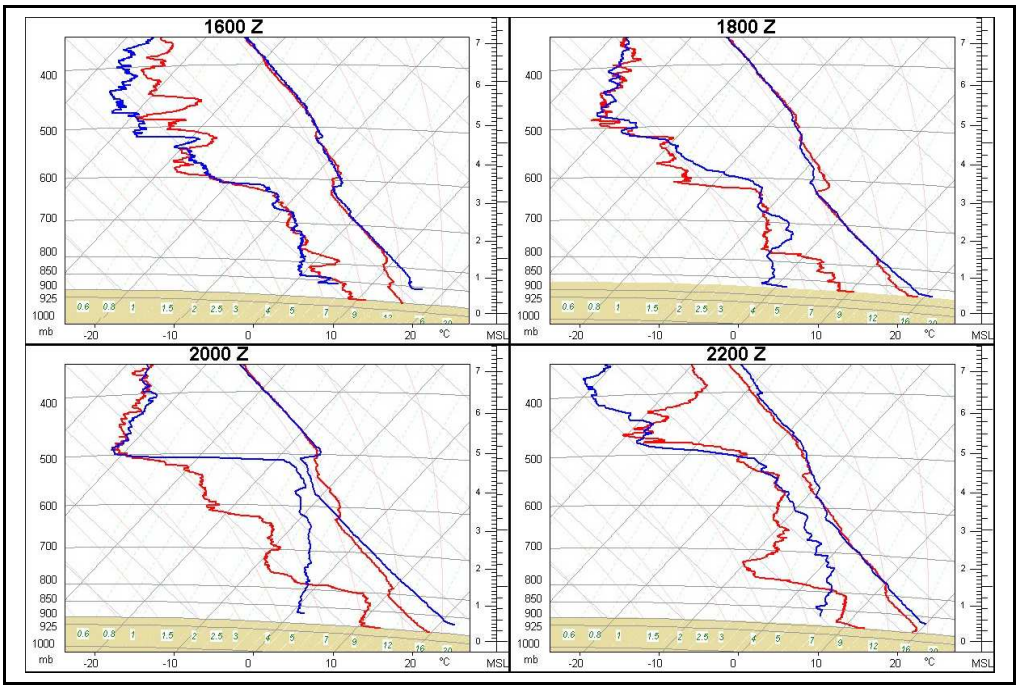

Figure 4.13: Comparison of thermodynamic soundings for different locations and times. The best textbook soundings in either the dry or the moist air are compared.

Left top: Soundings at 1600 UTC at EA3 (red) in the moist air and at MB1 (blue) in the dry air.

Right top: Soundings at 1800 UTC at WVX (red) in the moist air and at MB2 (blue) in the dry air.

Left bottom: Soundings at 2000 UTC at EA3 (red) in the moist air and at MB2 (blue) in the dry air.

Right bottom: Soundings at 2200 UTC at EA3 (red) in the moist air and at MB2 (blue) in the dry air.

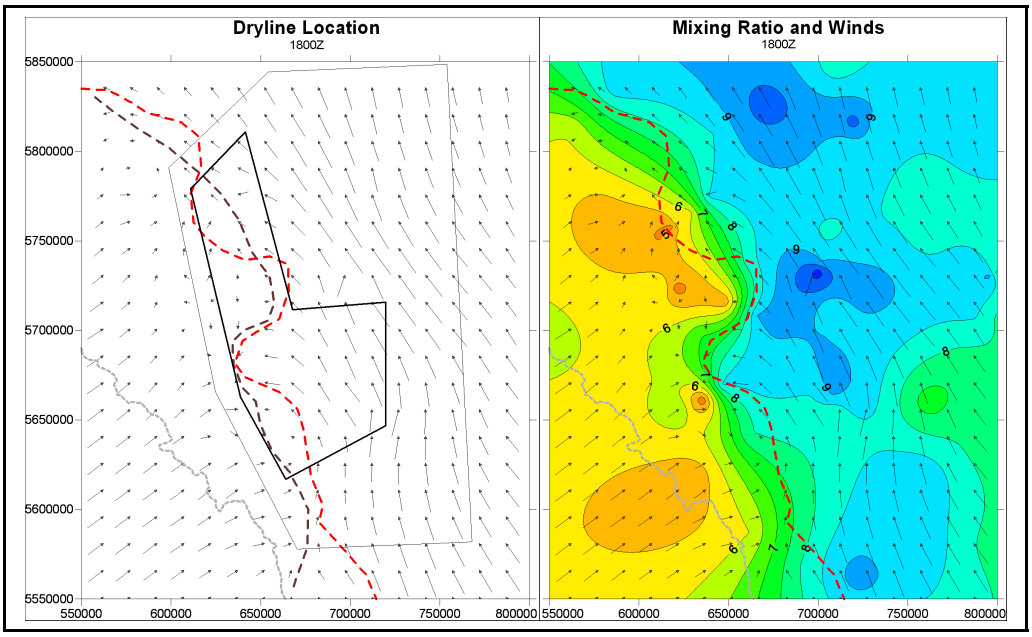

Figure 4.14: Comparison of the analysed dryline location with the location of the cloud – no cloud boundary from satellite images at 1800 UTC. The dryline is shown by a dashed brown line, while the boundary between clouds is shown by the dashed red line. The mixing ratio and winds are also shown with the scales on the map, with isohumes of mixing ratio labelled in g kg^{-1}. Again, dry air is indicated by orange and yellow colouring, while moist air is indicated by shades of blue.

Figure 4.15: This photo was taken near P3 (the tethersonde site) facing west south west at 1630 UTC. The line of convective clouds parallel to the Rocky Mountains is believed to indicate the convergence associated with the dryline.

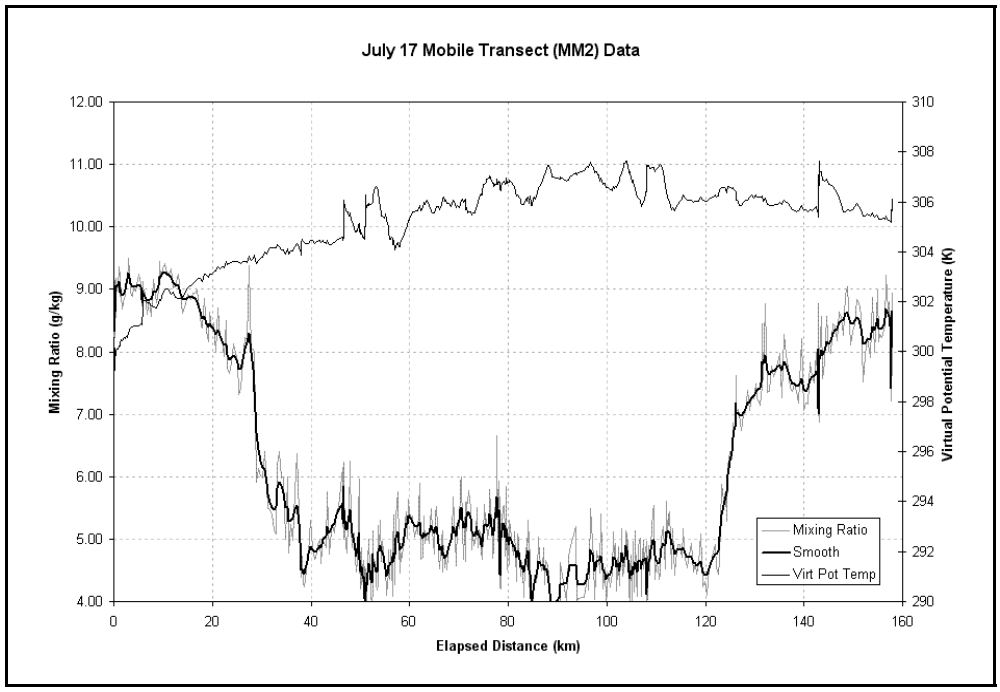

Figure 4.16: Measurements from a mobile surface transect across the dryline. The thin black line is the virtual potential temperature (K), the thin grey line is the mixing ratio (g kg^{-1}), and the thick black line is the mixing ratio after it has been smoothed. In this case, the vehicle was driven from the moist air, across the dryline into the dry air, turned around and driven back across the dryline into the moist air. The horizontal axis is the elapsed distance that the vehicle was driven. Both dryline crossings are evident: one at 30 km along the transect, and the other at 125 km along the transect.

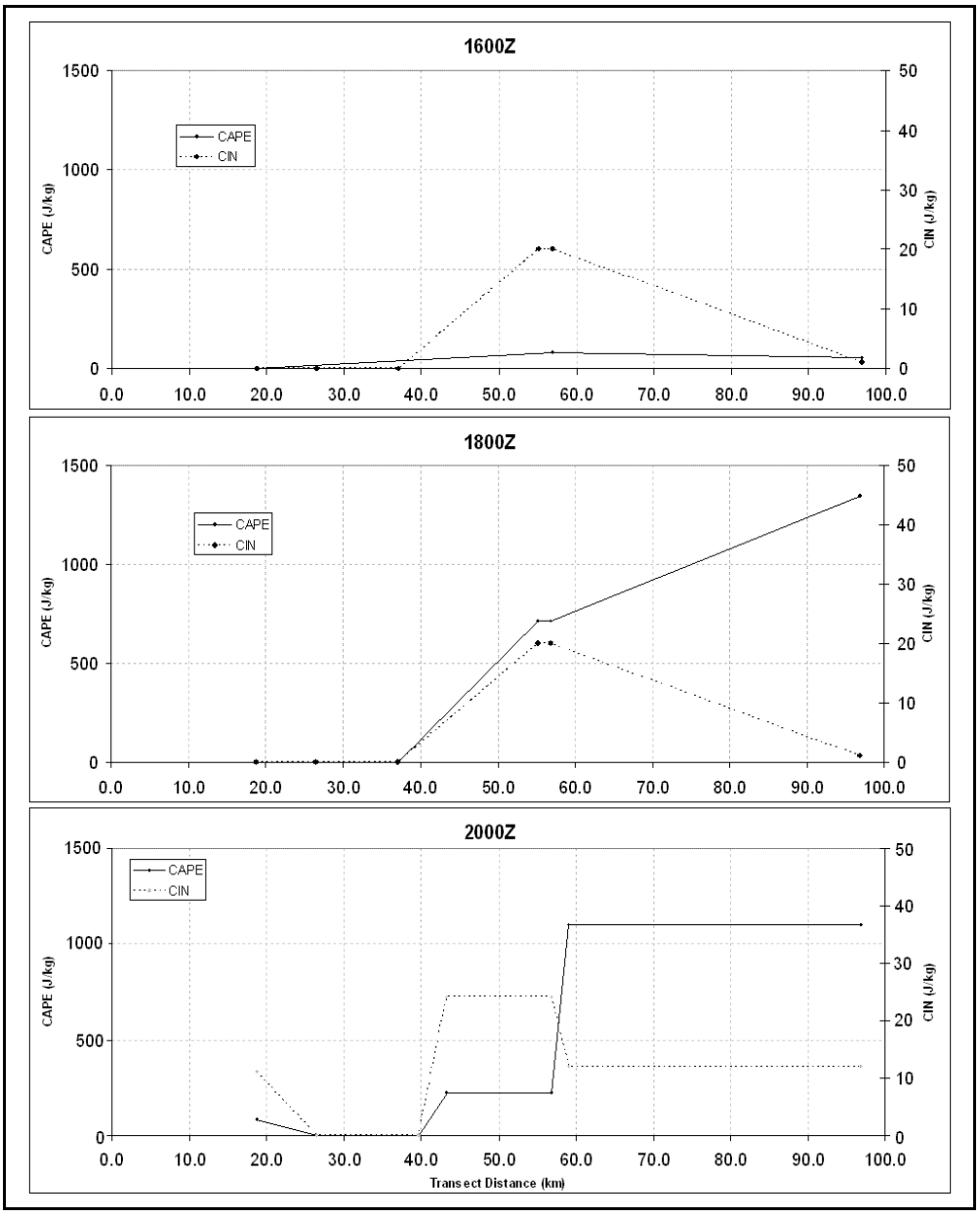

Figure 4.17: Transect of the CAPE and CIN across the dryline at different times. At 1800 UTC, the CAPE is anomalously high and the CIN is anomalously low due to a lack of data throughout the sounding (See section 3.4 c). Low CAPE values on the west side of the dryline prevent severe storms, while high values on the east side allow severe storms if they are triggered.

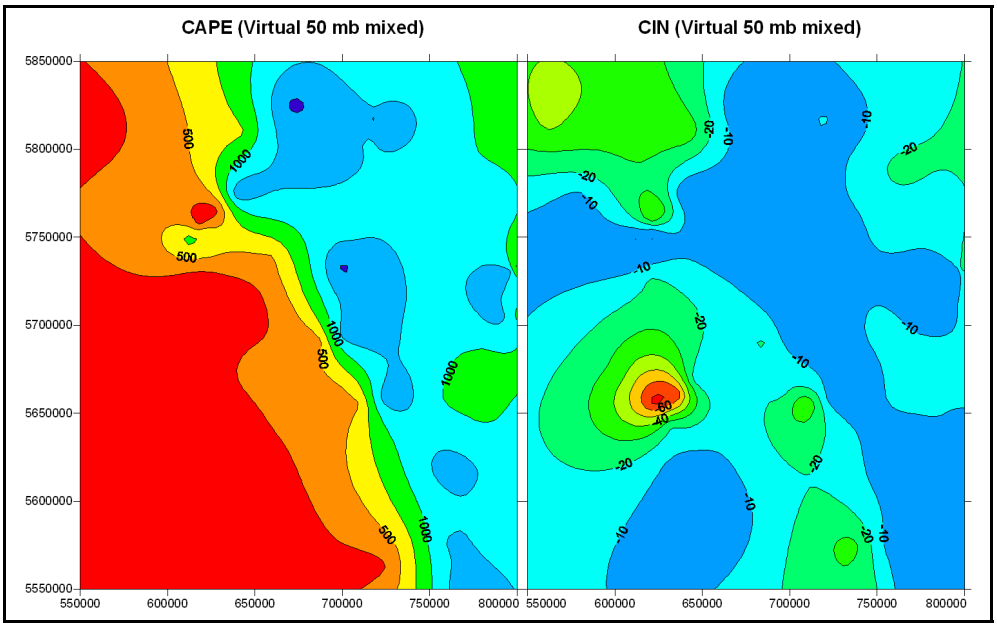

Figure 4.18: Contour maps of CAPE and CIN in the UNSTABLE study area at 1900 UTC. The contour interval for the CAPE is 250 J kg^{-1} while the contour interval for the CIN is 10 J kg^{-1}. Both are calculated using virtual temperature and are based on a lowest 50 mb mixed layer.

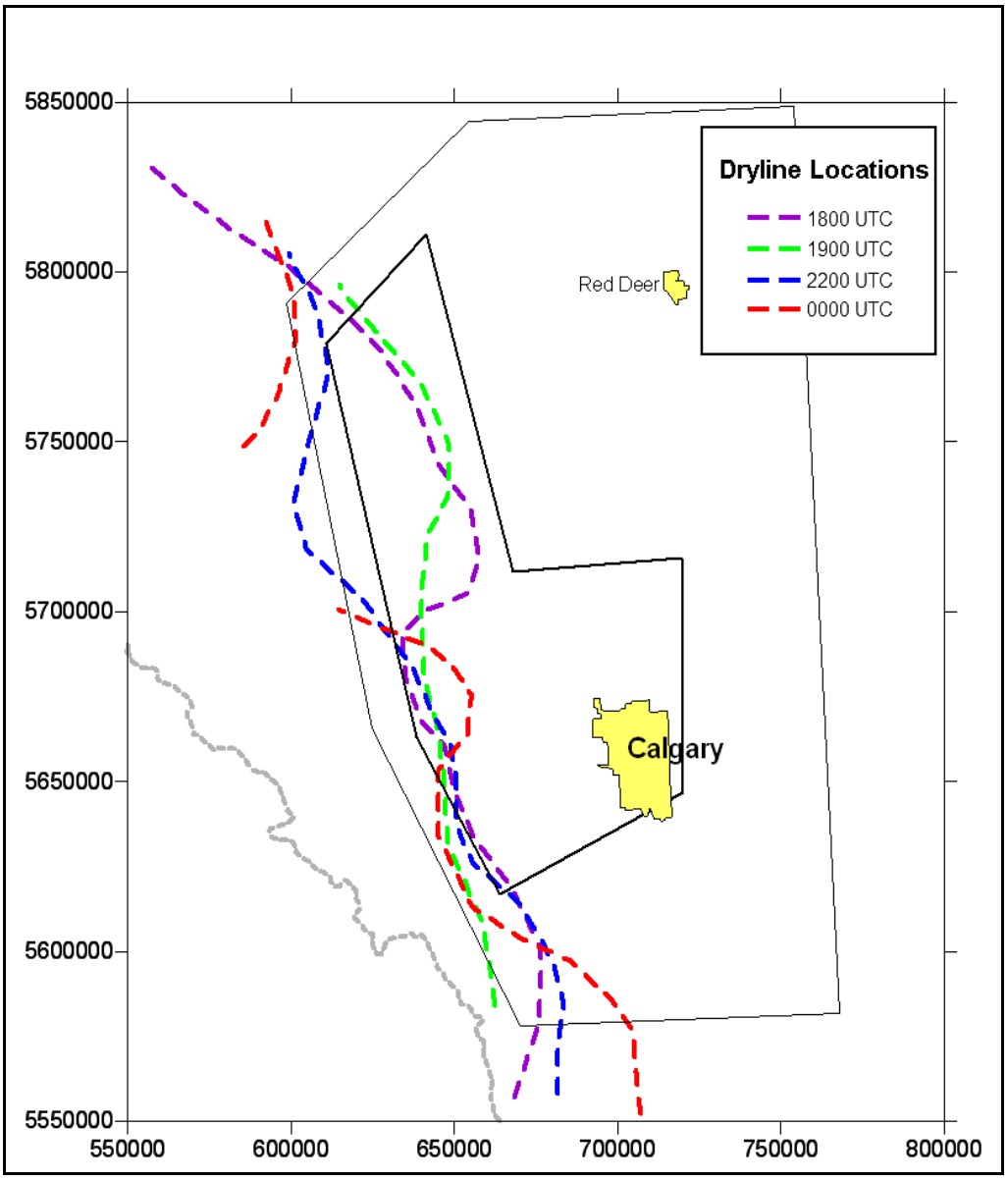

Figure 4.19: The location of selected dryline analyses throughout the day. Dryline locations are shown by the coloured dashed lines. The dryline was defined as the 7 g kg^{-1} isohume. This diagram shows the synoptic quasistationary nature of this dryline and the mesoscale variability.

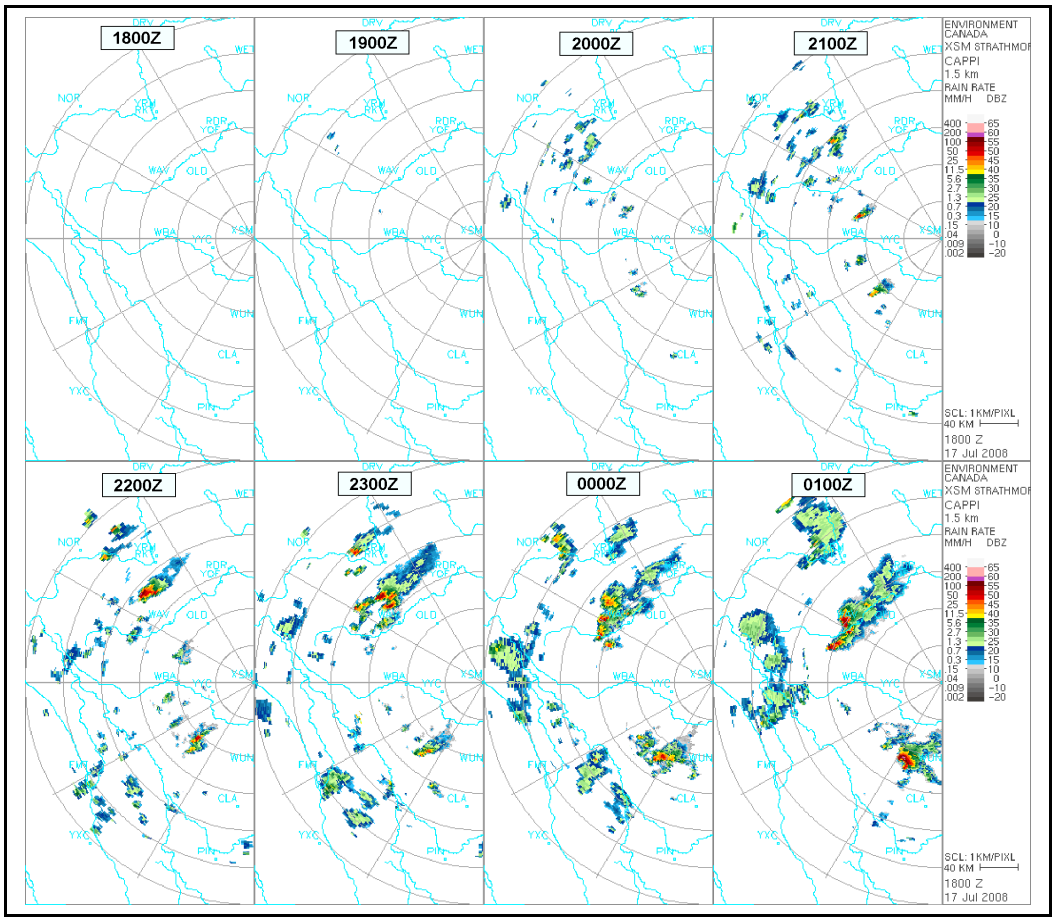

Figure 4.20: 1.5 km CAPPI radar reflectivity images from the Strathmore radar station near Calgary. Shown are images from 1800 UTC on 17 July 2008 through 0100 UTC on 18 July 2008 at 1 hour intervals. The colour scale on the right shows the rainfall rate in mm h^{-1}.

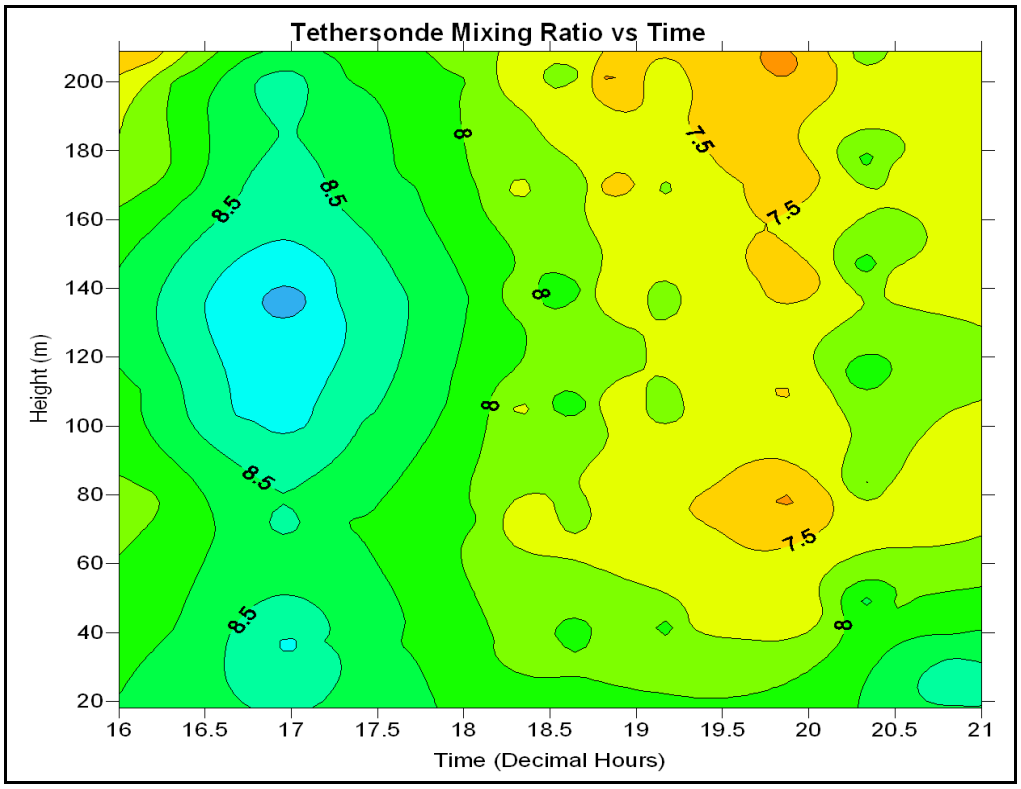

Figure 4.21: Time-height distribution of vapour mixing ratio measured by the tethersonde. This is contoured in 0.25 gkg^{-1} intervals, with the time is in decimal hours in UTC time. 6 measurements were taken between the ground and 200 metres above ground. This figure shows the mixing down of the dry air around 1830 UTC as the dryline mixing zone formed.

Figure 4.22: This photo shows a measurement of the hail size in one of the storms on 17 July 1008. A loonie (Canadian dollar coin – diameter: 26 mm) is provided for comparison. The maximum hail size was a diameter of 21 mm. Most of the hail was close to spherical and opaque.

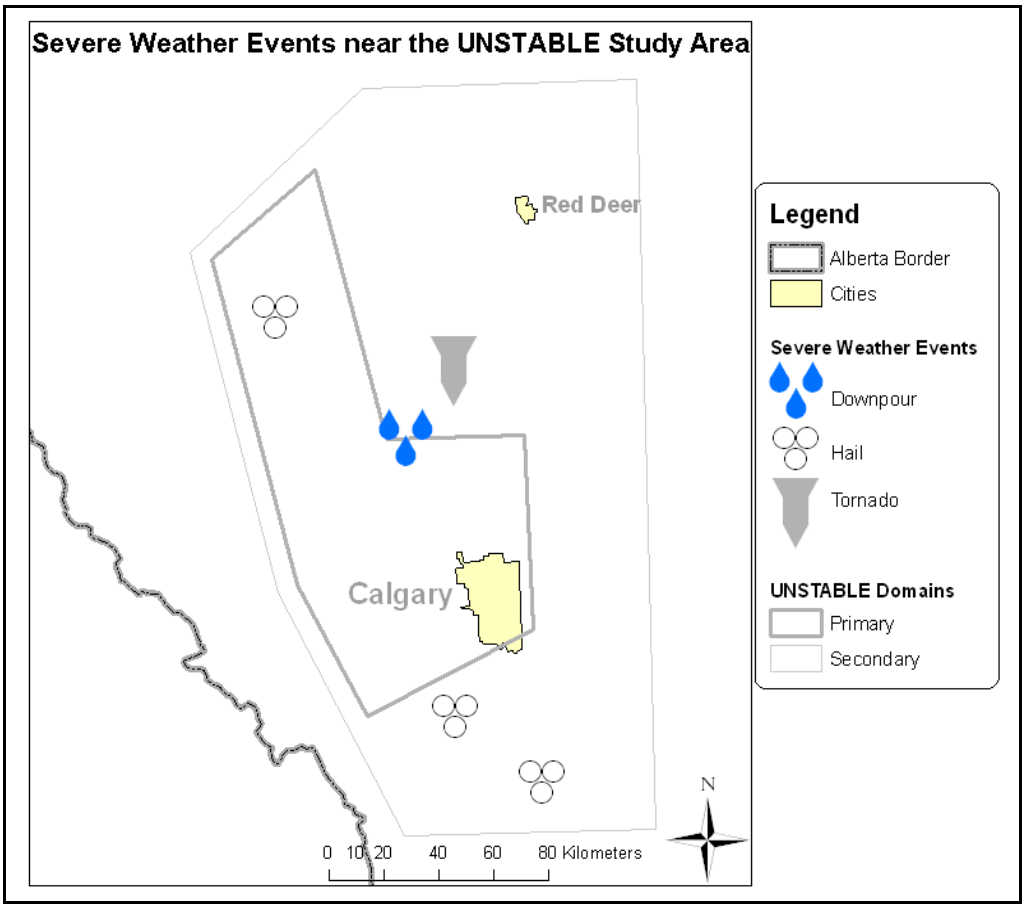

Figure 4.23: This figure shows all of the severe weather events reported to the Environment Canada Stormline on the 17 July 2008 within the UNSTABLE study area. There were a number of severe hail reports, one tornado report, and one report of a heavy downpour. The cities of Calgary and Red Deer and the UNSTABLE domains are included for reference.

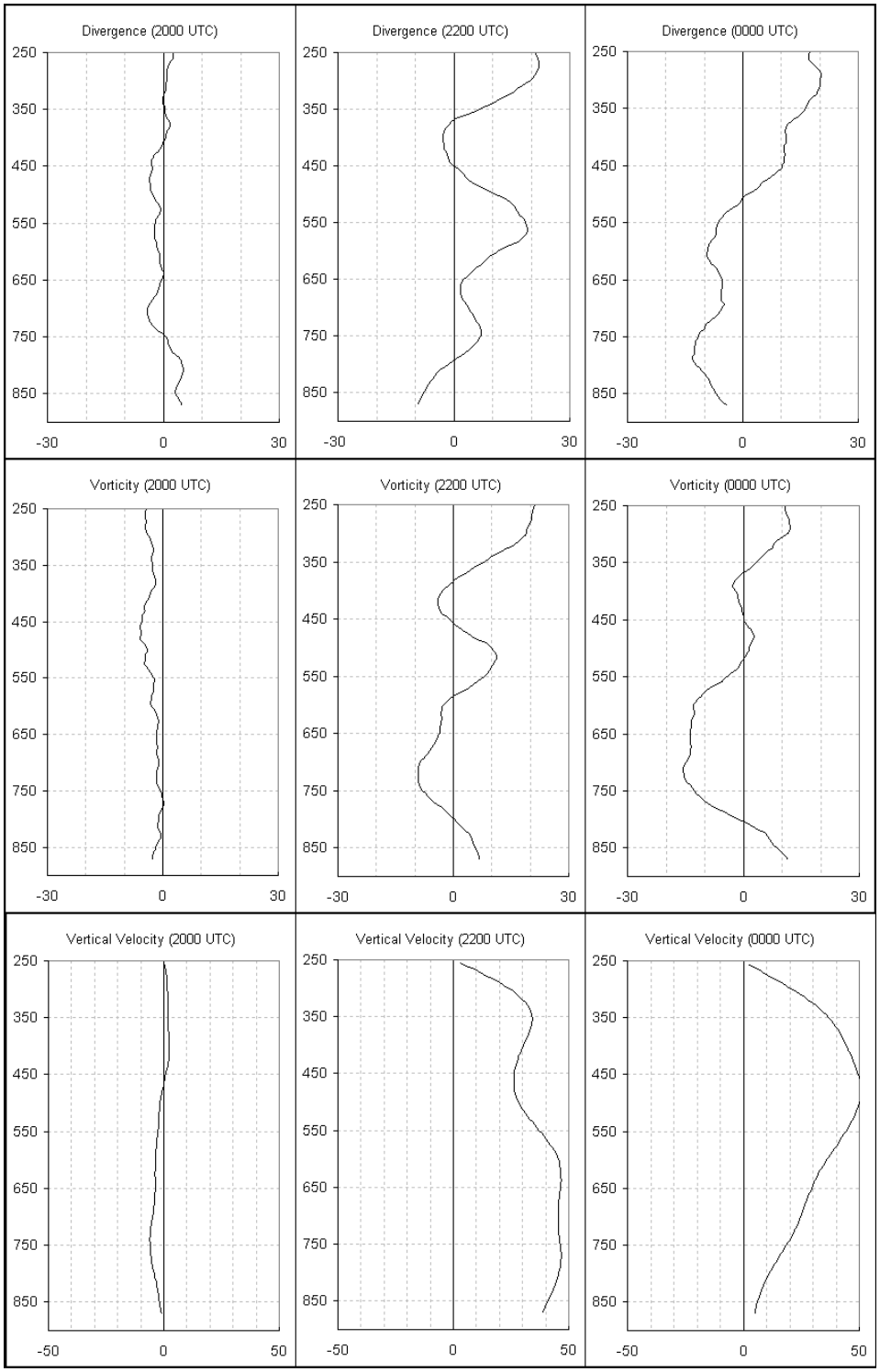

Figure 4.24: Vertical profiles of the divergence, vorticity, and vertical velocity as determined by the triangle depicted by the three soundings shown in Figure 3.3. Divergence and vorticity are given in 10^{-5} m s^{-1} m^{-1} while the vertical velocity is in cm s^{-1}. The vertical axis denotes the pressure in mb. The divergence, vorticity, and vertical velocity were evaluated at 2000 UTC, 2200 UTC, and 0000 UTC.

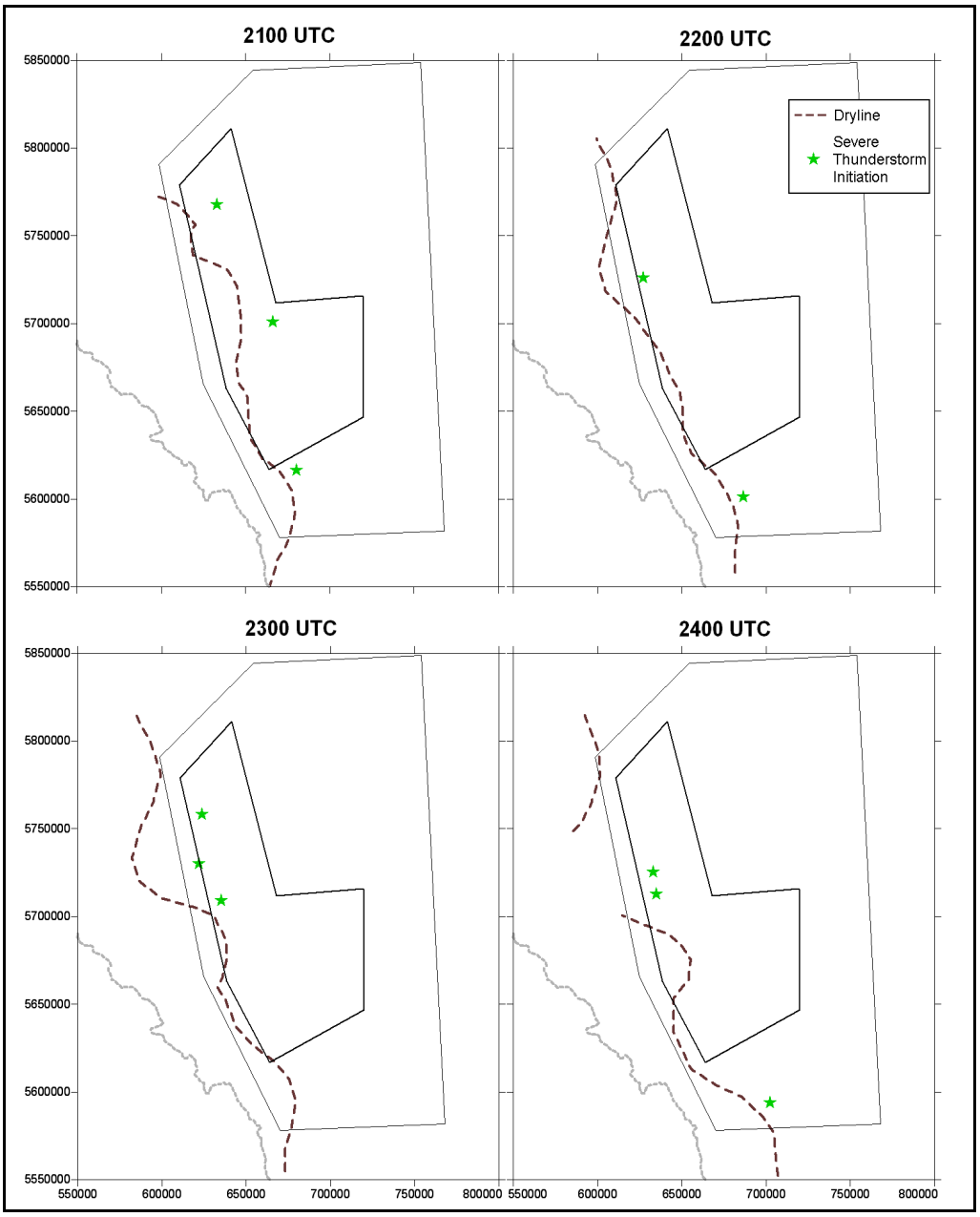

Figure 4.25: Location of the dryline and the initiation of severe convection at 2100 UTC, 2200 UTC, 2300, UTC, and 2400 UTC. The dashed brown line is the location of the 7 g kg^{-1} isohume (the dryline), while the green stars are the location of the initiation of severe thunderstorms (defined as radar echoes greater than 45 dBZ).

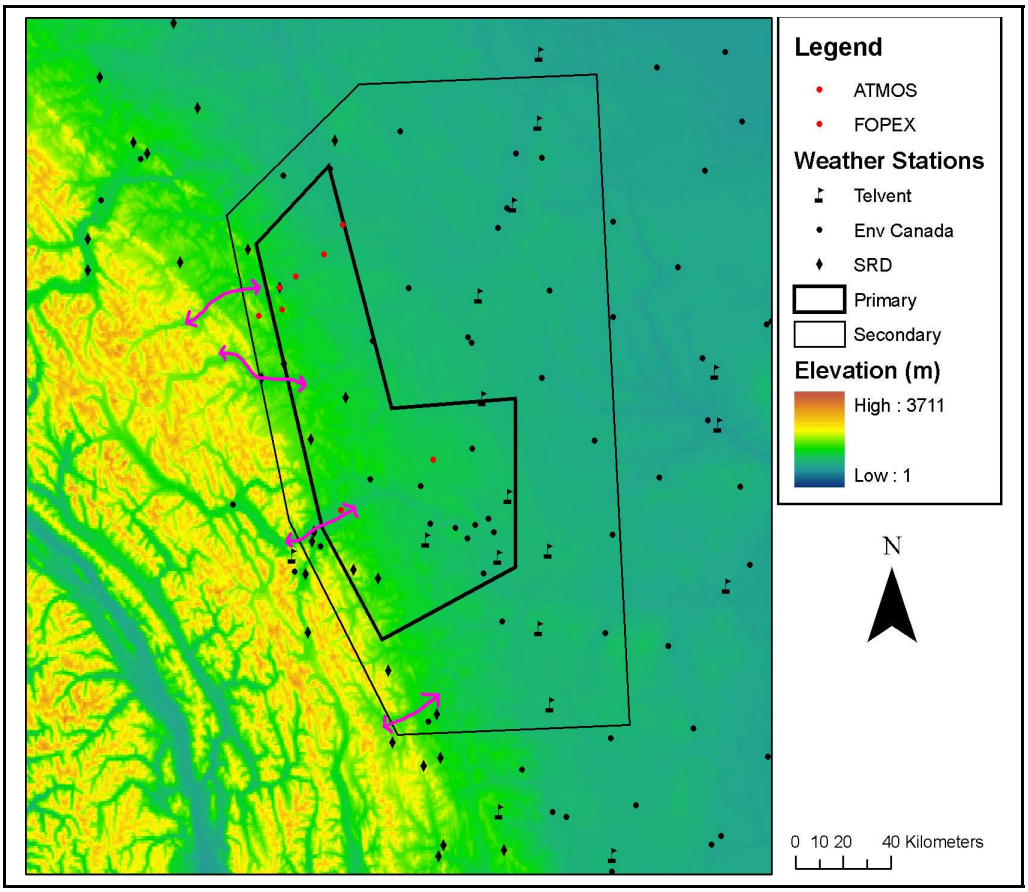

Figure 4.26: This is a digital elevation model in the UNSTABLE domains. The elevation is represented by the colours as indicated in the legend. The UNSTABLE Primary and Secondary domains are added, as are some of the UNSTABLE and operational weather stations. The pink arrows represent areas where there is a significant valley that could allow dry air to flow out of the mountains resulting in a mesoscale bulging dryline.

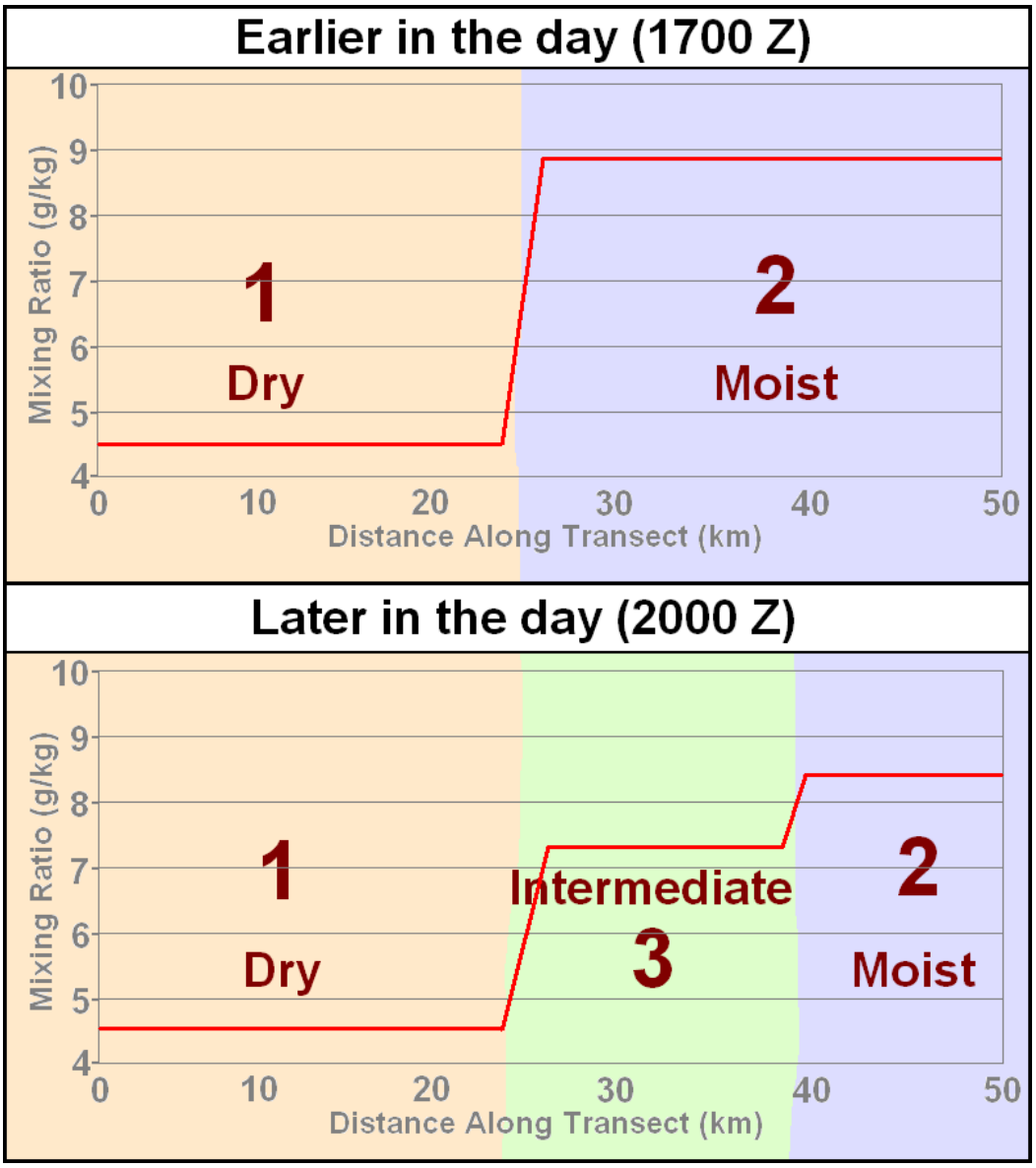

Figure 5.1: Schematic illustrating a transect across the dryline at different times of the day based on the results of the 17 July 2008 case. The red line indicates the mixing ratio (in g kg $^{-1}$) versus the distance along the transect. This figure shows the development of the mixing zone in the afternoon.

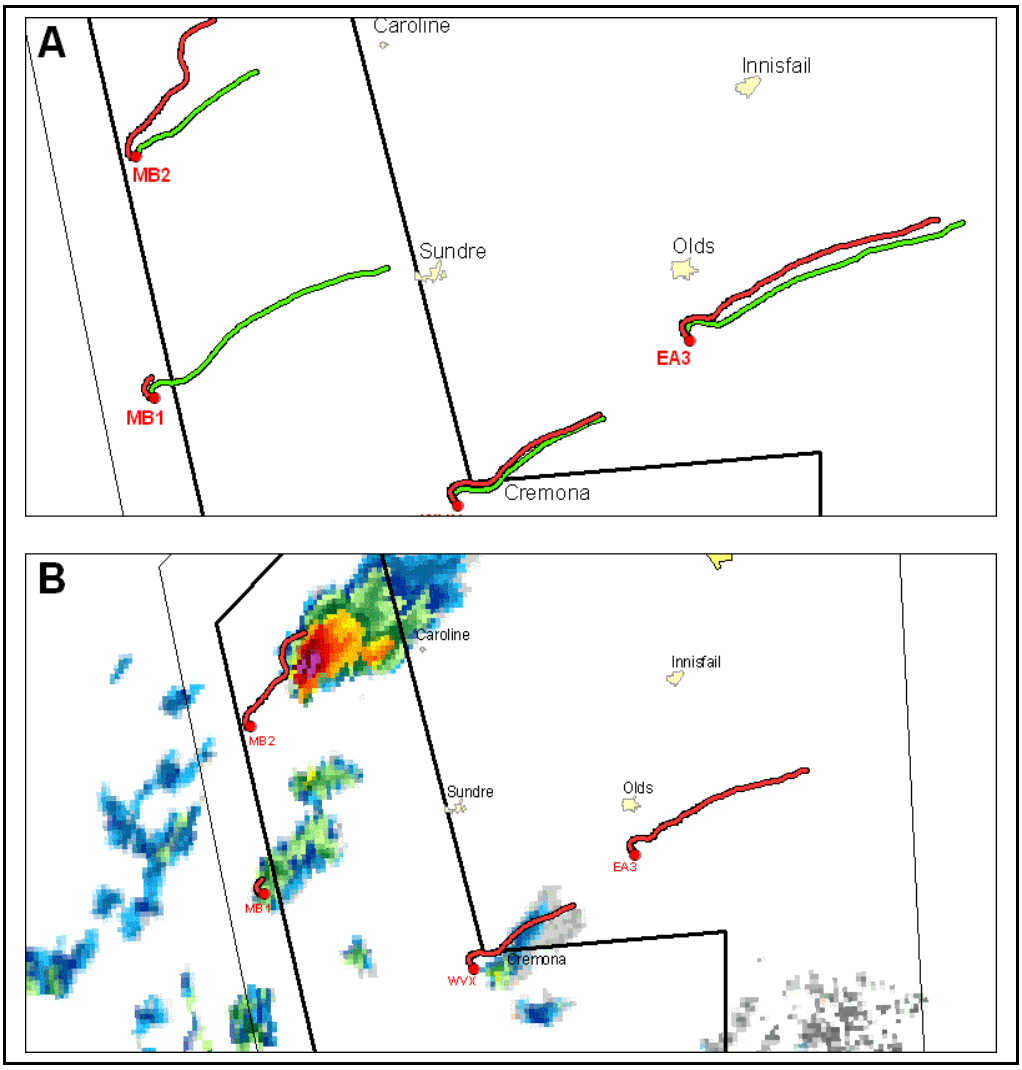

Figure 5.2: The tracks of the soundings compared to the radar images. The green tracks are the 2000 UTC soundings while the red tracks are the 2200 UTC soundings. Comparing the red and green tracks visually shows the increase in divergence in the upper levels. In figure B, the radar image is overlaid in order to show the deviation of the soundings due to storms. The colour scale of the radar is the same as in Figure 4.20.

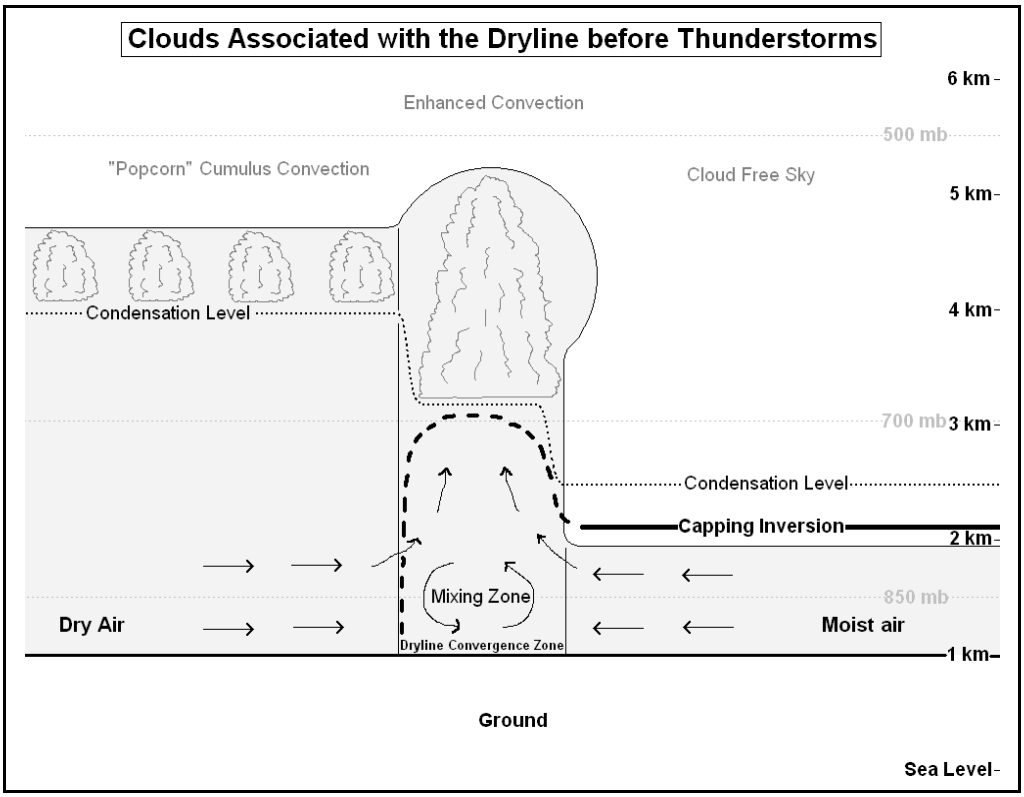

Figure 5.3: Schematic cross section perpendicular to the dryline. The dry air has a component of the wind towards the east, whereas the moist air has a component of the wind blowing west. The dry air and moist air converge creating the mixing zone in the middle of the figure along the dryline. The shaded light grey area is well mixed and shows the mixing height. The capping inversion (thick black line) is present in the moist air, which keeps the mixing height close to the surface, while the mixing height is much higher in the dry air. The thick black dashed line indicates a weakened cap within the mixing zone intersecting with the surface at the western edge of the dryline. The black dashed line indicates the level surface air must reach in order to condense into clouds. The mixing heights do not reach the condensation level in the moist air, preventing clouds from forming. The mixing height extends above the condensation level in the dry air and the mixing zone, allowing clouds to form. Convergence along the dryline and a lower condensation level in the mixing zone contribute to a line of enhanced convective clouds.

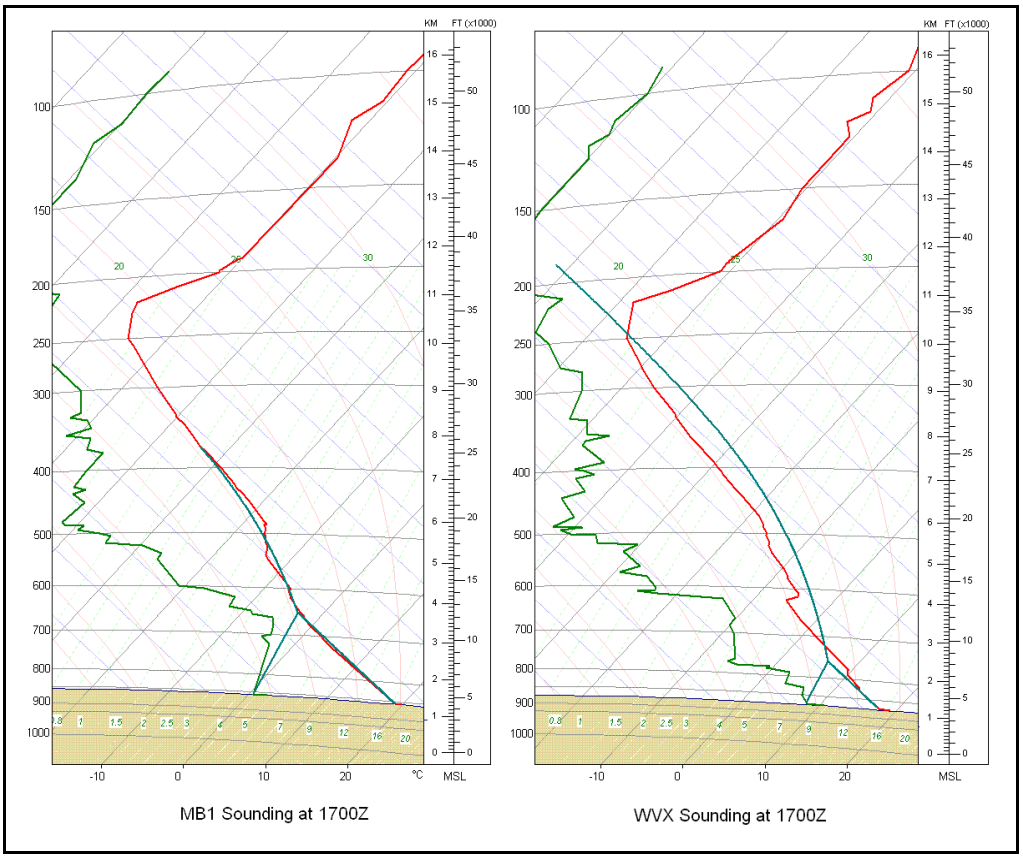

Figure 5.4: A comparison of a sounding in the moist air (WVX) and the dry air (MB2). The horizontal lines are the pressure level in millibars, the diagonal black lines are the temperature, the blue and red lines are the dry and moist adiabats, respectively while the dashed green lines are lines of constant mixing ratio. The thick red line is the temperature, the thick green line is the dewpoint, while the thick blue line is the temperature of an air parcel lifted up through the atmosphere.

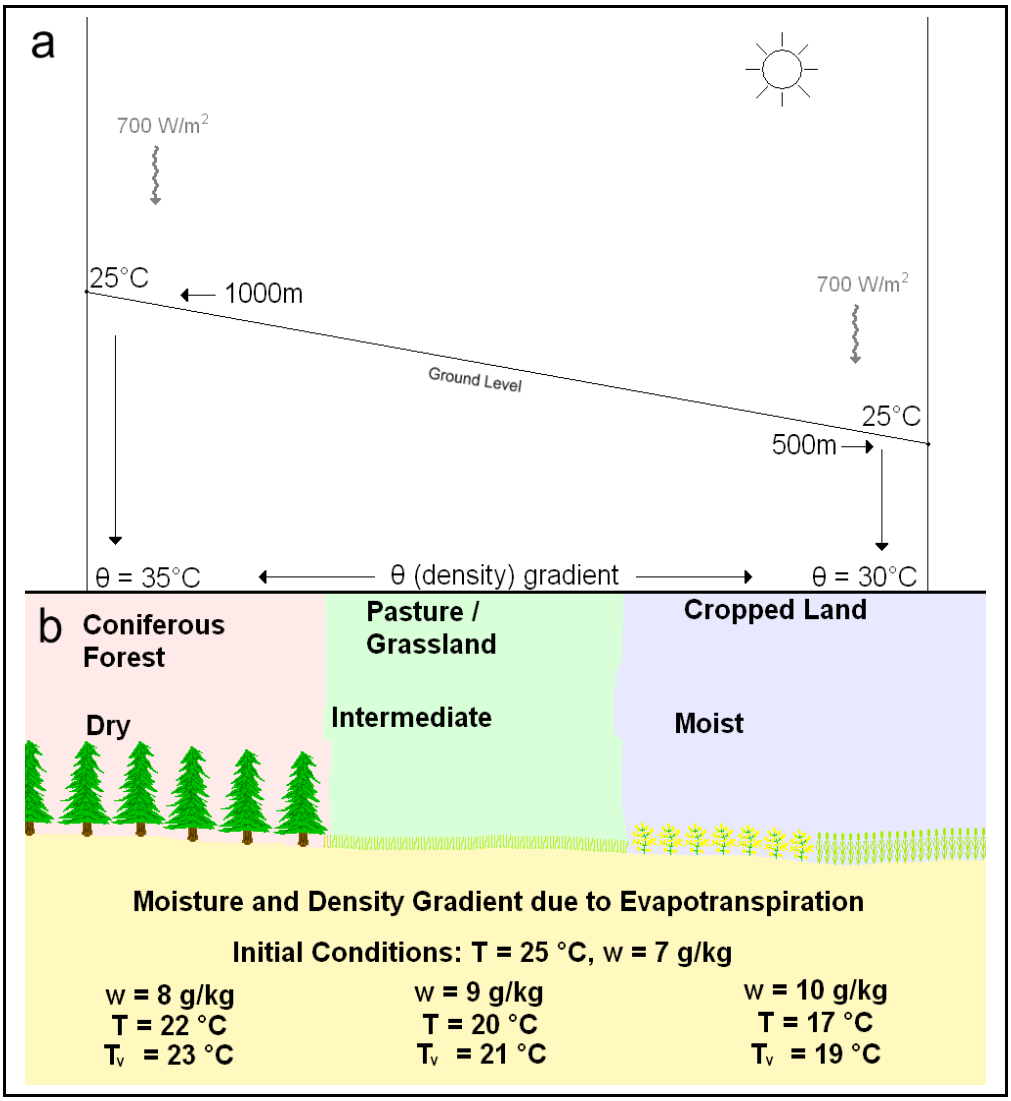

Figure 5.5: Different ways that a gradual density gradient could arise. The top panel shows the issues caused by elevation when using potential temperature to indicate density. Higher elevations could contribute higher potential temperatures (and thus lower densities) based on elevation alone. The bottom panel shows the potential effect of vegetation / land use changes on the virtual temperature. Increases in evapotranspiration can contribute to lowering temperatures and thus higher densities. Both of these effects can affect the density gradient across the dryline.

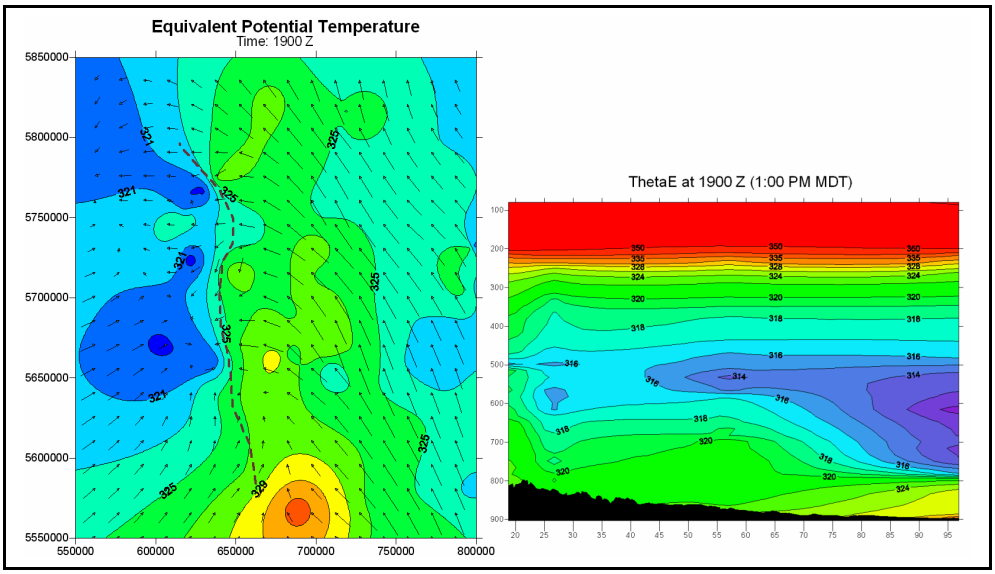

Figure 5.6: A surface analysis and cross section of the equivalent potential temperature. In the surface map, the equivalent potential temperature is contoured in 1 K intervals. The dryline is also shown on the surface map. In the cross section, the interval is variable. The pressure levels in the cross section are in mb, and the distances along the transect in km.

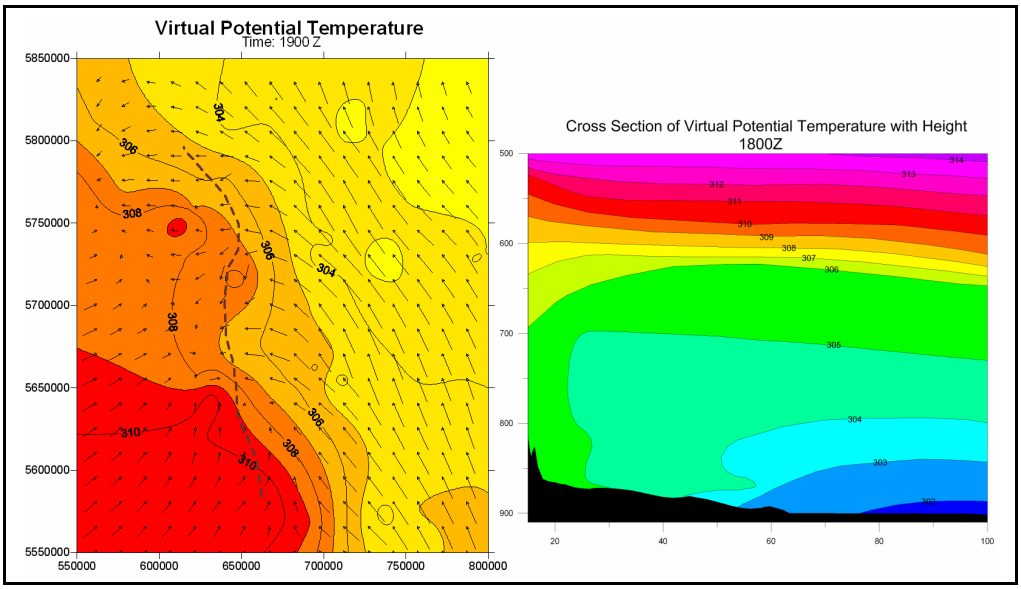

Figure 5.7: A surface analysis and cross section of the virtual potential temperature. Both are contoured in 1 K intervals. The scales on the surface map indicate the UTM coordinates in metres. On the cross section, the distance along the cross section is in km while the vertical scale is the pressure level in mb.

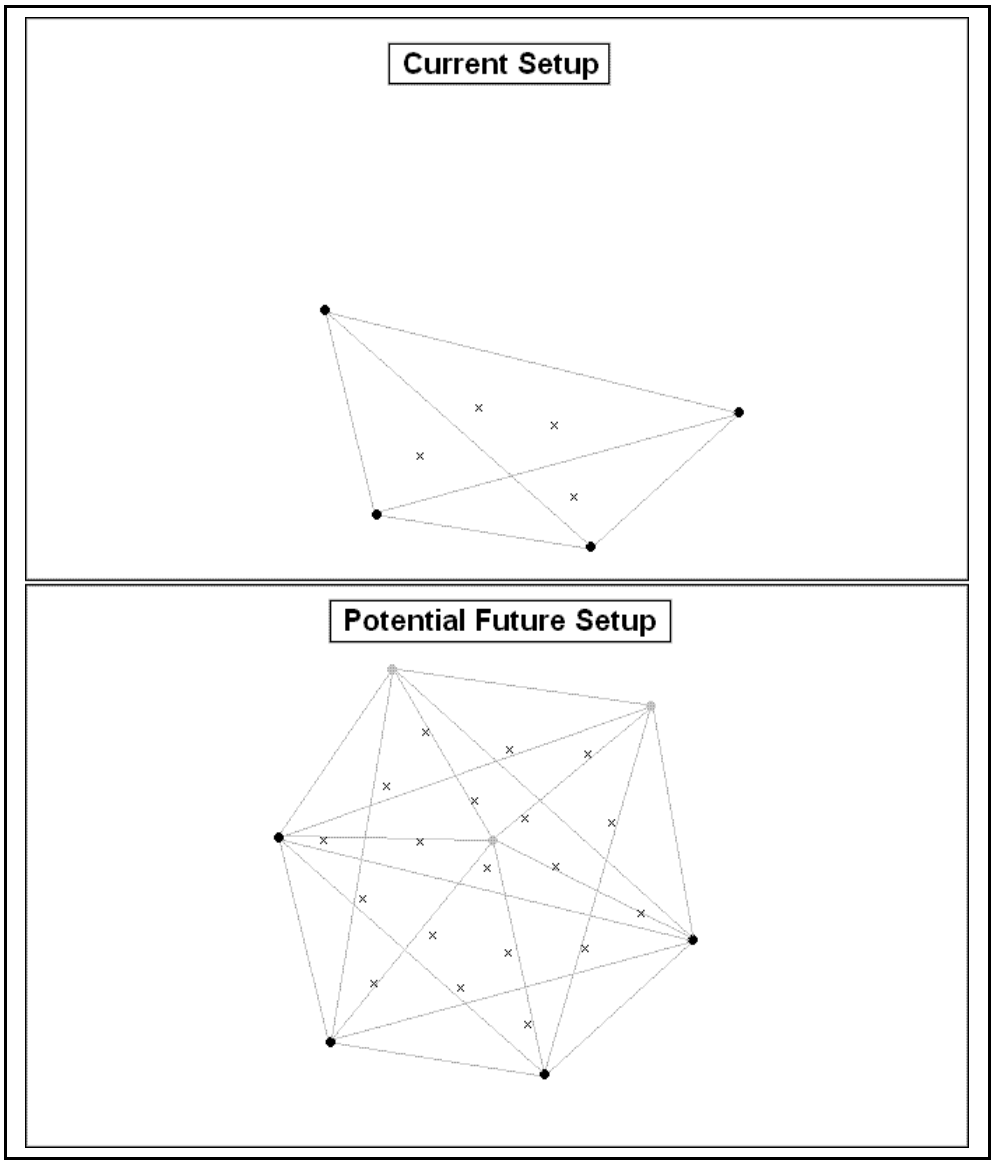

Figure 6.1: A schematic of the potential future setup of soundings. The black dots are the current soundings, the grey dots are the future soundings, the crosses are the potential points where vertical motion could be evaluated, and the lines delineate the triangles formed between soundings. The future setup would allow a three dimensional analysis of convergence, vorticity, and vertical motion.

Bibliography

Atkins, N. T., R. M. Wakimoto, and C. L. Ziegler, 1998: Observations of the Finescale Structure of a Dryline during VORTEX-95. *Monthly Weather Review*, 126, 525-550.

Beebe, R. G., 1958: An Instability Line as Observed by the Tornado Research Airplane. *Journal of Meteorology*, 15, 278-282.

Beebe, R. G., and F. C. Bates, 1955: A Mechanism for Assisting in the Release of Convective Instability. *Monthly Weather Review*, 83, 1-10.

Bluestein, H. B., E. W. McCaul, G. P. Byrd, and G. R. Woodall, 1988: Mobile Sounding Observations of a Tornadic Storm near the Dryline: The Canadian, Texas Storm of 7 May 1986. *Monthly Weather Review*, 116, 1790-1804.

Bluestein, H. B., E. W. McCaul, G. P. Byrd, G. R. Woodall, G. Martin, S. Keighton, L. C. Showell, 1989. Mobile Sounding Observations of a Thunderstorm near the Dryline: The Gruver, Texas Storm Complex of 25 May 1987. *Monthly Weather Review*, 117, 244-250.

Bluestein, H. B., and S. S. Parker, 1993: Modes of Isolated, Severe Convective Storm Formation along the Dryline. *Monthly Weather Review*, 121, 1354-1372.

Brennand, M. P., 1992: Convective Storms and Moisture Fields in LIMEX85: A Case Study. M.Sc. Thesis, University of Alberta, Edmonton, 136 pp.

Carlson, J. D., and R. E. Burgan, 2003: Review of Users' Needs in Operational Fire Danger Estimation: The Oklahoma Example. *International Journal of Remote Sensing*, 24, 8, 1601-1620

Charlton, R. B., B. M. Kachman, and L. Wojtiw, 1995: Urban Hailstorms: A View from Alberta. *Natural Hazards*, 12, 29-75.

Crawford, T. M., and H. B. Bluestein, 1997: Characteristics of Dryline Passage during COPS-91. *Monthly Weather Review*, 125, 463-477.

Djurić, D., 1994: *Weather Analysis*, Prentice Hall Inc., New Jersey, 300 pp.

Doswell, C. A., and E. N. Rasmussen, 1994: The Effect of Neglecting the Virtual Temperature Correction on CAPE Calculations. *Weather and Forecasting*, 9, 619-623.

Dupilka, M. L., 2006: On Forecasting Severe Storms in Alberta using Environmental Sounding Data. Ph.D. Thesis, University of Alberta, Edmonton, 235 pp.

Dupilka, M. L., and G. W. Reuter, 2005: An Examination of Three Severe Convective Storms that Produced Significant Tornadoes in Central Alberta. *National Weather Digest*, 29, 47-59.

Dupilka, M. L., and G. W. Reuter, 2006: Forecasting Tornadic Thunderstorm Potential in Alberta Using Environmental Sounding Data. Part I: Wind Shear and Buoyancy and Part II: Helicity, Precipitable Water, and Storm Convergence. *Weather and Forecasting*, 21, 325-346.

Environment Canada, 2008: Weather Watches, Warnings, and Advisories. <http:// www.msc-smc.ec.gc.ca/cd/brochures/warning_e.cfm>, Accessed February 29th, 2008.

English M., 1973: Part II: Growth of Large Hail in the Storm. *Alberta Hail-storms, Meteorology Monograph, American Meteorological Society,* 36, 37-98.

Etkin, D., and S. E. Brun, 2001: Canada's Hail Climatology: 1977 - 1993.

Fujita, T., 1958: Structure and movement of a dry front. *Bulletin of the American Meteorological Society*, 39, 574-582.

Fujita, T., 1970: The Lubbock Tornadoes: A Study of Suction Spots. *Weatherwise*, 23, 4, 161-173.

Fawbush, E. J., R. C. Miller, L. G. Starrett, 1951: An Empirical Method of Forecasting Tornado Development. *Bulletin of the American Meteorological Society*, 32, 1-9.

Hage, K., 2003: On Destructive Canadian Prairie Windstorms and Severe Winters: A Climatological Assessment in the Context of Global Warming. *Natural Hazards*, 29, 207-238.

Hane, C. E., H. B. Bluestein, T. M. Crawford, M. E. Baldwin, R. M. Rabin, 1997: Severe Thunderstorm Development in Relation to Along-Dryline Variability: A Case Study. *Monthly Weather Review*, 125, 231-251.

Hane, C. E., C. L. Ziegler, and H. B. Bluestein, 1993: Investigation of the Dryline and Convective Storms Initiated Along the Dryline: Field Experiments During COPS-91. *Bulletin of the American Meteorological Society*, 74, 11, 2133-2145

Hill, L. M., 2006: Drylines Observed in Alberta during AGAME. M.Sc. Thesis, University of Alberta, Edmonton, 111 pp.

Holt, A. R., P. I. Joe, R. McGuinness, E. Torlaschi, T. Nichols, F. Bergwall, and D. A. Holland, 1994: Simultaneous Polarization and Doppler Observations of Severe Convective Storms in Central Alberta. *Atmospheric Research*, 33, 37-56.

Kalnay, E. and Coauthors, 1996: The NCEP/NCAR Reanalysis 40-year Project. *Bulletin of the American Meteorological Society*, 77, 437-471.

Knott, R. J., and N. M. Taylor, 2000: Operational Aspects of the Alberta Severe Weather Outbreak of 29 July 1993. *National Weather Digest*, 24, 11-23.

Larochelle, B., 1994: Application of Synthetic Dual-Doppler technique to an operational Doppler Weather Radar. M.Sc. Thesis, University of Alberta, Edmonton, 158 pp.

Matteson, G. T. 1969. The West Texas Dry Front of June 1967. M. Sc. Thesis, University of Oklahoma, Norman, 63 pp.

McCarthy, J. and S. E. Koch, 1982: The Evolution of an Oklahoma Dryline. Part I: A Meso- and Subsynoptic-Scale Analysis. *Journal of the Atmospheric Sciences*, 39, 225-236.

McGuire, E. L., 1962: The Vertical Structure of Three Dry Lines as Revealed by Aircraft Traverses. National Severe Storms Project Report No. 7, Department of Commerce, Weather Bureau, Washington 25, D. C.

Miller, J. A., T. A. Kovacs, P. R. Bannon, 2001: A Shallow Water Model of the Diurnal Dryline. *Journal of the Atmospheric Sciences*, 58, 3508-3524.

Miller, R. C, 1959: Tornado-Producing Synoptic Patterns. *Bulletin of the American Meteorological Society*, 40, 465-472.

Natural Resources Canada, 2009: Geogratis. <http://geogratis.cgdi.gc.ca/geogratis/en/index.html>, Accessed May 3rd, 2009. © Department of Natural Resources Canada. All rights reserved.

Ogura, Y. and Y. Chen, 1977: A Life History of an Intense Mesoscale Convective Storm in Oklahoma. *Journal of the Atmospheric Sciences*, 34, 1458-1476.

Parsons, D. B., M. A. Shapiro, R. M. Hardesty, R. J. Zamora, and J. M. Intrieri, 1991: The Finescale Structure of a West Texas Dryline. *Monthly Weather Review*, 119, 1242-1258.

Peterson, R. E., 1983: The West Texas Dryline: Occurrence and Behaviour. Preprints, *13th Conference on Severe Local Storms*, American Meteorological Society, 9-11.

Pietrycha, A. E., and E. N. Rasmussen, 2004: Finescale Observations of the Dryline: A Mobile Mesonet Perspective. *Weather and Forecasting*, 19, 1075-1088.

Raddatz, R. L., 1998: Anthropogenic Vegetation Transformation and the Potential for Deep Convection on the Canadian Prairies. *Canadian Journal of Soil Science*, 657-666.

Raddatz, R. L., 2003: Agriculture and Tornadoes on the Canadian Prairies: Potential Impact of Increasing Atmospheric CO_2 on Summer Severe Weather. *Natural Hazards*, 290, 113-122.

Renick J. H., and J. B. Maxwell, 1977: Forecasting Hailfall in Alberta. *Hail: A Review of Hail Science and Hail Suppression, Meteorology Monograph, American Meteorological Society*, 38, 145-151.

Reuter, G. W., and C. D. Nguyen, 1993: Organization of Cloud and Precipitation in an Alberta Storm. *Atmospheric Research*, 30, 127-141.

Rhea, J. O., 1966: A Study of Thunderstorm Formation along Dry Lines. *Journal of Applied Meteorology*, 5, 58-63.

Rogers, R. R., and N. K. Sakellariou, 1986: Precipitation Production in Three Alberta Thunderstorms. *Atmosphere-Ocean*, 24, 145-168.

Rogers, R. R., and M. K. Yau, 1989: A Short Course in Cloud Physics. Pergamon Press, Ontario, Canada, 293 pp.

Schaefer, J. T., 1974a: A Simulative Model of Dryline Motion. *Journal of the Atmospheric Sciences*, 31, 956-964.

Schaefer, J. T., 1974b: The Life Cycle of a Dryline. *Journal of Applied Meteorology*, 13, 444-449.

Shaw, B. L., R. A. Pielke, and C. L. Ziegler, 1997: A Three Dimensional Numerical Simulation of a Great Plains Dryline. *Monthly Weather Review*, 125, 1489-1506.

Schaefer, J. T., 1986: The Dryline. *Mesoscale Meteorology and Forecasting*, P. S. Ray, Ed., American Meteorological Society, 549-572.

Smith, S. B., G. W. Reuter, M. K. Yau, 1998: The Episodic Occurrence of Hail in Central Alberta and the Highveld of South Africa. *Atmosphere-Ocean*, 36, 2, 169-178.

Smith, S. B., and M. K. Yau, 1993: The Causes of Severe Convective Outbreaks in Alberta. Part I: A Comparison of a Severe Outbreak with Two Nonsevere Events and Part II: Conceptual Model and Statistical Analysis. *Monthly Weather Review*, 121, 1099-1133.

Strong, G. S., 1986: Synoptic to Mesoscale Dynamics of Severe Thunderstorm Environments: A Diagnostic Study with Forecasting Applications. PhD Thesis, University of Alberta, Edmonton.

Strong, G. S., 1997: Atmospheric Moisture Budget Estimates of Regional Evapotranspiration from RES-91. *Atmosphere-Ocean*, 35, 1, 29-63

Summers, E, personal email communication, April 9, 2009.

Taylor, N., D. Sills, J. Hanesiak, J. Milbrandt, P. McCarthy, C. Smith, and G. Strong, 2007: The Understanding Severe Thunderstorms and Alberta Boundary Layers Experiment (UNSTABLE) Scientific Overview. <http://www.umanitoba.ca/faculties/environment/envirogeog/weather/unstable/>, Accessed February 29th, 2008.

Wallace, J. M., and P. V. Hobbs, 1977: *Atmospheric Science: An Introductory Survey*. San Diego, California, Elsevier Science, 467 pp.

Xin, L. and G. W. Reuter, 1998: VVP Technique Applied to an Alberta Storm. *Journal of Atmospheric and Oceanic Technology*, 15, 587-592.

Ziegler, C. L., and C. E. Hane, 1993: An Observational Study of the Dryline. *Monthly Weather Review*, 121, 1134-1151.

Ziegler, C. L., T. J. Lee, and R. A. Pielke, 1997: Convective Initiation at the Dryline: A Modelling Study. *Monthly Weather Review*, 125, 1001-1026.

Ziegler, C. L., W. J. Martin, R. A. Pielke, and R. L. Walko, 1995: A Modelling Study of the Dryline. *Journal of the Atmospheric Sciences*, 52, 2, 263-285.

Ziegler, C. L, and E. N. Rasmussen, 1998: The Initiation of Moist Convection at the Dryline: Forecasting Issues from a Case Study Perspective. *Weather and Forecasting*, 13, 1106-1131.

Appendices

Appendix A: Method of calculating kinematic variables
(Summarised from Djurić, 1994)

Consider a field variable U that varies continuously in x and y where (x, y) denotes the coordinates in a horizontal Cartesian plane. Suppose that $U(x_0,y_0) = U_0$. For a point (x, y) close to (x_0, y_0), we can approximate U(x, y) by the first order Taylor series expansion:

$$U(x,y) = U_0 + (x - x_0)\frac{\partial U}{\partial x} + (y - y_0)\frac{\partial U}{\partial y} \qquad \text{(A-1)}$$

Here $\partial U / \partial x$ and $\partial U / \partial y$ denote partial derivatives in x and y at point (x_0, y_0).

Let A, B, and C denote locations of three points with co-ordinates (x_A, y_A), (x_B, y_B), and (x_C, y_C), respectively. Let $u_A = u(x_A, y_A)$, $u_B = u(x_B, y_B)$, and $u_C = u(x_C, y_C)$ denote the x component of horizontal wind vector at points A, B , and C. Substituting into (1) we derive a system of three linear equations:

$$u_A = u_0 + (x_A - x_0)\frac{\partial u}{\partial x} + (y_A - y_0)\frac{\partial u}{\partial y} \qquad \text{(A-2)}$$

$$u_B = u_0 + (x_B - x_0)\frac{\partial u}{\partial x} + (y_B - y_0)\frac{\partial u}{\partial y} \qquad \text{(A-3)}$$

$$u_C = u_0 + (x_C - x_0)\frac{\partial u}{\partial x} + (y_C - y_0)\frac{\partial u}{\partial y} \qquad \text{(A-4)}$$

We can solve (2)-(4) by substitution to find the two unknown variables $\partial u / \partial x$ and $\partial u / \partial y$.

$$\frac{\partial u}{\partial x} = \frac{u_A(y_B - y_C) + u_B(y_C - y_A) + u_c(y_A - y_B)}{x_A(y_B - y_C) + x_B(y_C - y_A) + x_c(y_A - y_B)} \qquad \text{(A-5)}$$

$$\frac{\partial u}{\partial y} = \frac{u_A(x_B - x_C) + u_B(x_C - x_A) + u_c(x_A - x_B)}{y_A(x_B - x_C) + y_B(x_C - x_A) + y_c(x_A - x_B)} \qquad \text{(A-6)}$$

Similarly, we can derive two components of the horizontal gradient of the horizontal y component of the wind vector v, to get:

$$\frac{\partial v}{\partial x} = \frac{v_A(y_B - y_C) + v_B(y_C - y_A) + v_c(y_A - y_B)}{x_A(y_B - y_C) + x_B(y_C - y_A) + x_c(y_A - y_B)} \qquad \text{(A-7)}$$

$$\frac{\partial v}{\partial y} = \frac{v_A(x_B - x_C) + v_B(x_C - x_A) + v_c(x_A - x_B)}{y_A(x_B - x_C) + y_B(x_C - x_A) + y_c(x_A - x_B)} \qquad \text{(A-8)}$$

After evaluating these equations, $\partial u / \partial x$, $\partial u / \partial y$, $\partial v / \partial x$, and $\partial v / \partial y$ are all known, and it is possible to calculate the horizontal divergence and vorticity using the following equations:

$$Divergence = \nabla \cdot V = \frac{\partial u}{\partial x} + \frac{\partial v}{\partial y} \qquad \text{(A-9)}$$

$$Vorticity = \nabla \times V = \frac{\partial v}{\partial x} - \frac{\partial u}{\partial y} \qquad \text{(A-10)}$$

This allows for the computation of divergence and vorticity at any level for which the winds are known at all three soundings, giving a detailed profile of the mesoscale atmospheric dynamics.

b) Vertical velocity

By integrating the divergence from the surface to the tropopause, and assuming a zero velocity at the tropopause, one can determine the vertical velocity. This is done as follows:

We start off with the continuity equation:

$$\frac{\partial u}{\partial x} + \frac{\partial v}{\partial y} = -\frac{\partial \omega}{\partial p} \qquad \text{(A-11)}$$

The left hand side of the equation is just the horizontal divergence, while the right hand side is the partial derivative of the vertical velocity in pressure coordinates with respect to the pressure in units of Pa^{-1}. Integrating this equation from any

given pressure level to the tropopause allows for the calculation of the vertical velocity. This is done as follows:

$$\int_{p1}^{p2} \frac{\partial \omega}{\partial p} dp = -\int_{p1}^{p2} (\nabla \cdot V) dp \qquad \text{(A-12)}$$

$$\omega(p_2) - \omega(p_1) = -\sum_{p1}^{p2} (\nabla \cdot V) dp \qquad \text{(A-13)}$$

Since the tropopause is the beginning of an extremely stable layer (the stratosphere) with little vertical motion, it is reasonable to assume a zero vertical velocity at the tropopause. This allows for a simplification of the equations and the calculation of the vertical velocity at every level in the sounding.

$$\omega(p_1) = -\sum_{p1}^{p2} (\nabla \cdot V) dp \qquad \text{(A-14)}$$

This can be converted from pressure coordinates to metres per second by using the following formula:

$$w = \frac{\omega}{g\rho} \qquad \text{(A-15)}$$

Here, w denotes the vertical competent of the velocity vector, or updraft (in ms^{-1}), g denotes the gravitational acceleration ($g = 9.8\ ms^{-2}$), and ρ denotes the density of the air (in kg m^{-3}). Note that the air density varies with height.

Appendix B: Calculation of thermodynamic variables
(summarised from Wallace and Hobbs, 1977)

a) Surface pressure estimation

Atmospheric pressure is measured at some surface weather stations, but not at all stations. In order to compute derived variables such as mixing ratio, the pressure must be known. In order to get the pressure, the sea level pressures of the stations with known pressures are calculated. After averaging these out for the whole area, the pressure of the unknown station can be estimated knowing its elevation and the approximate average sea level pressure for the area using the following equation:

$$P = SLP \exp\left(-\frac{gh}{R_d (T + \Gamma h)} \right) \qquad \text{(B-1)}$$

P is the station pressure, SLP is the sea level pressure, g is 9.8 ms^{-2}, h is the elevation of the weather station, R_d is the gas constant for dry air, T is the temperature in Kelvin, and Γ is the standard temperature lapse rate of 6.5 °C/km.

b) Calculation of water vapour pressure, vapour mixing ratio and dewpoint

The water vapour pressure is calculated using a variation of the Clausius–Clapeyron equation. The following equation defines the saturated vapour pressure at a specific temperature.

$$e_s = 6.11 \exp\left(\frac{L_v}{R_v} \left(\frac{1}{273.15} - \frac{1}{T} \right) \right) \qquad \text{(B-2)}$$

e_s is the water vapour pressure, L_v is the latent heat of vaporisation at 15 °C, R_v is the gas constant for water vapour, and T is the temperature in Kelvin.

The actual vapour pressure is calculated using the relative humidity, RH (expressed in percentages):

$$e = e_s \left(\frac{RH}{100} \right) \qquad \text{(B-3)}$$

The mixing ratio can be derived from knowing the vapour pressure and the actual pressure. It is defined as:

$$w = \frac{R_d}{R_v}\frac{e}{(P-e)} \qquad \text{(B-4)}$$

w is the mixing ratio, R_d is the gas constant for dry air, R_v is the gas constant for water vapour, e is the vapour pressure of water vapour, and P is the atmospheric pressure.

The dewpoint is calculated using the Clausius–Clapeyron in the reverse way that the vapour pressure is calculated:

$$T_d = \frac{1}{\frac{1}{273.15} - \frac{R_v}{L_v}\ln\left(\frac{e}{6.11}\right)} \qquad \text{(B-5)}$$

T_d is the dewpoint, R_v is the gas constant for water vapour, L_v is the latent heat of vaporisation of water, and e is the vapour pressure.

c) Calculation of air density, potential temperature, equivalent potential temperature and virtual potential temperature

The density of air is due to the variation of pressure, temperature, and humidity. It is calculated with the following equation, which accounts for the variation of humidity.

$$\rho = \frac{P\left(\left(\frac{w}{1+w}\right)M_v + \left(\frac{1}{1+w}\right)M_d\right)}{RT} \qquad \text{(B-6)}$$

ρ is the density, P is the pressure, w is the mixing ratio, M_v is the molar mass of water, M_d is the molar mass of air, R is the universal gas constant, and T is the temperature in Kelvin.

The potential temperature is the temperature a parcel of air could reach if brought adiabatically to 1000 mb. This is given by the following equation:

$$\theta = T\left(\frac{P_0}{P}\right)^{\frac{R_d}{c_P}} \qquad \text{(B-7)}$$

θ is the potential temperature in Kelvin, T is the actual temperature in Kelvin, P_0 is the reference pressure (1000 mb), P is the actual air pressure, R_d is the gas constant for dry air, and c_p is the specific heat capacity of dry air.

The equivalent potential temperature is the potential temperature a parcel of air could reach if brought adiabatically to 1000 mb and had the latent heat of all water vapour in it released. It is based on the above potential temperature equation, and is given by:

$$\theta_e = \theta \exp\left(\frac{L_v w_s}{cpT}\right) \qquad \text{(B-8)}$$

θ_e is the equivalent potential temperature, θ is the potential temperature defined above, L_v is the latent heat of vaporisation of water, w_s is the saturated mixing ratio, c_p is the heat capacity of air, and T is the temperature of the air.

The virtual temperature T_v is what the temperature of an air parcel would be if it had the same density as dry air with the same humidity. It is calculated with the following equation:

$$T_v = \frac{T}{1-\left(e/p\right)\left(1-\varepsilon\right)} = T\left(1+\left(\frac{1-\varepsilon}{\varepsilon}\right)w\right) \qquad \text{(B-9)}$$

Where T is the temperature, e is the partial pressure of water vapour, p is the atmospheric pressure, w is the mixing ratio, and ε is the ratio of the gas constants for water vapour and dry air (which is 0.622). T_v can be replaced by θ_v and T can be replaced by θ to give the virtual potential temperature.

Appendix C: Estimating severe weather indices

To analyse the potential for convection sounding data can be used to estimate severe weather indices such as Convective Available Potential Energy (CAPE), Lifted Index (LI), Convective INhibition energy (CIN), and Precipitable Water (PW). With only four upper air soundings over our domain, it is not feasible to construct maps with contour intervals of these weather indices. However, it is possible to substitute the surface values for the soundings with surface values for the surface stations. This allows for the calculation of the severe weather indices at surface stations where there are no upper air observations.

The main premise for this is the fact that the upper atmosphere doesn't change much, and that the variation in the parameters is mostly caused by boundary layer changes, which can be approximated by the variables recorded at surface stations.

The procedure involves taking the sounding, adding in the surface temperature, dewpoint, and pressure, removing any sounding measurements from elevations below the surface station, and then recalculating the severe weather indices. This can be done at any surface station and allows for the creation of contour maps. For this case study, upper air variables are calculated using virtual temperature (density), and by mixing the lowest 50 millibars.

This seems reasonable for coming up with values for CAPE, lifted index, and CIN. There is some variation with elevation, but it appears to be a real variation and not an artefact of the substitution of surface stations. In general, raising the elevation of a surface station while keeping the same temperature and humidity will result in higher CAPE, and lower CIN. The difference in elevation does not have to be much in order to change these values significantly.

Using this procedure becomes problematic when dealing with precipitable water. Precipitable water is the total mass of water integrated to the top of the atmosphere (Usually 250 mb is more than high enough to catch most of the moisture). Because the majority of the moisture that contributes to precipitable

water is found within the boundary layer, changes in boundary layer depth greatly affect precipitable water. When looking at a capped situation, stations that are higher in elevation are closer to the cap, which defines the top of the boundary layer. This gives them a shallower layer of moisture, and a much smaller amount of precipitable water. Likewise, stations at low elevations (such as in river valleys) get abnormally high precipitable water values while having the same surface humidity. The variation of precipitable water with elevation can make it a poor indicator of the location of the dryline.

Appendix D: Surface weather station data quality and usability

Certain surface data obtained from different sources do not conform to what is required for completing an analysis of the surface humidity field, especially in the dry air. Some stations (especially from ASRD) are positioned at very high altitude on the tops of mountains, and are pushed into the upper level dry air, and are not representative of what would be at the surface. These stations are excluded from the surface analysis. The cut off elevation was decided to be 2000 m. They include:

Nakiska	(Environment Canada)	Elevation: 2543 m
Barrier Lake	(ASRD)	Elevation: 2021 m
Hailstone Butte	(ASRD)	Elevation: 2370 m
Moose Mountain	(ASRD)	Elevation: 2431 m
Raspberry Ridge	(ASRD)	Elevation: 2360 m
Baldy	(ASRD)	Elevation: 2082 m
Cline	(ASRD)	Elevation: 2050 m

The forestry stations that were removed only report at 1200Z and 1800Z, so this is not a significant loss of data. The loss of Nakiska from Environment Canada is a major loss in the dry air, but necessary for consistency. Summers (2009) also notes that ASRD weather stations tend to report slightly higher relative humidity than Environment Canada Stations due to their being located in forested areas.

In the dataset from Alberta Transportation, Okotoks was not reporting most of the day, and there were two stations which consistently reported anomalously low humidity with no apparent reason. These two stations have also been excluded from the analysis on the basis that the humidity sensor is in error. The pressure sensors on the Alberta Transportation weather stations are also not reporting accurate pressure. The pressures reported are not consistent with anything that should be reported in Alberta. In order to fix this, the atmospheric pressures at the stations have been calculated using equation B-1 to provide an estimate of the pressure. The excluded Alberta Transportation weather stations include:

Airdrie	(Telvent)	Reason: Abnormally low humidity
Ponoka	(Telvent)	Reason: Abnormally low humidity

Both of these weather stations are well into the moist air, and are in areas with many other weather stations to supplement data.